
UNIVERSITÀ DEGLI STUDI DI PADOVA

Scuola di Ingegneria

Dipartimento di Ingegneria Civile, Edile ed Ambientale

Corso di Laurea Magistrale in Ingegneria Civile


Tesi di Laurea

# CALIBRATION AND VALIDATION OF ATENA CONCRETE MATERIAL MODEL WITH RESPECT TO EXPERIMENTAL DATA


Laureando: Alessio Pizzocchero

Relatori: Prof. Ing. Carlo Pellegrino

Dott. Ing. Jan Vorel



A.A. 2014-2015

# Contents

# Figures index

# Chapter 1

# INTRODUCTION

Concrete is certainly the most used and important construction material of this era, but even some mathematical models of it exist in specialist literature, this model can't represent, with precision, the particular material characteristics under all loading conditions. The principal fault is the limited knowledge towards calibration and validation requirements and the availability of complete methods. Another problem for the progress in this area is the computational cost, the difficultly to solve the nonlinear systems, and the scarcity of comprehensive experimental data sets.

The Experimental database used in this work, was done to promote the study about concrete models by providing an overview of required tests and data preparation techniques and making a comprehensive set of concrete test data, cast from the same batch, available for a model development, calibration and validation.

In recent years many new construction materials have been created, these have novel properties, like strengths of up to 200 Mpa, superior rheology, or increased ductility .There are, for example fiber reinforced concretes (FRC), ultra-high performance concretes (UHPC) , sefl consolidating concretes (SCC) and engineered cementitious composites (ECC) . The main difficulty for a spread of these novel materials is a scarcity of experience.

Traditionally, large experimental investigation and many years of practical experience has led to the development of suitable design codes and design rules which are very safe and characterized by cautious assumptions. However, for the clean materials this approach is difficult to realize because the time on your hands is

short, thus, the only solution is complement experiments with analytical predications founded on correct, reliable and validated models.

The cracking and strain softening are the main characteristics of the tensile behavior of the quasi-brittle materials, like concrete. Such behavior, characterized from a loss of carrying capacity for increasing deformation, is normally described by non-linear fracture mechanics and fitting strain softening laws.

In literature we can find many constitutive models to describe the behavior of concrete. They utilize different concepts, like the plasticity, damage mechanics or fracture mechanics. They are included in the continuum mechanics and are formulated in tensorial form. Another formulation is the microplane models, these are formulated in vectorial form, which has some advantages that tensorial formulations. Microplane models don't use the functions of macroscopic stress and strain tensor invariant, and its constitutive laws are actuate by utilizing either the kinematic or the static constraints. Kinematically constrained formulations can be used with microplane constitutive laws exhibit softening and for this reason they have been adopted for quasi-brittle materials.

The solution for continuum formulations are independent of the numerical solution about the finite element discretization, and have to be inherent to the constitutive model, indeed methods that don't suffer from mesh sensitivity use the cohesive discrete cracks for strain softening.

The lattice is another formulation to simulate quasi-brittle materials, this class of models are discretized deducting their internal structure and utilize the characteristic lengths to furnish the formulation for example to particle size, particle models or size of the contact area among particles.

This allows there to have suitable ability of simulating the geometrical characteristic of material internal structure and thanks to it the simulation of damage initiation and crack propagation are accurate.

In conclusion, there are many different concrete material models in the literature, but difficulty still lies in choosing the model that is most suitable for a specified application. Even for the input parameters it's difficult to find the suitable values, these can be model parameters that have to be inversely identified or can have direct physical meaning.

To determinate and validate the model parameters the experimental data is required and the data of test types have to be of a sufficient number, meaning there have to be an adequate number of samples to obtain significant results. The most important necessary tests are uniaxial compression, confined compression of triaxial tests, and direct or indirect tension tests.

The 3-point-bending test or splitting test, to define the indirect tension, is usually preferred for the brittle nature of concrete. At least two sizes or otherwise two different types of tests have to be obtained to assure unique softening parameters and softening post-peak data.

For the clean materials, or for predictions under high loading rates, other tests are obligatory, and for the predictive capabilities this new model is not enough to be satisfactory after calibration, but they also need to be validated. This step includes a division of test and specimens into subpopulations for calibration and prediction. In this investigation a specific size of three- point bending (beam C) and the cube 40x40mm of unconfined compression, were chosen and allocated to calibration, the rest of the specimens of three point bending test were used for prediction and validation.

All specimens of this comprehensive set of tests were cast from the same batch and tested at an age of more than 400 days with the exclusion of standard 28-day compressive tests because their influence of ageing is of importance. For all the tests, including uniaxial compression, confined compression and size-effect tests (3-point bending and splitting), the raw data obtained has been pre-processed with the

purpose to find statistical indicators for material properties and the curves trend including post-peak softening.

Even if there is plenty of experimental data in the literature which is about different phenomena and mechanisms, there isn't an abundance of publications reporting response curves for uniaxial compression, confined compression and indirect tension with the same batch of concrete, and none at the same time provide post-peak response for various sizes.

## 1.1 Aims and Objectives

This thesis presents the numerical calibration and validation of the concrete material model formulated and used in ATENA software. The model parameters are firstly calibrated through optimum fitting of typical basic material test data. Then the model is verified through comparing the numerical simulation results with a large group of experiment data. The simulated experiments include three point bending tests scaled in four size and unconfined compression of cubes. Conclusions from the current research efforts and recommendations for future studies are included.

Finite element method (FEM) models were developed to simulate the behavior of four full-size beams and two size cubes from linear through nonlinear response and up to failure.

In the calibration methods proposed and discussed in this thesis, traditional experimental information consisting of stress-strain curves. It was comparison stress-strain curves obtained through experimental tests and stress-stain curves obtained through numerical simulation

Three-point bending tests and unconfined compression tests are often employed for calibrating and validating mechanical models of homogeneous materials. Mechanical calibration means here identification of parameters which are contained

in constitutive elastic-plastic and fracture models and turn out to be not directly measurable by traditional elementary tests.

Either semi-empirical formulae can be used for such calibration, finite element simulations of the test allows to exploit wider sets of experimental data and to increase the number of estimated parameters and estimation accuracy.

.The response of a concrete structure is determined in part by the material response of the plain concrete of which it is composed. Thus, analysis and prediction of structural response to static or dynamic loading requires prediction of concrete response to variable load histories. The fundamental characteristics of concrete behavior are established through experimental testing of plain concrete specimens subjected to specific, relatively simple load histories. Continuum mechanics provides a framework for developing an analytical model that describe these fundamental characteristics. Experimental data provide additional information for refinement and calibration of the analytical model.

In this paper the concrete material model used in this investigation for finite element analysis of the three-point bending and unconfined compression tests will be presented.

## 1.2 Organisation of the thesis

This thesis is formed of 9 chapters.

In the first chapter the aims and objectives were explained after an introduction to the work.

In the second chapter the laboratory tests available, and the experimental data obtained from them, were analyzed, while the different types of specimens used and the individual tests performed have been described.

In the third chapter the behavior of concrete under the action of the laboratory tests has been explained, explaining the failure mechanisms and the problem called "size effect" based on the difference in size of the specimens.

In the fourth chapter a general overview of all existing constitutive models for concrete has been made, focusing on aspects that could affect the constitutive model calibrated and validated in this work.

The fifth chapter talks about the software ATENA, describing the implemented Material Model and the various solution methods of nonlinear analysis used to solve the FEM model. It also describes the finite elements used for the creation of the FEM model.

In the sixth chapter the creation of FEM models is described, explaining the procedure and the Characteristics.

In the seventh chapter the calibration of Material Model was addressed, describing the process and the results obtained. A parametric analysis of the most significant parameters considered in the calibration has also been conducted.

In the eighth chapter the validation of the model Material was performed, analyzing the different aspects and describing the results obtained.

In the ninth chapter, the conclusions found and possible future studies were reported

# Chapter 2

# THE EXPERIMENT USED

## 2.1 The speciment used

The investigation used in this research represents an extension of a size-effect investigation in 3-point bending conducted by Hoover et al. where 164 concrete specimens were cast in one batch in early 2011 and tested in 2012. After that, 105 specimens were cut from remaining shards in order to supplement, among others, con_ned compression tests, Brazilian splitting tests, direct tension tests, and hysteretic loading-unloading tests.

In detail, response curves for the following tests were done in the experimental tests treated:

- 128 three-point bending tests of 400 day old geometrically scaled unreinforced concrete beams of four sizes with a size range of 1:12.5 including un-notched specimens and beams with relative notch depths of $\alpha = a/D$ = 0.30, 0.15, 0.075, 0.025.

- 12 centrically and eccentrically loaded 466 day old 3-point bending specimens of size D = 93 mm, with and without unloading cycles in the softening regime.

- 40 Brazilian splitting tests, of roughly 475 day old prismatic specimens of 5 sizes with a size range of 1:16.7.

- 12 standard ASTM modulus of rupture tests at 31 days and 400 days.

- 24 uniaxial compression tests of 3"x6" (75x150 mm) cylinders at 31 days and 400 days.

- 22 uniaxial compression tests of approximately 470 day old cubes with D = 40 mm and D = 150 mm, loaded partly monotonically and partly with several loading-unloading cycles in the softening regime.

- 6 uniaxial compression tests of approximately 950 day old cubes with D = 40 mm.

- 6 uniaxial tension tests of approximately 950 day old prisms.

- 4 confined compression tests of 560 day old cored cylinders with D = 50 mm and L = 40 mm including 4 unconfined uniaxial compression tests of cored companion specimens.

- 11 torsion tests of prisms with W = 40 mm and D = 40; 60; 80 mm.

It was not possible to treat all tests in this thesis, for this reason the most significant tests for doing a complete numerical simulation were chosen. All of three-point bending tests and one unconfined compression tests were chosen. In Figure 2.1 is shown the beam of three-point bending test and in Figure 2.2 is shown the cube 40x40mm chosen.

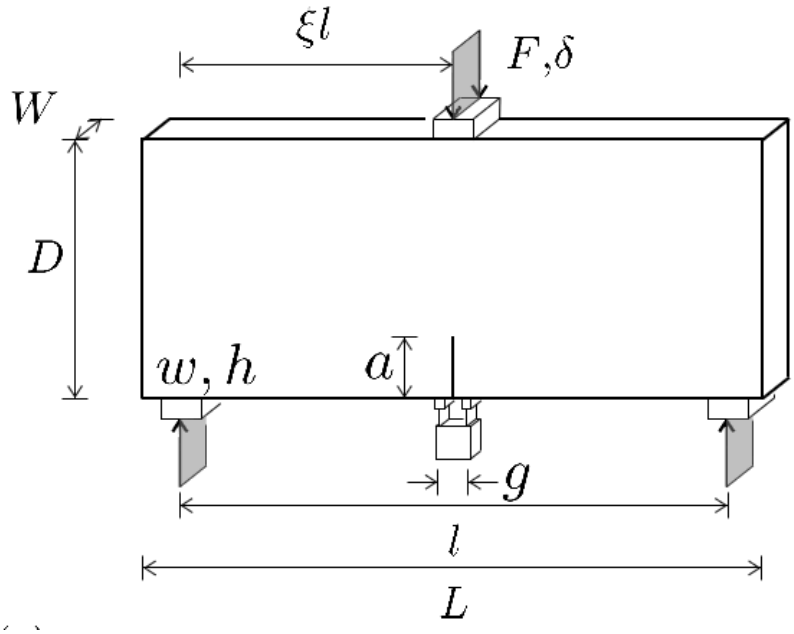


*Figure 2.1: Specimen geometry, three point bending tests, geometrically scaled in four sizes*

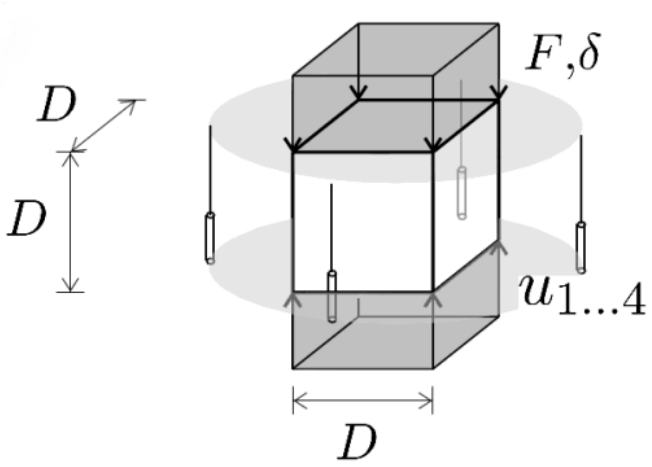


*Figure 2.2: Specimen geometry, unconfined compression of cubes of two sizes*

## 2.2 Mix properties and curing

One batch of ready-mixed concrete was used. All 164 specimens of the initial investigation include 128 beams, 12 ASTM beams, 24 cylinders. The specified compressive strength was $f'_c$ =31MPa. The coarse aggregate was pea gravel, with a maximum diameter of 10 mm, a water-cement ratio *w/c* = 0.41, and a water-binder ratio *w/b* = 0.35. A slump retention admixture guaranteed workability for the full 3 hours duration of casting period with a consistent of 150 mm of slump. The depth for the 128 beams is constant, your value is *W*=40 mm.

All specimens were cast horizontally and later were vibrated. The remaining shards of the original investigation had been exposed to additional analysis and special attention was focus on avoiding areas of high stress concentration and pre-damaged areas. Beams and cylinders, after the casting, remained covered with plastic and untouched for 36 hours. Until testing they stayed in a ambient with around 23°C and approximately 98% relative humidity.

## 2.3 Overview of material properties

In the table 2.1 there are the basic concrete properties, that their results come from various tests perfomed at different ages. The fracture parameters are given in table 2.2. The coefficient of variation *CoV =std/mean* have been utilized, where possible, for the inherent scatter.

The casting and specimen preparation were done highly carefully and caused low experimental scatter with coefficient variation less 10%. Also the statistical outliers was suitable because just one beam and two of early age compression cylinders didn't pass the Grubb's test for outliers, and obviously these specimens were excluded from the investigation. Compressive strength was settled relating on 75x150 mm cylinders, 40 mm and 150 mm cubes. The value of poisson ratio is $\nu = 0.172$ it was determined based on the circumferential expansion of standard cylinder in compression.

| Material property | | unit | mean | CoV [%] |
|---|---|---|---|---|
| Compressive cylinder strength | $f_{cyl,75}(31)$ | MPa | 46.5 | 3.2 |
| Compressive cylinder strength | $f_{cyl,75}(400)$ | MPa | 55.6 | 3.7 |
| Compressive cube strength | $f_{cu,40}(470)$ | MPa | 56.16 | 9.5 |
| Compressive cube strength | $f_{cu,150}(470)$ | MPa | 57.1 | 5.5 |
| Compressive cube strength | $f_{cu,40}(950)$ | MPa | 61.2 | 8.2 |
| Modulus of elasticity,75 mm cyl | $E_{cyl,75}(31)$ | GPa | 27.74 | 6.2 |
| Modulus of elasticity,75 mm cyl | $E_{cyl,75}(400)$ | GPa | 34.38 | 3.9 |
| Modulus of elasticity,D=40 mm | $E_{r,40}(400)$ | GPa | 35.70 | 7.0 |
| Modulus of elasticity,D=93 mm | $E_{r,93}(400)$ | GPa | 41.29 | 6.8 |
| Modulus of elasticity,D=215 mm | $E_{r,215}(400)$ | GPa | 43.68 | 9.4 |
| Modulus of elasticity,D=500 mm | $E_{r,500}(400)$ | GPa | 43.66 | 12.7 |
| Modulus of elasticity, inverse | $E_{r,inv}(400)$ | GPa | 37.94 | |
| Poisson ratio | $\nu$ | - | 0.172 | 10.0 |

*Table 2.1: Material properties extracted from cylinder tests and ASTM modulus of rupture tests*

According to the fib Model code 2010, the Eq. (2.1) can be used to determinate the strength and modulus development, with parameter $s$=0.25 for R-type cement.

$$f(t) = f_{28}\beta_{fib}(t),\ \ E(t) = E_{28}\sqrt{\beta_{fib}(t)},\ \ \beta_{fib}(t) = e^{s(1-\sqrt{28/t})} \tag{2.1}$$

Another equivalent formulation is from ACI, given by Eq. (2.2) with $a$=*4.0* and $b$ = 0.85 for type-I cement.

$$f(t) = f_{28}\beta_{ACI}(t),\ \ E(t) = E_{28}\sqrt{\beta_{ACI}(t)},\ \ \beta_{ACI}(t) = \frac{t}{a+bt} \tag{2.2}$$

While these two formulations fail to predict the modulus development, the strength development calculate with the model code is very good, and the prediction with the ACI formulation is fair. Strength an modulus values extracted 28-day are given including the 95% confidence bounds, and they are reported in table (2). With the ACI formulation (Eq. 2.3) or the fib formulation (Eq. 2.4) can be predicted the Young modulus utilizing the compressive strength. About the fib formulation the parameters $E_0$ and $\alpha_E$ are dependent on aggregate type.

$$E_{28,ACI} = 4734\sqrt{f_{28}} \tag{2.3}$$

$$E_{28,ci,fib} = E_0\alpha_E\left(\frac{f_{28}}{10}\right)^{1/3} \tag{2.4}$$

| Parameter | model | value | unit | RMSE |
|---|---|---|---|---|
| $f_{cyl,75(}28)$ | fib | 46.1 | MPa | 0.184 |
| $f_{cyl,75(}28)$ | *ACI* | 46.8 | MPa | 1.243 |
| $f_r(28)$ | fib | 6.8 | MPa | 0.158 |
| $f_r(28)$ | *ACI* | 6.9 | MPa | 0.314 |
| $E_{cyl,75}(28)$ | fib | 29.63 | GPa | 1.988 |
| $E_{cyl,75}(28)$ | *ACI* | 29.81 | GPa | 2.313 |
| $E_{cyl,75}(28)$ | Fib* | 27.31 | GPa | - |
| $E_{cyl,75}(28)$ | ACI* | 26.78 | GPa | - |

*Table 2.2: Strength and modulus development: quality of fit.*

In the table 2.3 there are the values of fracture energy. They were obtained from the study of size-effect in 3-point-bending push through to Hoover et al. With the Bazant's Size Effect Law he obtained the initial fracture energy $G_f$ whereas the total fracture energy $G_F$ based on the work of fracture method. As thought probable, the total fracture energy is around double the initial fracture energy.

| Material property | unit | mean | CoV [%] |
|---|---|---|---|
| *Fitting of Type 2 SEL α = 0.30* | | | |
| Initial fracture energy $G_f$ | N/m | 51.87 | - |
| Characteristic length $c_f$ | m | 23.88 | - |
| *Fitting of Type 2 SEL α = 0.15* | | | |
| Initial fracture energy $G_f$ | N/m | 49.78 | - |
| Characteristic length $c_f$ | m | 20.99 | - |
| *Work of fracture energy α = 0.30* | | | |
| total fracture energy $G_f$ | N/m | 96.94 | 16.9 |
| *Work of fracture energy α = 0.15* | | | |
| total fracture energy $G_f$ | N/m | 111.1 | 20.7 |

*Table 2.3: Fracture parameters according to Hoover et al.*

## 2.4 Detailed description of tests

For all the tests three MTS closed-loop testing machines with sevo-hydraulic system and tree different capacities were used. For the uniaxial compression and the confined compression tests the machines with 4.5 MN load frame were used. For the three-point bending tests and splitting tests of specimens with the size D= 215 mm and D= 500 mm were carried out in the 980 KN load frame. For all remaining specimens the 89 kN load frame was used. The dimensions of each specimen, during the preparation, and the crack pattern were recorded and documented with pictures. The displacement of the piston measured inside the machine (stroke), force and loading time were recorded. All the test specific quantities (load-point displacement, axial shortening, circumferential expansion and crack mouth opening displacement)

were also recorded. Every day the machines were exposed to rigorous control to calibrate the load cells.

### 2.4.1 Test control and stability

About the testing of quasi-brittle materials, an issue to calibrate the model parameters which control softening in tension, shear-tension, or compression under low confinement is to obtain the suitable values for the post–peak softening curves for different types of tests and various sizes. The energetic stability condition is used to describe the stability problem in the softening regime, that represents the ability to control a specimen. This problem is formulated in terms of the second variant of the potential energy ($\delta^2 II > 0$) and represent a limit state called "snap-down". This issue happens when under displacement control the stability path remains, providing that no point with vertical slope is reached. This phenomenon is characterized by an equilibrium path with global energy release and represents the transition to a "snap-back" instability.

The practical problem of a specimen with elastic stiffness $K_{el}$ in a load-frame with stiffness $K_m$ is equivalent to a serial system with total current tangential stiffness $K(u)=(1/K_m+1/(K_{el}-\Delta K(u)))^{-1}$. The term $( K_{el}-\Delta K(u))$ represents the true tangential specimen stiffness and $\Delta K(u)$ is a total stiffness change due to softening. Basically if $K(u)$ tend to minus infinite there is a snap-down, therefore the only solution for a stable test in displacement control in the softening regime is that $K(u)$ is finite along the entire equilibrium path. The features of the specimen or by means of the test setup are the most common reasons for the instability. The condition $\Delta K(u) < K_{el}$ or mathematically $K_{crit} < \infty$ guarantee the stability if assuming an ideal load frame with infinite stiffness. If in elastically unloading parts of the specimen more energy is released than required to propagate the crack the snapback is noted on the other side. The condition $K_m > K_{crit}$ represents a minimum stiffness of the machine frame

indispensable for the stability of the test. Essentially, if it is possible to continuously find an increase of the quantity for the control, the post-peak test will be stable.

The success of fracture tests ultimately depends on the proper selection of specimen geometry, test setup, sensor instrumentation, and control mode. Thus, during the development of experimental campaigns compliance tests of the load frame, fixtures, and preliminary simulations of the specimens to determine a stable mode of control are highly advised.

### 2.4.2 Data preparation and analysis

All data obtained from the experimental are impartial and objective because they were processed automatically. The pre-processing set only the statistics of the specimen dimensions, and all the automatic operations of removal of pre-test and post-test data were normalized with a limit frequency of 0.10.

During the initial setting, the load displacement diagrams is extracted by linear extrapolation of the elastic part of the loading branch and the constant movement by the respective displacement intercept. The values of the linear region considered are (0.50-0.90)$\sigma_{peack}$ for beam, (0.25-0.90)$\sigma_{peack}$ for compression specimens and (0.60-0.90)$\sigma_{peack}$ for Brazilian beams. The figures referential showed the result for each specimen family in terms of a mean response curve and envelope. In the depiction of the curves, it averaged the pre-peak and post-peak branches separately

## 2.5 Unconfined Compression

The compression tests are the most traditional test used to characterize the concrete. The Eurocode indicate two kinds of specimen, cylinders or cubes, the first one has 150 mm of diameter and 300 mm height, while the second one has 150 mm side length.

Unconfined compression tests not only yield a material's uniaxial compressive strength but also provide insight into the softening behavior already starting before the peak-load.

From the undamaged part of the ASTM modulus of rupture specimens eight 150 mm cubes were cut and from the remainder of the 3-point-bending size effect investigation fourteen 40 mm cubes were cut. These cubes were tested at about an age of 470 days like the Brazilian splitting size effect investigation. The ASTM test standard specifies that during the application of the load, only the top load platen can rotate. Before the tests, it was used solfur compound to cover the top of the cubes to ensure initially co-planar and smooth loading surfaces and the load was applied in both surface up and down. According to ASTM C39, the observed fracture patterns were conformed to Type 1, with the form similar a cone.

To obtain an adequate friction especially when there were the peak loads, between specimen and load platens some degree of lateral confinement in the contact surface was introduced. This procedure can be reproduced without problem in the numerical analyses by suitable interface elements, but in the standard analyses assuming just the ideal uniaxial conditions. In these tests solely sulphur compound capping was applied.

Before and after capping the specimen dimensions recorded were length of all edges and the height. The force F and machine stroke $\delta$ was measured during the tests where the second one was the stable mode of control. With four equiangularly distributed LVDTs the load platen to platen distance $u$ was also measured.

In The diagram of uniaxial compression originated to the experimental tests, in the x-coordinate there is the nominal strain $\varepsilon_N$ and in the y-coordinate the nominal stress $\sigma_{N.}$ These two parameters are defined by Eq. (2.5) and Eq. (2.6) respectively. In the first formula $\bar{u}$ is the mean shortening of the specimen and D is the mean of the specimen dimension in the respective axis, obtained from four measurements.

$$\sigma_N = \frac{kF}{D^2} \tag{2.5}$$

$$\varepsilon_N = \frac{u}{D} \tag{2.6}$$

In Figure 2.3 and 2.4 the nominal stress $\sigma_N$ versus nominal strain $\varepsilon_N$ diagrams for uniaxial compression tests of 40 mm and 150 mm cubes is shown in terms of mean response curves and envelope. Specimen dimension, peak stresses and elastic module is given by mean values and coefficients of variation.

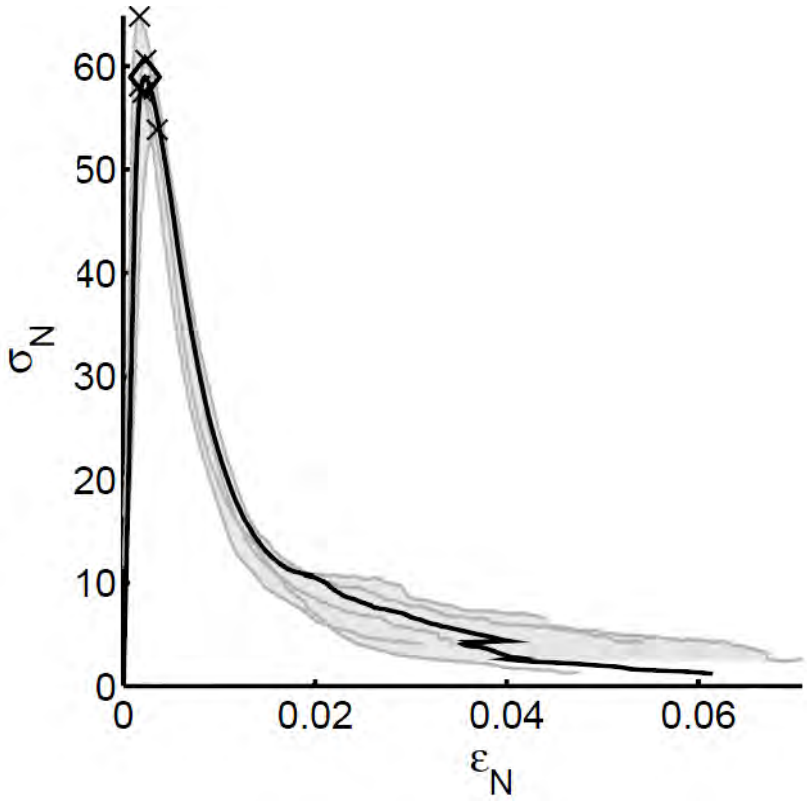


*Figure 2.3: Nominal stress $\sigma_N$ versus nominal strain $\varepsilon_N$ for uniaxial compression tests: cubes 40x40 mm at 470 days*

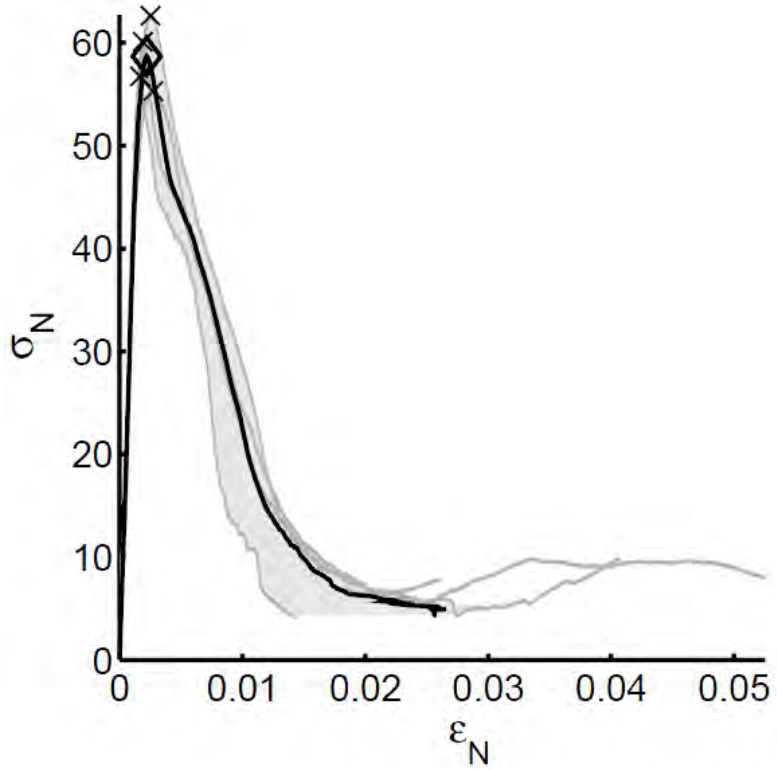


*Figure 2.4: Nominal stress $\sigma_N$ versus nominal strain $\varepsilon_N$ for uniaxial compression tests: cubes 150x150 mm at 470 days*

## 2.6 Flexural fracture by 3-point-bending

The investigation considered focus on the flexural fracture, where, in total, 128 beams were tested. There were four sizes of beams with a size range of 1:12:5.The principal survey about size dependency focused on flexural strength and toughness, however, the parameters, including the relative notch depth $\alpha = a/D$, and the relative load eccentricity $\xi = x/l$ were studied. The notch depths were studied in different values of $\alpha$= 0.3,0.15,0.075 for all sizes and $\alpha$= 0.025 for the two larger sizes. Therefore, six specimens for each size and notch depth combination were tested. For each different size, only the thickness W and the notch width were left constant, while all dimensions including the steel support block were geometrically scaled. The notches were cut after 96 days with a diamond coated band saw with a width of 1.8 mm.

In 11 days, all 128 beams of the bending size effect investigation were tested around 400 days after casting. For notched specimens the stable mode of control was CMOD and for un-notched beams was average tensile strain. The large specimens of sizes A and B were loaded in the 220 kip load frame whereas specimens of size C and D were tested in the 20 kip load frame (figure 2.5). Force, stroke and center-point displacement were obtained by averaging two LVDT measurements. In addition to these, there was an extensometer that read the tension side of the beam for all tests.

Where the elastic deformation within the gauge length *g* is negligible, the CMOD (crack mouth opening displacement) corresponds to measurements for the notch depths. For un-notched specimens and also for specimens with shallow notch sensors of larger gauge length *g* were instrumental to guarantee a crack localization within.

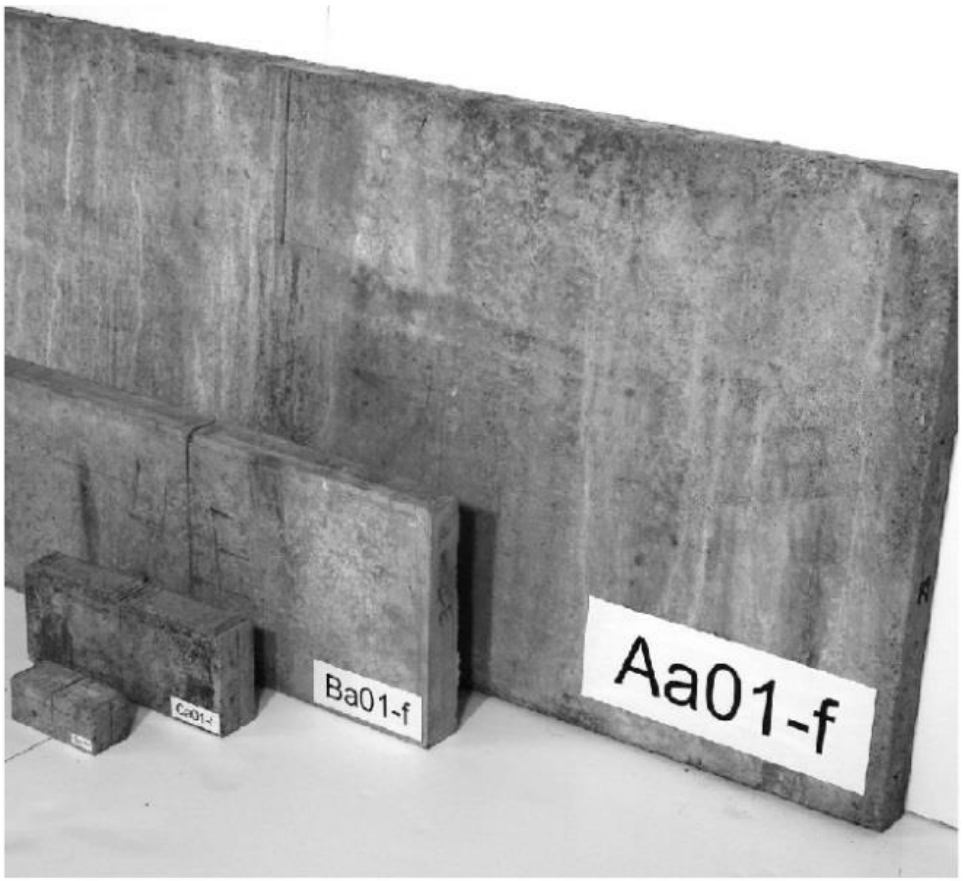


*Figure 2.5 Three point bending: size comparison*,

| Property | A[mm] | B[mm] | C[mm] | D[mm] |
|---|---|---|---|---|
| Thickness,*W* | 40.0 | 40 | 40.0 | 40.0 |
| Height, *D* | 500 | 215 | 92.8 | 40.0 |
| Length,*L* | 1200 | 517 | 223 | 96.0 |
| Span, *l* | 1088 | 469 | 202 | 87.0 |
| Guage length,*g* | 162;218 | 94.5;137 | 60.0;25.4 | 25.4 |
| Guage length,*g (α = 0.3)* | 25.4 | 25.4 | 12.7 | 12.7 |
| Loading block width,*w* | 60 | 26 | 11.0 | 5.2 |
| Loading block height, *h* | 40 | 20 | 10.0 | 5.0 |

*Table 2.4: Nominal geometry of 3-point-bending specimens*

For notched or un-notched specimens of all different sizes, the response is pictured in terms of nominal strain $e_N$ (x-coordinate) and nominal stress $\sigma_N$ (y-coordinate). The nominal stress is defined by Eq. (2.7) and the nominal strain is defined by Eq. (2.8) where *u* is the measured opening of the extensometer, *g* is the gauge length and the nominal stress is based according to beam theory.

For both equations D is the height of the specimen and W is the thickness. For specimens with deep notch the extensometer reading at the surface of the beam is proportional to the CMOD, therefore the crack mouth opening can be well approximated by the first ones. For small specimens with short notch elastic deformation within, the gauge length is small if it is compared to the total extensometer reading, and this characteristic is more accentuated for specimens with wide sizes.

The gauge length can therefore be neglected to calculate the nominal strain for a notched specimen. However, for a meticulous research, the gauge length and consequently the contributions of elastic deformation should be considered.

$$\sigma_N = \frac{6F(1-\xi)\xi l}{WD^2} \tag{2.7}$$

$$\varepsilon_N = \begin{cases} \frac{\beta u}{g} \; for & \alpha = 0 \\ \frac{u}{D} \; for & \alpha > 0 \end{cases} \tag{2.8}$$

For un-notched specimens a correction factor β is required because the gauge length is finite and not negligible compared to span length *l*, this matter doesn't change for different sizes.

As expected, with specimen size D, strength decreases and the post-peak regime shows a transition from ductile to rather brittle behavior. For all five geometrically similar beam sets, the slope in the elastic regime coincides.

Being that cement is a heterogeneous material, its distribution of strength can be random as it has a significant scatter in structural response. This characteristic shows that the macroscopic strength of specimens without initial notch have a wide-spread crack localization on the tension side.

The specimen response is plotted in terms of nominal stress $\sigma_N$ and nominal strain $\varepsilon_N$ for the un-notched and notched specimens of all four sizes in Figure 2.6 - 2.7 - 2.8 - 2.9 - 2.10.

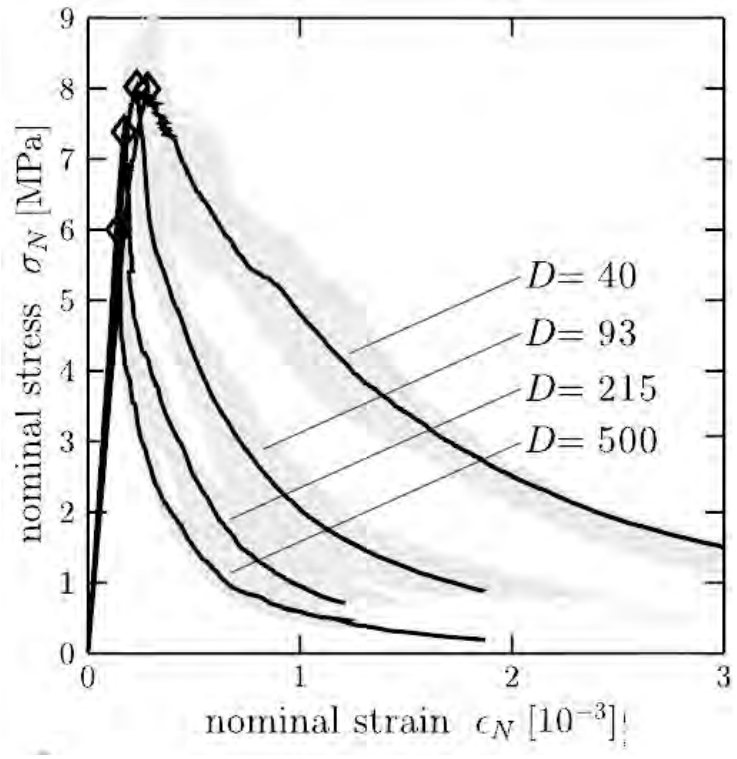


*Figure 2.6: Three point bending: nominal stress-strain diagram for un-notched beams*

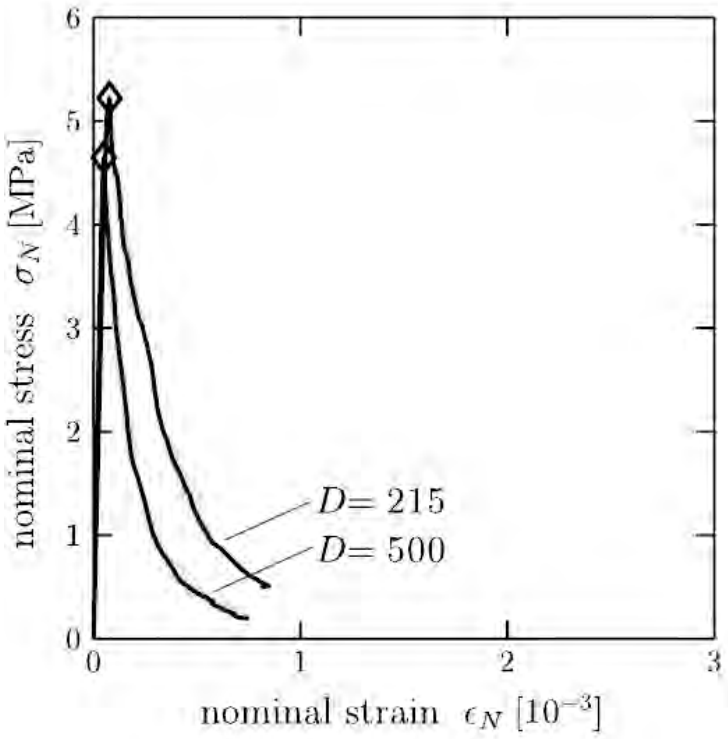


*Figure 2.7: Three point bending: nominal stress-strain diagram for beams with α = 2.5%,*

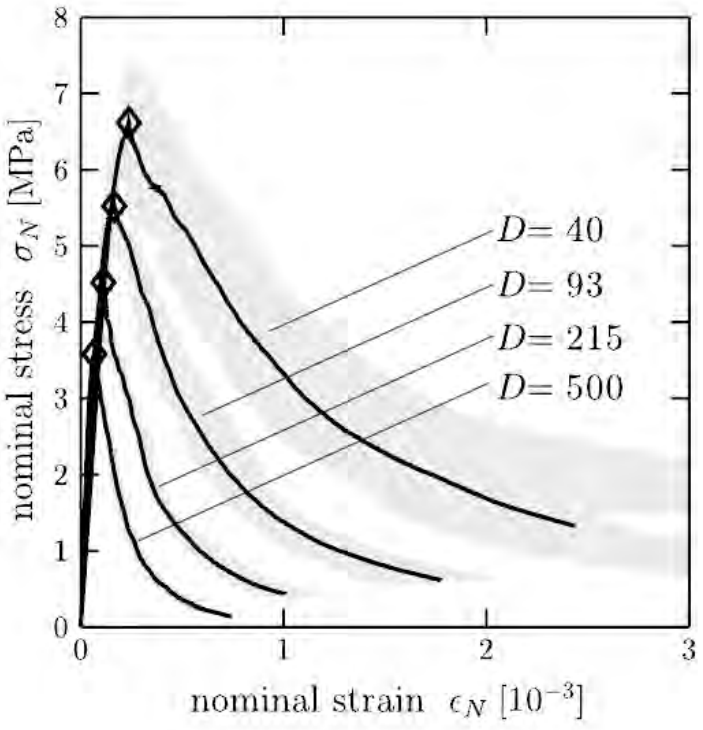


*Figure 2.8: Three point bending: nominal stress-strain diagram for beams with α = 7.5%,*

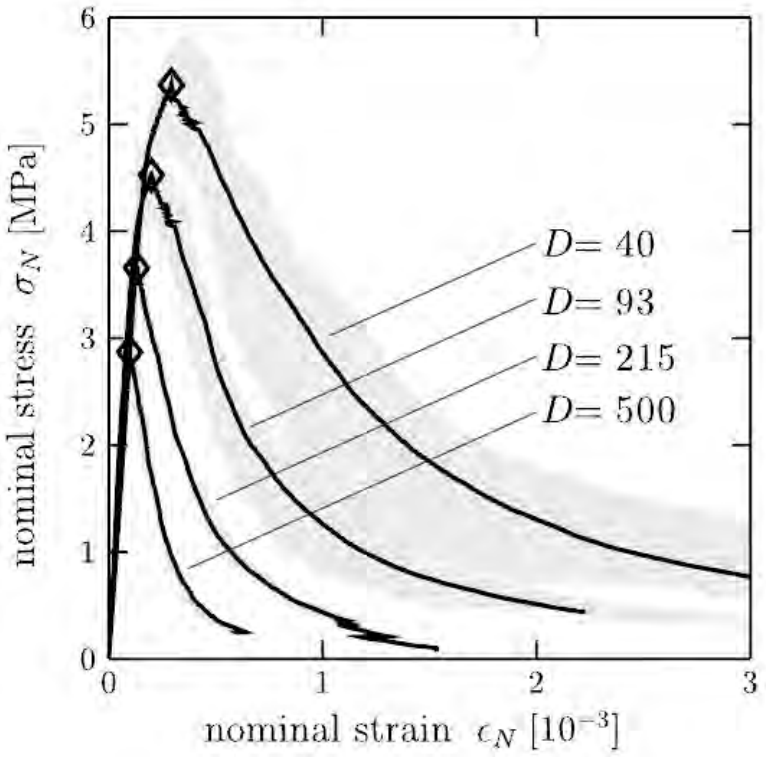


*Figure 2.9: Three point bending: nominal stress-strain diagram for beams with α = 15%,*

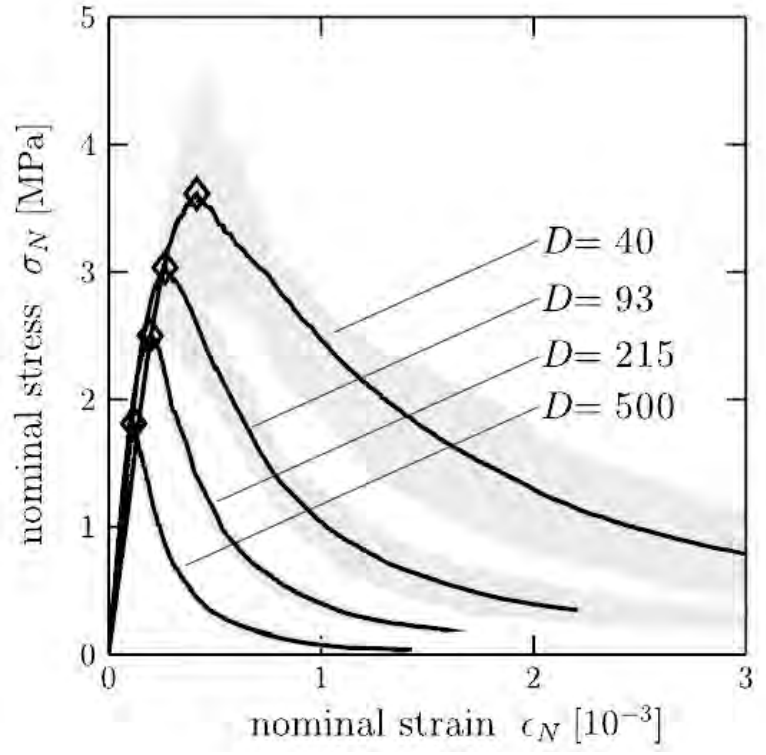


*Figure 2.10: Three point bending: nominal stress-strain diagram for beams with α = 30%,*

# Chapter 3

# EXPERIMENTAL BEHAVIOUR OF CONCRETE

## 3.1 Brief literature review on fracture mechanics of plain concrete

How material fails can be described by two basic fracture mechanics approaches.

- When the intensity of stress concentration at micro-flaw (say, a crack tip) exceeds the intrinsic cohesive strength of the material (stress intensity approach) a material fails.

- When the energy stored in it during loading exceed the energy required for creating fresh macro-flaws (say, crack surfaces), the energy balance approach a material fails.

Single Edged Notched (SEN) beams using the fictitious crack model also known as Damage zone model have been analyzed by Hillerborg et al. The tensile stress is assumed not to fall to zero immediately after the attainment of limiting value but to decrease slowly with increasing crack widths. To describe the tensile fracture behavior of concrete Modulus of elasticity E, uniaxial tensile strength $\sigma_t$ and fracture energy $G_F$; defined as the area under post-peak stress vs. COD diagram are the material properties required. The concept of crack band theory for fracture of concrete was introduced by Bazant & Oh. The fracture front is modeled as a blunt smeared crack band.

Three parameters $G_F$; $\sigma_t$ and the width of crack band $W_C$ (fracture process zone) characterize the material fracture parameters. $G_F$ is however defined as the product of $W_C$ and the area under the tensile stress-strain curve. The maximum load carrying capacity of several beams are predicted using this model. $G_F$ is found to depend on

the specimen size. The values of $G_F$ so obtained are used to obtain an empirical relationship to predict $G_F$ from the knowledge of material properties. These model irrespective of the approach adopted requires a complete stress-crack opening relation. They are particularly well suited for numerical techniques like the finite element method. Some models also proposed do not require the finite element technique. Wecharatana & Shah based on some simple and approximate extensions of the concepts of LEFM, have predicted the extent of the non-linear fracture process zone in concrete. Critical COD equal to 0.025mm and a constant closing pressure to exist along the length of the fracture process zone are assumed.

Fracture loads of a large number of notched beams are reported to have been estimated with a reasonable degree of accuracy. Two parameter fracture models have been proposed by Jenq & Shah. The two parameters are critical stress intensity factor calculated at the tip of the effective crack and critical COD. Based on their test results, the two parameters are found to have size dependency. A critical review of works dealing with concrete fracture has been presented by Alberto Carpinteri. He concludes that heterogeneity is only a matter of scale and notch sensitivity is necessary but not sufficient condition for the applicability of the linear elastic fracture mechanics. Tests on cement mortar and concrete beams in two stages have been performed by Nallathambi & Karihaloo, with a view to study the influence of several variables upon the fracture behavior of concrete.

On the basis of the results from the first stage of test in which a single water/cement ratio and type of coarse aggregate were used, a simple formula was ascertained to estimate the fracture toughness of concrete in terms of specimen dimensions, maximum aggregate size and notch depth together with the mix compressive strength and modulus of elasticity (determined from separate standard cylinder test). It was found to predict with satisfactory accuracy, the results from the second stage of test in which, besides variation of the type of coarse aggregate and water/cement ratio, some of the specimen sizes were outside the range used in the first series. Peterson determined fracture energy GIC using load-deflection curve. The test

results indicate that GIC is independent of both notch depth and beam depth. Raghu Prasad et al proposed a simple numerical method called Initial stiffness method and Modified lattice model. to analyze fracture behavior of plain concrete beam (strain softening material) in mode-I using finite element method.

A new parameter namely, strain softening parameter has been introduced. By analyzing a significant number of beams tested and reported by various researchers the method is validated.

## 3.2 Behaviour of concrete under uniaxial compression

This is the most commonly used test (Figure 3.1). It is carried out on cylinders or cubes of concrete. In general, the normalized test is controlled at an imposed stress rate, but an imposed displacement allows the post-peak regime of the response to be obtained.

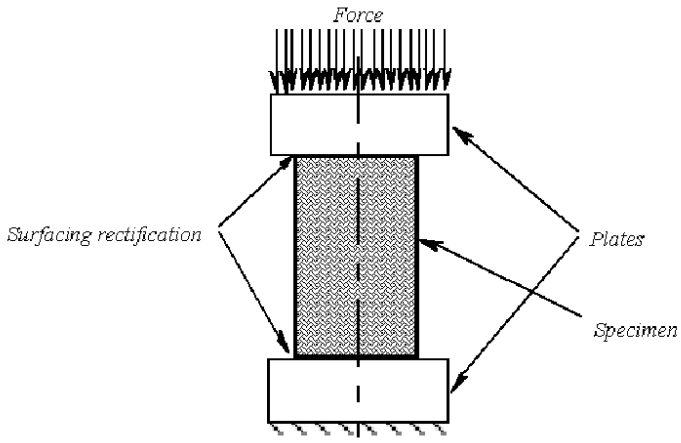


*Figure 3.1:Principe of simple compression test*

The typical curve stress-strain of concrete when exposed to uniaxial compression is presented in Figure (3.2). There are three levels of deformation: the elastic phase, the inelastic phase and the phase where there the deformation is. The first phase is shown until the value of stress is about 30% of $f'_c$, where $f'_c$ is a cylindrical uniaxial compressive strain. For higher stress, there is the second phase, where the reaction is nonlinear and becomes more clear if the stress is about the value of the pick $f'_c$.

After that, it becomes the descending branch where increasing the deformation decrease the stress up to breakage for crushing. If the material is exposed cyclic loads, remaining deformations and a decline of the stiffness is observed.

During loading, deformations perpendicular to the principal compressive stress appear, creating micro-cracks as the tensile deformation threshold is being exceeded. Micro-cracks coalescence leads to the collapse of the specimen. Moreover the elastic characteristics of the material evolve; the elasticity modulus decreases during the loading whereby the material becomes damaged due to micro-cracking. Some irreversible deformations appear. The boundary conditions of the specimen play an important role on the characterization of the behavior of the material during simple compression. Due to friction, bracing cones appear at failure. Just the central part of the specimen is subjected to a uniaxial compression stress. After the peak load, the Poisson coefficient suddenly increases. In the same way, damage growth is occurring more rapidly.

Experimental observation shows that after the pick, the deformation is no longer uniform, but tends to localize in one section. In this phase a better representation of the behavior has to be in terms of stress-displacement instead of stress-strain. These examinations were studied from Van Mier where the geometry of the specimen has influence on stress-strain branch. The results are shown in Figure (3.3).

Before the pick, the curves trend is almost identical, but after the pick, with the reduction of the height of the specimen there is a decrease of the slope of the stress-strain branch instead. However, if the same results are represented in terms of stress-displacement, this different response of the specimen practically disappears Figure (3.4).

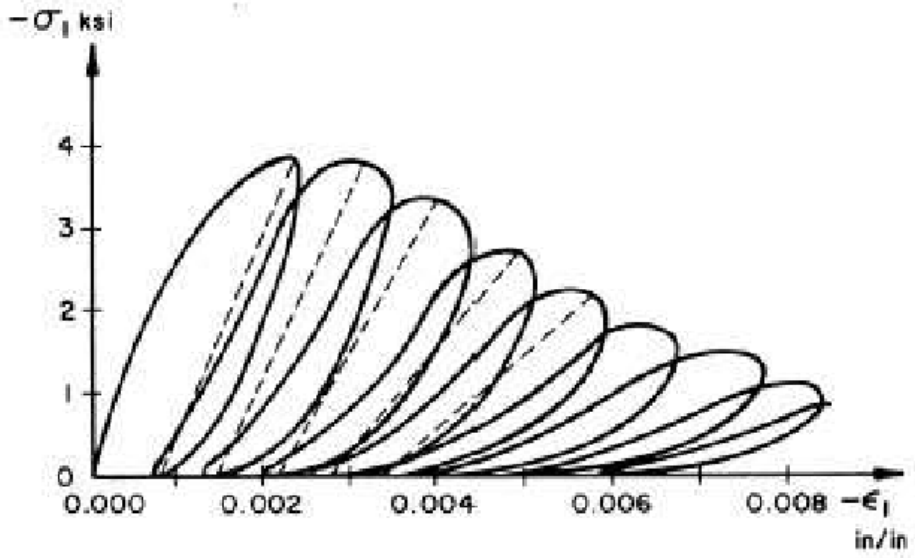


*Figure 3.2: stress-strain curve for cyclic uniaxial compression*

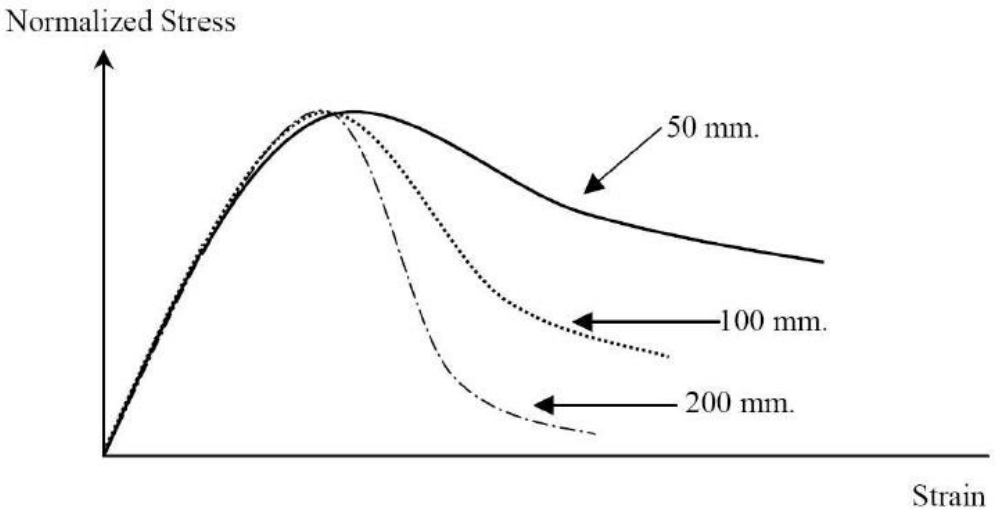


*Figure 3.3:dependence of stress-strain curve due to specimen size*

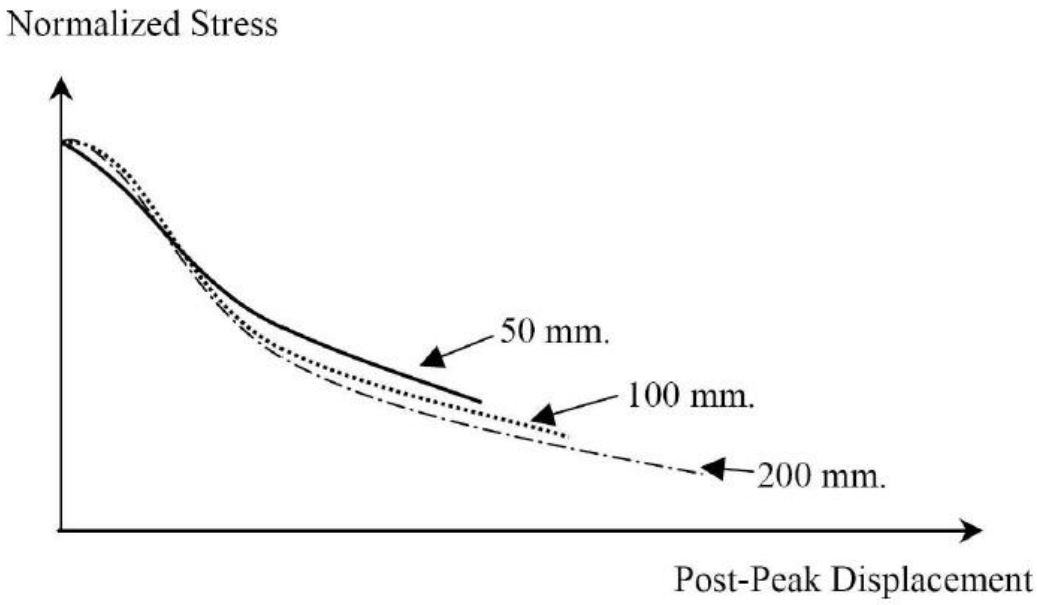


*Figure 3.4: independence of stress-displacement curve due to specimen size*

Interlayer water within the material influences its visco-elastic behavior. Several other phenomena are related to the water content and the presence of hard inclusions (aggregates) within a cementitious matrix, which retracts as the water leaves. Concrete and mortar strengths increase when free water leaves, because of the capillary effect and increased suction within the partially saturated porous medium.

Concrete can be considered as an initially isotropic material. The elastic parameters of the material are Young's modulus (E) and Poisson coefficient (ν). Regarding common concretes, those usual values of the parameters are *30,000 MPa* and *0.2*, respectively, and are used in numerous constitutive laws and numerical calculations for concrete structures, as well as for the determination of the delayed (time dependent) deformations of concrete.

The peak corresponds to the maximal value reached by the compression stress. In general, at this state, we observe the formation of macro-cracking parallel to the direction of compression. Experimentally, it is difficult to obtain the softening

response because redistribution inside the specimen occurs and the strain distribution is no longer homogenous over the specimen

The post-peak response of concrete is necessary, for example, in studies related to the durability of the material as transport properties are very sensitive to the cracking of the material. In the axial stress-strain curve, Stress is calculated from the force of the machine and strain is global, that is to say computed from the variation of distance between the supports of the specimen. This type of curve cannot be used for the absolute measurement of elastic parameters or behavior, but allows comparisons between the tests performed under the same conditions.

## 3.3 Behaviour of concrete under uniaxial tensile

Due to the experimental difficulty of carrying out direct traction tests, different tests are more commonly used, relying on the dissymmetry of the compressive and tensile strengths of the concretes. In some specific experimental situations, it is possible to obtain locally a tensile fracture of the specimen being loaded in compression. The most commonly used test is called the “Brazilian” or splitting test.

Another type of indirect traction test is the three-point bending test on a concrete specimen that may or may not be notched. The principle is to develop a moment within the beam, and therefore, to call upon the tensile lower fibers, the higher fibers being elastic due to dissymmetry behavior. The boundary conditions used are roll supports at the ends of the beam, to enable shrinkage during loading. The applied force and the deflection at the center of the beam are measured. It is possible to stick deformation gages on the beam in order to get local information, or cracking recording gages above the notch. The test control is achieved through an imposed displacement or an imposed force.

In this experimental test the tensile strain is not homogenous within the body of the specimen so the interpretation of the obtained results is sometimes difficult. For the

simplicity of the distribution of the normal stress within the median section of the beam, in the three-point bending test it is possible to determine the tensile response of the material using a reverse analysis. Moreover, a notch is generally placed in this median cross section in order to introduce a defect minimizing the resistant section, and therefore to enable better control of the cracking and collapse process. It is then possible to control the test as a function of the crack propagation, which allows the tensile softening response of concrete to be determined because loss of stability of the loading process is avoided. This test is most often used for the determination of rupture parameters. The three-point bending test requires some caution. Crushing of concrete at the supports often occurs.

The typical curve trend stress-strain for a concrete under a uniaxial tensile is shown in Figure

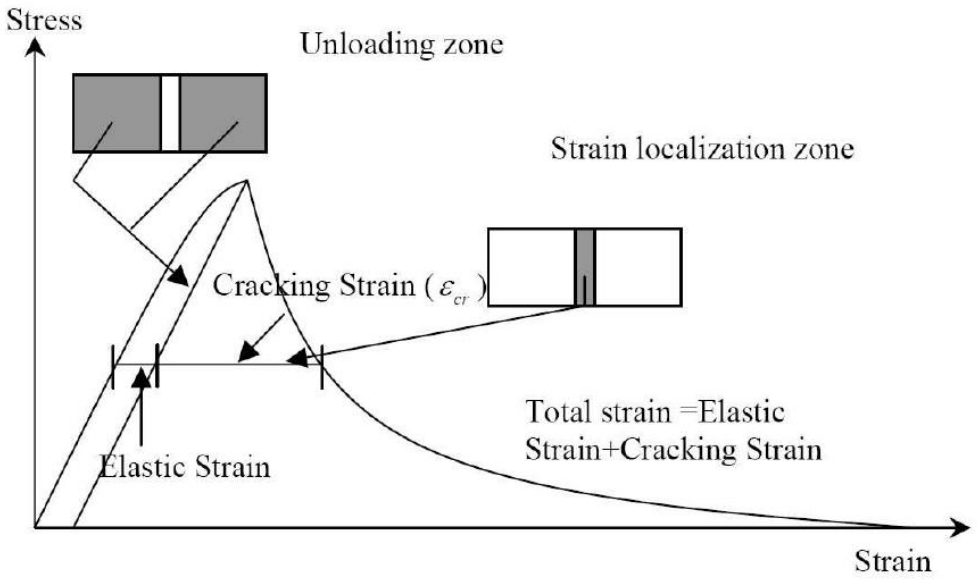


*Figure 3.5: Typical stress-strain curve for concrete under a uniaxial tensile*

Behavior of concrete is almost linear up to last strength. After the pick, there is the development of the crack, and the stress decreases while the stretch increases. This phenomenon is known like tensile strain softening. In this phase the deformation is not uniform in the specimen, but is localized in one area called “fracture zone”, while the remainder of the structure gets unloaded. The total deformation is

composed of two separate parts: the elastic strain of the compression concrete and the cracking strain.

It was demonstrated experimentally that the stress-strain reaction depends on specimen size, therefore it is better to describe the crack behavior with a relationship stress-opening of the crack as shown in Figure (3.6).

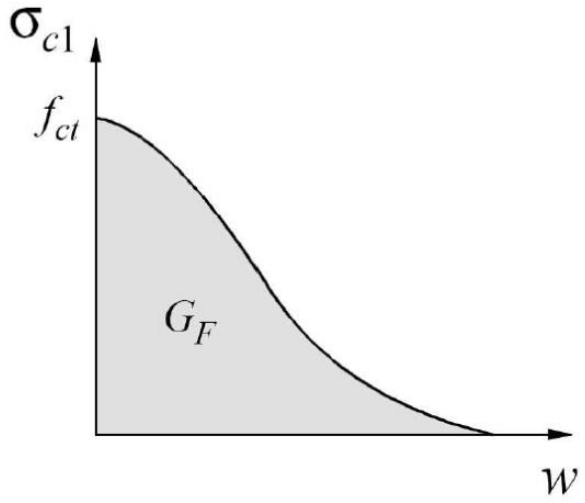


*Figure 3.6: Relationship stress-opening in the crack*

## 3.4 Size Effect of Structural Concrete

Traditional laboratory tests are aimed at the characterization of the mechanical response of materials, assuming of course that the constitutive relations deduced from the tests are not dependent on the type of test performed. Another important assumption is that the response of the material should be independent of the size of the structure, the considered structure being a laboratory specimen or a real-size structure. This is not always true, at least some deviations to this basic principle have been observed quite a number of times. This phenomenon is called *structural size effect* and it will be considerate in this thesis.

Structural size effect is defined here as the dependence of the mechanical response on the size of the structure. This is a well known phenomenon has demonstrated that geometrically similar concrete beams subjected to three-point bending exhibited a structural size effect. From experimental results, the material strength has been computed using standard elasticity and the results show that the larger the beam, the smaller the material strength (Figure 3.7).

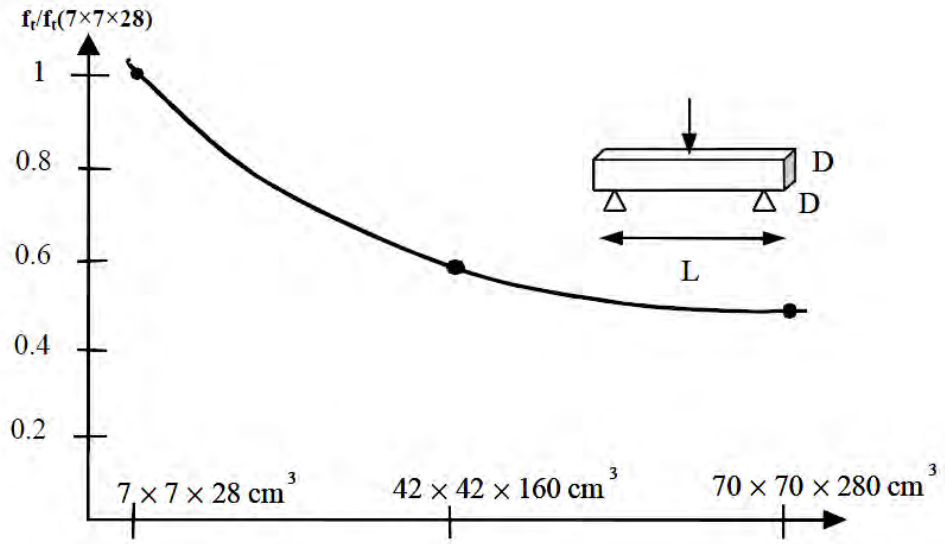


*Figure 3.7: Size effect observed on three-point bending beams. ft is the tensile strength computed on the bottom fiber according to elasticity at peak load*

Based on the results of Mariotte [MAR 86], Weibull [WEI 39] proposed a probabilistic theory constructed on the weakest link principle. The strength of a structure is the smallest strength of the elements from which the structure is assembled. As the probability of finding a weak element of any given strength decreases as the volume of the structure decreases, the apparent strength of a structure increases as its size decreases. This probabilistic model relies on a specific distribution of the local strength, more precisely on a specific description of the tail of this distribution.

In the weakest link theory, structures are considered to fail at crack initiation and the fracture process zone is considered to be very small – negligible compared to the size of the crack and to the size of the structure.

Inspired by several works dealing with the fractality of cracks devised a size effect law based on the geometry of the crack and fracture surface. The three principal theories are:

– the probabilistic theory due to Weibull;

– the deterministic theory due to Bazant ;

– the fractal size effect theory due to Carpenteri *et al*.

The foregoing probabilistic structural size effect law is based on the idea of random structural strength combined with Weibull distribution of probability of failure. A salient characteristic of this size effect law is that it does not contain an internal length because it is a power law. In a physical theory where the scaling law is expressed as a power law, there is no characteristic length. The structure size is compared to a reference, but the comparison is performed through a ratio and the actual size of the reference does not appear in the scaling law.

A second source of size effect, besides a random distribution of strength, is due to the redistribution of stresses ahead of the crack tip, in the fracture process zone. This size effect applies typically to quasi-brittle materials which possess a fracture process zone whose size may not be considered as negligible

# Chapter 4

# CONSTITUTIVE MODEL FOR CONCRETE

In the last three decades, the constitutive modelling of concrete evolved considerably. This chapter describes various developments in this field based on different approaches analyzing the plastic fracturing. It is the constitutive model that will be studied in this paper.

Concrete is a heterogeneous, cohesive-frictional material and exhibits complex non-linear inelastic behavior under multi-axial stress states. The increased use of concrete as primary structural material in building complex structures necessitates the development of sophisticated material models for accurate prediction of the material response to a variety of loading situations. The new developments regarding concrete technology which resulted in a new generation of concretes, which are better in terms of performance, such as high strength concrete (HSC), reactive powder concrete (RPC), high performance light weight concrete (HPLC) and self compacting concrete, further stressed the need for new material models.

Concrete structures are often analyzed by means of the finite element method. This kind of Analysis, for structural engineering problems is based on solution of a set of equilibrium equations and a kinematically admissible displacement field. Every problem is combined with boundary and initial conditions. The statically and kinematically admissible sets of equations are independent of each other, and the constitutive relations are required to connect them.

Concrete contains a large number of micro-cracks, especially at the interface between aggregates and mortar, even before the application of the external load.

Many theories proposed in the literature for the prediction of the concrete behavior are studied, such as empirical models, linear elastic, nonlinear elastic, plasticity based models, models based on endochronic theory of inelasticity, fracturing models and continuum damage mechanics models, micromechanics models.

In the following section these kinds of models will be briefly discussed.

## 4.1 Empirical models

Usually the material constitutive law is obtained through a series of experiments, where the experimental data is used to propose functions, which describe the material behavior, by curve fitting. Obtaining the experimental data is not always easy, especially in cases of multiaxial stress situations. The experimental information after peak is often insufficient due to difficulties associated with the testing techniques of materials. One reason for the scarcity of test data is scatter of the test data associated with machine precession, testing technique and statistical variation of material properties from sample to sample. Fortunately, in literature there were many attempts that overcame these difficulties for specific loading situations such as uniaxial, biaxial, triaxial and cyclic loading.

Many uniaxial and biaxial stress-strain relations are available in the literature. Typical uniaxial compressive and biaxial stress-strain curves are shown in Figure (4.1) and Figure (4.2) respectively.

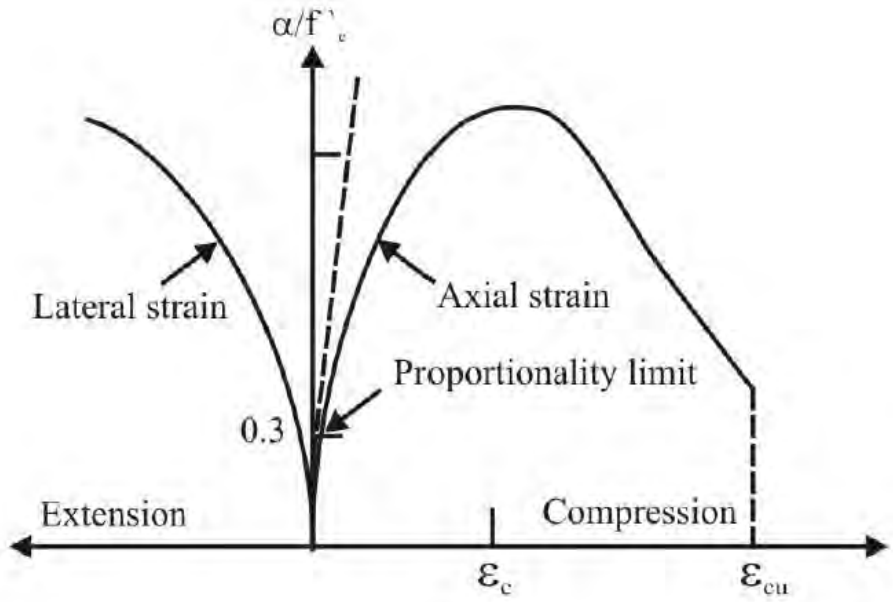


*Figure 4.1: Uniaxial stress-strain curve*

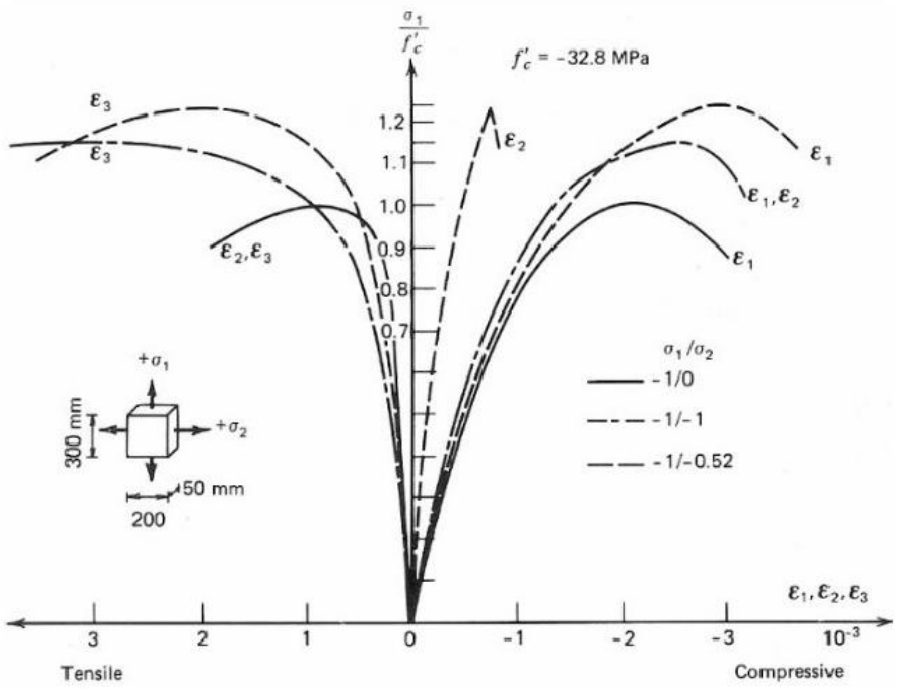


*Figure4.2: Biaxial stress-strain curve*

## 4.2 Linear elastic models

Linear elastic models are the simplest constitutive models available in the literature. In this model concrete is treated as linear elastic until it reaches ultimate strength and subsequently fails in brittle manner. For concrete under tension, the linear elastic model is quite accurate and sufficient to predict the behavior of concrete from the failure strength. Linear elastic stress-strain relation can be written using the general notation as:

$$\sigma_{ij} = F_{ij}\,(\varepsilon_{kl}) \tag{4.1}$$

$$\sigma_{ij} = C_{ijkl}\varepsilon_{kl} \tag{4.2}$$

where $F_{ij}$ is a function and $C_{ijkl}$ represents material stiffness.

A problem of this constitutive law is that it is often inappropriate, as concrete falls under the pressure sensitive group of materials whose general response under an imposed load is highly nonlinear and inelastic.

## 4.3 Non linear elastic models

Nonlinear constitutive models are used for concrete under multiaxial compressive stress, therefore where there is a significant nonlinearity. The two basic approaches used for nonlinear modeling are secant formulation (Total stress-strain) and tangential stress-strain (Incremental) formulation. Incremental stress-strain relation can be written in the following form:

$$d\sigma_{ij} = C^{t}_{ijkl}d\varepsilon_{kl} \tag{4.3}$$

Where $C^{t}_{ijkl}$ is the tangent material stiffness.

Secant formulations are reversible and applicable primarily to monotonic or proportional loading situations. These models are simple extensions of linear elastic models and formulated by assuming functional relations for secant bulk modulus, secant shear modulus and assuming stresses and strains are derived as gradients of stress and strain potentials. Inelastic deformations and cyclic loading can be resolved using incremental or hypoelastic models with variable tangent moduli.

For a complete description of the ultimate strength surface a suitable failure criterion is incorporated in the elasticity based models. Criteria such as yielding, load carrying capacity and initiation of cracking have been used to define failure. Failure can be defined as the ultimate load carrying capacity of concrete and represents the boundary of the work-hardening region. In the literature many failure criteria for normal, high strength, light weight and steel fiber concrete can be found. The most commonly used failure criteria are defined in stress space by a number of constants varying from one to five independent control parameters. In literature there are various criteria for concrete, the more familiar are Mohr-Coulomb criteria, Drucker-Prager, Chen and Chen, Ottosen, Hsieh-Ting-Chen, Willam and Warnke. A more sophisticated criterion was developed by Menetrey and Willam, which is also utilized in ATENA. This criterion predicts the behavior of concrete in a better manner and is expressed by the following expression.

$$F(\xi,\rho,\theta) = \left[\sqrt{15}\frac{\rho}{f_c'}\right] + m\left[\frac{\rho}{\sqrt{6}f_c'}r(\theta,e) + \frac{\xi}{\sqrt{3}f_c'}\right] - c = 0 \qquad (4.4)$$

where ξ = Hydrostatic stress invariant, ρ = Deviatoric stress invariant and θ = Deviatoric.

Polar angle and $r(\theta,e)$ is an elliptic function.

$$\xi = \frac{I_1}{\sqrt{3}}, \qquad I_1 = \sigma_{ii}$$

$$\rho = \sqrt{2J_2}, \qquad J_2 = \frac{1}{2}S_{ij}S_{ji}$$

$$cos3\theta = \frac{3\sqrt{3}J_3}{2J_2^{\frac{3}{2}}}, \qquad J_3 = \frac{1}{3}S_{ij}S_{jk}S_{ki}$$

## 4.4 Plasticity based models

In literature there are many Classical plasticity based models developed in the recent past. The mechanism of material non-linearity in concrete consists of both plastic slip and micro cracking. The models which characterize the stress-strain and failure behavior of material under multidimensional stress states can have advantages and disadvantages, which depend, to a large extent on their particular application.

In plasticity theory the total strain increment tensor is assumed to be the sum of the elastic and plastic strain increment tensors

$$d\sigma_{ij} = d\sigma_{ij}^{e} + d\sigma_{ij}^{p} \tag{4.5}$$

### 4.4.1 Yield criteria

Yield criteria of material should be known from experiments. The behavior of concrete is influenced by the effect of hydrostatic pressure. In the literature, it is possible to find the yield criterion with the hydrostatic pressure dependent or with hydrostatic pressure independent. Some failure models, developed specifically for concrete are also used as yield function by applying some corrections and by being integrated into the theory of plasticity to compute strains and stresses in the yielded materials.

Any yield surface needs to satisfy certain physical requirements such as condition of irreversibility of plastic deformation and positive work which is expended on plastic deformation in a cycle. Non-smooth yield surfaces are often included in the

constitutive description of a material, these (Tresca or Mohr-Coulomb) cause an indeterminate situation while determining the direction of the plastic strain increment.

The Drucker-Prager criterion represents moderately well the response of plain concrete subjected to multi-axial compression and provides a smooth yield surface (Figure 4.3). This criterion is incorporated into some currently proposed concrete material models and is defined in the Eq. (4.6).

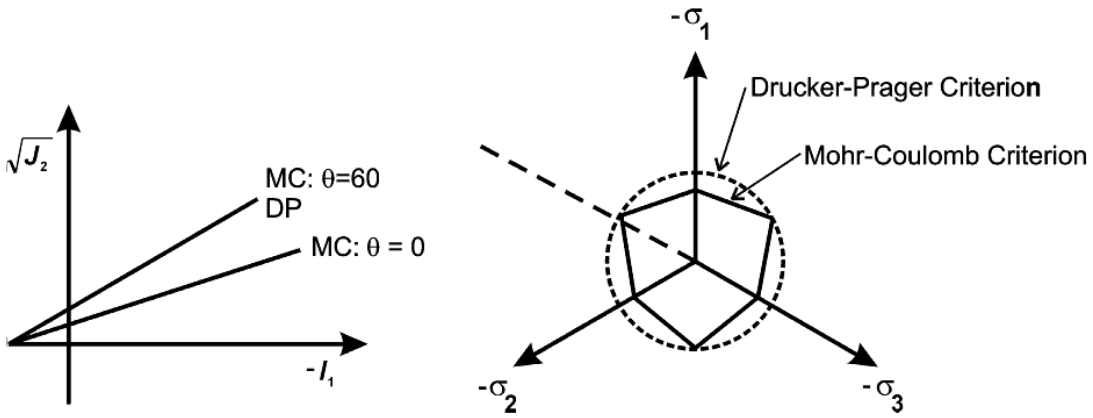


*Figure4.3: Mohr-Coulomb and Drucker-Prager Failure Criteria*

$$\sqrt{J_2} + \alpha I_1 + y = 0 \tag{4.3}$$

In Equation (4.6) $\alpha$ and $y$ are material parameters that, in the original formulation, are considered to be constant but vary with load history in more recent implementations.

### 4.4.2 Flow rules

Definition of a plasticity-based constitutive model requires establishing flow rules that define the evolution of a set of internal variables. Of particular interest is the plastic flow rule that defines the orientation of the plastic strain.

A stress increment $d\sigma$ to the current state of stress $\sigma$ results in elastic as well as plastic strain, if the stress state falls outside the elastic region. To describe the stress-strain relationship for an elastic-plastic deformation, we must define the flow rule which defines the direction of the plastic strain increment without any information regarding magnitude. Flow rule may or may not be associated with the yield criteria.

$$d\varepsilon_{ij}^{p} = d\lambda \frac{\partial Q}{\partial \sigma_{ij}} \tag{4.4}$$

where $d\lambda$ is a non-negative scalar; $Q$ is plastic potential function.

Experimental data, however, indicates that associated flow may not be the most appropriate assumption for characterizing the response of concrete. Some researchers have noted that concrete displays shear dilatancy characterized by volume change associated with shear distortion of the material. In order to improve modelling of concrete material response, non-associated flow models, in which the yield and plastic potential functions are not identical, in the form of equation 18, were used.

### 4.4.3 Hardening rules

The law, which governs the phenomenon of configuration change in yield surface, which occurs during loading process, is the hardening rule. One of the major problems of work/strain hardening plasticity is finding the evolution of the yield surface (Ohtami and Chen).

Several hardening rules have been proposed in the literature. Depending on the hardening rule used, the material response after initial yielding differs considerably. The hardening rules available in the literature are isotropic hardening, kinematic hardening, independent hardening and mixed hardening. In isotropic hardening, the basic assumption is uniform expansion of the yield surface. Yield surface does not undergo any distortion or translation. The concrete behavior under monotonic loading has been modeled by many, such as Imran et al, Smith et al. using isotropic hardening.

Prager proposed a model in connection with his kinematic model to predict the translation of the yield surface. The Kinematic model assumes that, during plastic loading, the yield surface translates as a rigid body in stress space without any expansion.

## 4.5 Strain softening and strain space plasticity

In the classical plasticity-based models, finding the yield surface poses many problems and an attempt was made to develop a continuous model for inelastic behavior which did not require the existence of the yield condition. This model is based on the concept of intrinsic (or endochronic) time, defined in terms of strain or stress and used to measure the degree of damage occurred to the internal structure of the material. This model was primarily developed for metals by Valanis. Sandler studied its stability and uniqueness and Rivlin critically evaluated the theory. The Endochronic model can describe inelastic volume dilatancy, unloading, strain softening, hydrostatic pressure sensitivity and pinching of hysteresis loops under cyclic loading. Even though this model gives superior results, its popularity is restricted by its complexity. The numerous numerical coefficients required for the development of a constitutive law are estimated by curve fitting of available experimental data. The main obstacle in the development and application of this method is the large number of parameters required.

A typical constitutive equation for linear endochronic theory with pseudo-time measure ξ is as follows in Eq. (4.5)

$$\sigma_{ij} = \int_0^{\xi} E_{ijkl}(\xi - \xi') \frac{\partial \varepsilon_{kl}}{\partial \varepsilon'} \tag{4.5}$$

## 4.6 Fracturing and continuum damage models

These models are based on the concept of propagation and coalescence of microcracks, which are present in the concrete even before the application of the load. Damage based models are often used to describe the mechanical behavior of concrete in tension. In the earlier class of models plastic deformation is defined by usual flow theory of plasticity and the stiffness degradation is modelled by fracturing theory. The second class of models is based on the use of a set of state variables quantifying the internal damage resulting from a certain loading history. The fundamental assumption in these models is that the local damage in the material can be averaged and represented in the form of damage variables, which are related to the tangential stiffness tensor of the material. The models of this category can describe progressive damage of concrete occurring at the microscopic level, through variables defined at the level of the macroscopic stress-strain relationship Krajcinovic and Fonseka.

Kratzig (1998) derived a strain based damage theory by assuming a Helmholtz free energy expression of the Eq. (4.6)

$$\Psi\left(\varepsilon_{ij}, C_{ijkl}, p\right) = \frac{1}{2\rho} \tag{4.6}$$

where ρ= Material density, $C_{jkii}$ is current stiffness tensor, and $\varepsilon_{ij}$ represents Strain tensor. $P$ represents an internal variable describing the radius of the limit state surface. Among the variety of theories that describe the behavior of concrete, CDM has the advantage to be founded on a rational frame work of the material theory,

therefore having a sound physical background. The CDM formulations are also finite element oriented.

## 4.7 Microplane models

Micromechanical models attempt to develop the macroscopic stress-strain relationship from the mechanics of the microstructure. The only popular model in this category, which reached up to implementation stage, is the microplane model proposed by Bazant and his associates.

Unlike the other constitutive models, which characterize the material behaviour in terms of second order tensors, the microplane model characterizes in terms of stress and strain vectors. The macroscopic strain and stress tensors are determined as a summation of all these vectors on planes of various orientations (Microplanes) under the assumption of static or kinematic constraint. The static constraint (the stress vector acting on a given plane is the projection of the macroscopic stress tensor) used in the earlier models, acts as an obstruction for the generalization of the microplane model for post peak strain softening quasi-brittle materials. The basic relations of the microplane model are briefly explained below. The normal strain on the microplane is in the Eq. (4.7)

$$\varepsilon_N = N_{ij}\varepsilon_{ij} \tag{4.7}$$

where $N_{ij} = n_i\, n_j$.

In conclusion the three major steps of the microplane model are projecting macro stress/strain tensor to microplane using static or kinematic constraint, defining a constitutive law at microplane level and getting the constitutive law at macro level by summing up all the stress/strain vectors on microplane. The main advantage of the microplane model is its conceptual clarity as the model is formulated in terms of vectors and the inherent nature of satisfying tensorial invariance requirements. The

microplane model treats apparent corners (Vertex) which appear in the conventional yield surface based material models. The disadvantage in the microplane model is the huge computational work and storage requirements.

# Chapter 5

# ATENA SOFTWARE: MATERIAL MODEL and NONLINEAL ANALYSIS

## 5.1 Introduction to FEM (Finite Element Method)

For structural design of concrete members, the non-linear finite element analysis has become an important tool. Over the last one or two decades numerical simulation of engineering materials has become a major research area. A successful numerical simulation demands choosing suitable elements, formulating proper material models and selecting proper solution methods.

The finite element method (FEM) or finite element analysis is a numerical technique for finding approximate solutions of partial differential equations as well as of integral equations. The solution approach is based either on eliminating the differential equation completely, or rendering the partial differential equations into an approximating system of ordinary differential equations, which are then numerically integrated using standard techniques.

The first challenge to solve this kind of problem, is to create an equation that approximates the equation to be studied, but the numerically stable do not accumulate and cause significant errors. The Finite Element Method is a good choice for solving partial differential equations over complex domains.

The basic concept of FEM modelling is the subdivision of the mathematical model into disjoint components of simple geometry. The response of each element is expressed in terms of a finite number of degrees of freedom characterized as the value of an unknown function, or functions or at set of nodal points. The response of

the mathematical model is then considered to be the discrete model obtained by connecting or assembling the collection of all elements.

## 5.2 Material model implemented in ATENA

The program system ATENA offers a variety of material models for different materials and purposes. For metal von Mises plastic model is available, for rock and solids Ducker-Prager plasticity can be used, while for steel, reinforcement multilinear uniaxial model is determined. Nevertheless, the most important material models in ATENA are the material models for concrete. These advanced models evaluate all the important aspect of real material behavior in tension and compression.

Three nonlinear material models for concrete are available in ATENA: SBETA model, Fracture-Plastic constitutive model, and Microplace material model. The following sections present the concrete material model used in this investigation for finite element analysis of the three-point bending and unconfined compression tests.

### 5.2.1 Sbeta model

SBETA is a damaged-based model in which a smeared approach is used to model both cracks and reinforcement. This model comprises non-linear compressive behavior that is capable of modeling hardening and softening. SBETA model also includes other effects of concrete behavior, like fracture of concrete in tension, based on the nonlinear fracture mechanics, biaxial strength failure criterion, reduction of compressive strength after cracking; and it can also find the tension stiffening effect, the reduction of the shear stiffness after cracking, and has two crack models: fixed crack direction and rotated crack direction.

Nonlinear elastic approach is used for the material matrix, where the elastic constants are derived from a stress-strain function which, in ATENA, is called the equivalent uniaxial law. This approach can also be considered as an isotropic damage model, where the damage modulus is represented from unloading modulus.

### 5.2.1.1 Stress-strain relations for concrete

Concrete shows a vast number of micro-cracks, especially, at the interface between aggregates and mortal, even before being loaded. The presence of these micro-cracks has an important effect on the mechanical behavior of concrete, because their propagation during loading contributes to the nonlinear behavior at low stress levels and causes volume expansion of the mortal. Between aggregates and mortal there is a different stiffness that can develop some micro-cracks during loading. One of the most important reasons for the low tensile strength of concrete is that the aggregate-mortal interface has a significantly lower tensile strength than mortal.

The response of a structure under load depends on the stress-strain relation of the constituent materials and the magnitude of stress.

### 5.2.1.2 Equivalent uniaxial law

The nonlinear behavior of concrete in the biaxial stress state is described by means of the so-called effective stress $б_c^{ef}$, and the equivalent uniaxial strain $\varepsilon^{eq}$. The effective stress is in most cases a principal stress.

The equivalent uniaxial strain is introduced in order to eliminate the Poisson's effect in the plane stress state.

$$\varepsilon^{eq} = \frac{б_{ci}}{E_{ci}} \tag{5.1}$$

The equivalent uni-axial strain can be considered as the strain, that would be produced by the stress $б_{ci}$ in a uniaxial test with modulus associated $E_{ci}$ with the direction *i*. Within this assumption, the nonlinearity representing damage is caused only by the governing stress $б_{ci}$.

The complete equivalent uniaxial stress-strain diagram for concrete is shown in Figure (5.1). The numbers of the diagram parts in Figure (5.1), (material state numbers) are used in the results of the analysis to indicate the state of damage of concrete.

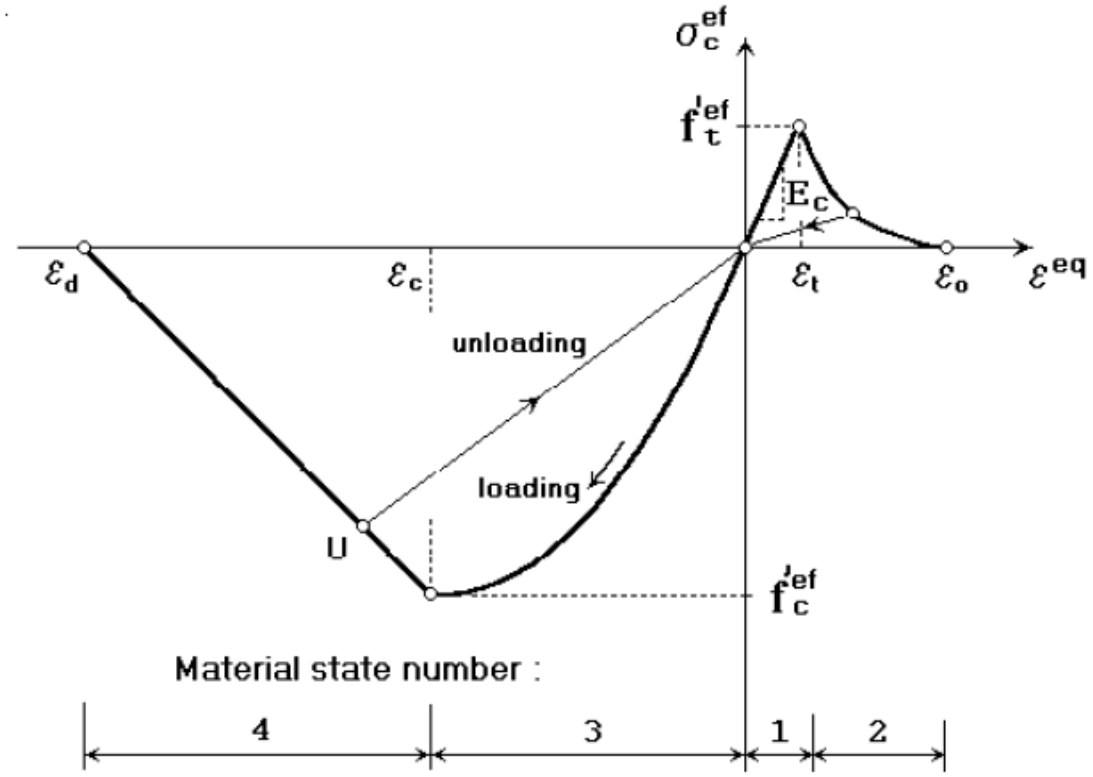


*Figure 5.1: Uniaxial stress-strain law for concrete*

Unloading is a linear function to the origin. An example of the unloading point *U* is shown in Figure (5.1). Thus, the relation between stress $б_c^{ef}$ and strain $\varepsilon_{eq}$ is not unique and depends on a load history. A change from loading to unloading occurs, when the increment of the effective strain changes the sign. If subsequent reloading

occurs, the linear unloading path is followed until the last loading point *U* is reached again. Then, the loading function is resumed.

The peak values of stress in compression $f'^{ef}_c$ and in tension $f'^{ef}_t$ are calculated according to the biaxial stress state. Thus, the equivalent uniaxial stress-strain law reflects the biaxial stress state. The above defined stress-strain relation is used to calculate the elastic modulus for the material stiffness matrices. The secant modulus is calculated as Eq. (5.2)

$$E_c^s = \frac{б_c}{\varepsilon^{eq}} \tag{5.2}$$

It is used in the constitutive equation to calculate stresses for the given strain state. The tangent modulus *Ec* is used in the material matrix $\mathbf{D}_c$ for construction of an element stiffness matrix for the iterative solution. The tangent modulus is the slope of the stress-strain curve at a given strain. It is always positive. In cases where the slope of the curve is less than the minimum value $E_{min}{}^t$ the value of the tangent modulus is set $E_c{}^t = \mathrm{E_{min}}^{\mathrm{t}}$. This occurs in the softening ranges and near the compressive peak.

### 5.2.1.3 Tension before Cracking

When the concrete is in tension without cracks, the behavior is assumed linear elastic. The elastic modulus of concrete is $\mathrm{E_c}$, and the effective tensile strength derived from the biaxial failure is $f'^{ef}_t$.

$$б_c^{ef} = E_c \varepsilon^{eq}, 0 \leq б_c \leq f'^{ef}_t \tag{5.3}$$

### 5.2.1.4 Tension after Cracking

Atena uses two types of formulation for the crack opening. The first one expresses that a fictitious crack model utilizes the crack-opening law and fracture energy. This formulation is suitable for modeling of crack propagation in concrete and it is used in combination with the crack band, the second one is a stress-strain relation in a material point. This formulation is not suitable for normal cases of crack propagation in concrete and should be used only in some special cases. In the following subsections five softening models included in SBETA material Model are described. The first is shown in fig (5.2) and is the Exponential Crack Opening Law.

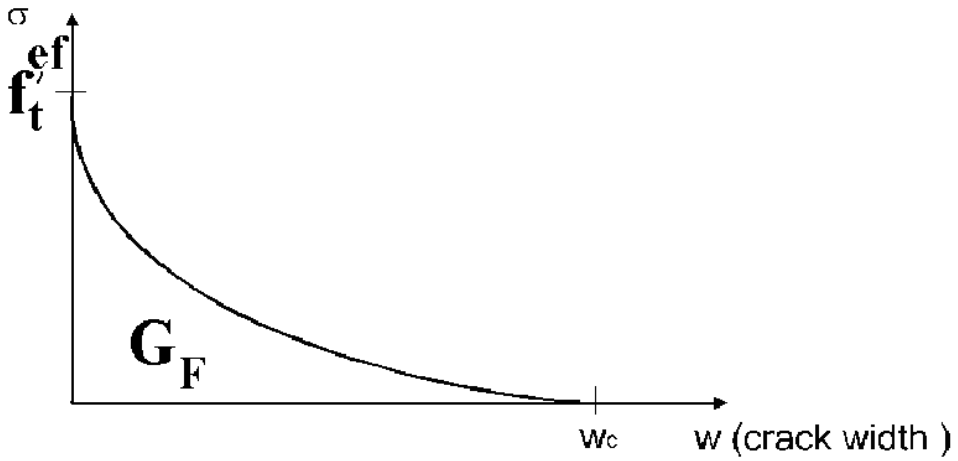


*Figure 5.2:Exponential Crack Opening Law*

$G_f$ is the fracture energy needed to create a unit area of stress-free crack. This Model uses the effective tensile strength derived from a failure function. The crack opening displacement *w* is derived from strains according to the crack band theory.

The second one is the Linear Crack Opening Law shown in fig (5.3).

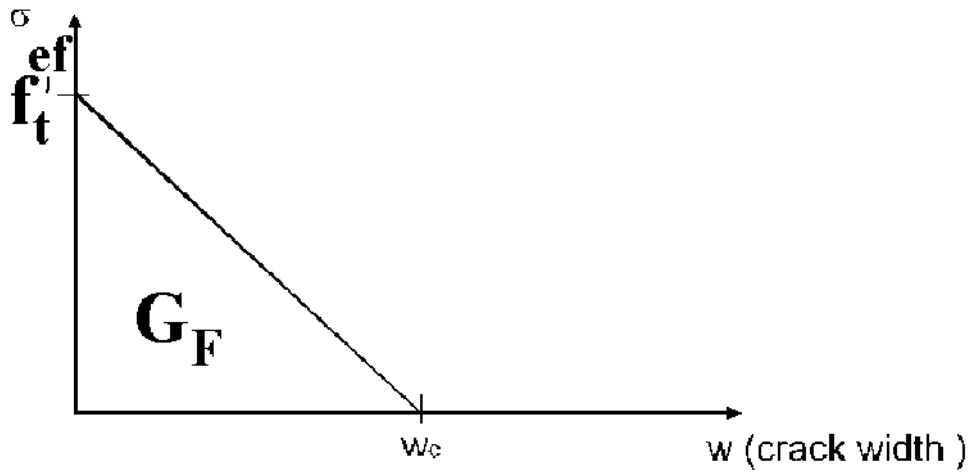


*Figure 5.3:Linear Crack Opening Law*

The last one used is Linear Softening Based on Local Strain shown in fig (5.4)

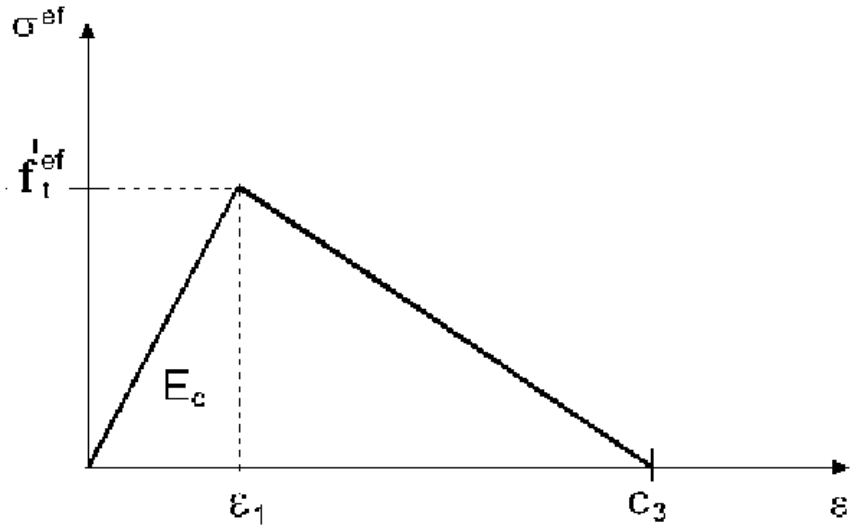


*Figure 5.4: Linear Softening Based on Local Strain*

### 5.2.1.5 Compression before Peak Stress

For the ascending branch of the concrete stress-strain law, ATENA used the formula recommended by CEB-FIP model Code 90, Figure(5.5). This formula allows curve

forms from linear to curved, and is appropriate for normal as well as high strength concrete.

$$\sigma_c^{ef} = f'^{ef}_c \frac{kx - x^2}{1 + (k-2)x}, x = \frac{\varepsilon}{\varepsilon_c}, k = \frac{E_o}{E_c} \tag{5.4}$$

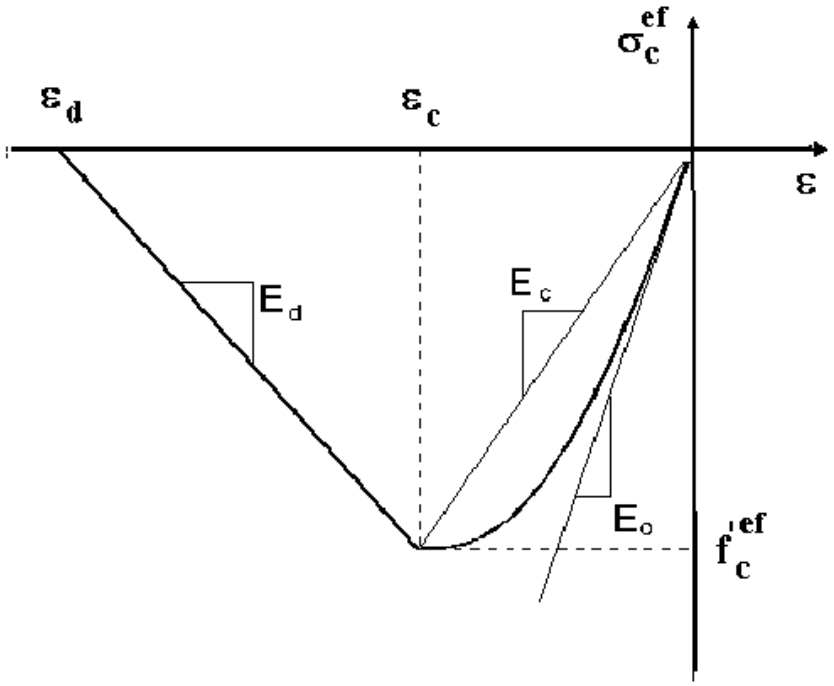


*Figure 5.5: Compressive stress-strain diagram.*

Meaning of the symbols in the Eq. (5.4) are:

- $\sigma_c^{ef}$ concrete compressive stress,
- $f'^{ef}_c$ concrete effective compressive strength
- $x$ normalized strain,
- $\varepsilon$ strain
- $\varepsilon_c$ strain at the peak stress $f'^{ef}_c$
- $k$ shape parameter,
- $E_o$- initial elastic modulus
- $E_c$ - secant elastic modulus at the peak stress.

In this case distributed damage is considered before the peak stress. Contrary to the localized damage, which is considered after the peak.

### 5.2.1.6 Compression after Peak Stress

The softening law in compression is linearly descending. The model of strain softening in compression is founded on dissipated energy. This model is based on the assumption, that compression failure is localized in a plane normal to the direction of compressive principal stress. In this plane all post-peak compressive displacements and energy dissipation are localized. This model assumes that the displacement is independent on the size of the structure.

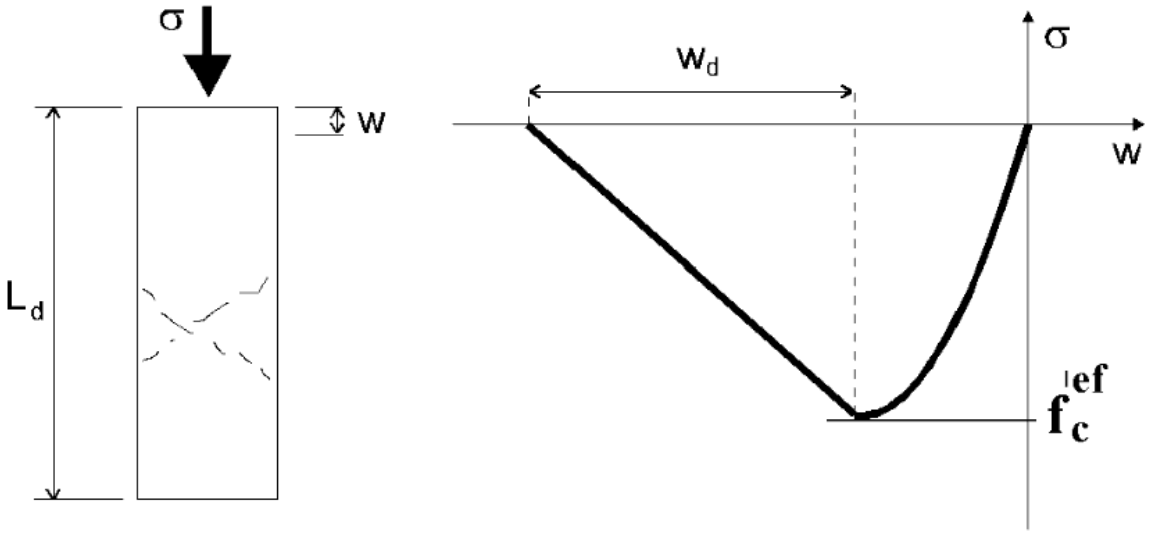


*Figure 5.6: Softening displacement law in compression*

When there is compression, the plastic displacement $w_d$ characterizes the end point of the softening curve, thus is defined the energy for generation of a unit area of the failure plane. For normal concrete the value of $w_d$ is around 0.5mm and it is used as a default for the definition of the softening in compression. In this case, for the

corresponding volume of continuous material the softening law is transformed from a fictitious failure plane, Figure (5.6), to the stress-strain relation.(fig). In the stress-strain diagram two points define the slope of the softening part: a peak of the diagram at the maximal stress and a limit compressive strain $\varepsilon_d$ at the zero stress. To calculate this strain the Eq. (5.5) is used, where $w_d$ is a plastic displacement, and $L'_d$ is a band size.

$$\varepsilon_d = \varepsilon_c + \frac{w_d}{L'_d} \tag{5.5}$$

The advantage of this formulation is reduced dependency on finite element mesh.

### 5.2.2 Fracture–Plastic Constitutive Model -CC3DNonLinCementitious

The Fracture-plastic model implemented in ATENA software and used in this thesis is a three dimensional model that combines constitutive models for tensile (fracturing) and compressive plastic) behavior. The fracture model is based on the classical orthotropic smeared crack formulation and crack band model. It employs Rankine failure criterion, exponential softening, and it can be used as rotated or fixed crack model. The hardening/softening plasticity model is based on Menétrey-Willam failure surface. Return mapping algorithm is used for the integration of constitutive equations. The algorithm for the combination of the two models is based on a recursive substitution. The two models have to be developed and formulated separately. The model can be used to simulate concrete cracking, crushing under high confinement, and crack closure due to crushing in other material directions. The material model formulation is based on the strain decomposition into elastic $\varepsilon^e_{ij}$, plastic $\varepsilon^p_{ij}$, and fracturing $\varepsilon^f_{ij}$ components.

$$\varepsilon_{ij} = \varepsilon^e_{ij} + \varepsilon^p_{ij} + \varepsilon^f_{ij} \tag{5.6}$$

The stress state is then computed by the formula:

$$\sigma_{ij}^{n} = \sigma_{ij}^{n-1} + E_{ijkl}\left(\Delta\varepsilon_{kl} - \Delta\varepsilon_{kl}^{p} - \Delta\varepsilon_{kl}^{f}\right) \tag{5.7}$$

where the increments of plastic strain $\Delta\varepsilon^{p}_{kl}$ and fracturing strain $\Delta\varepsilon^{f}_{kl}$ must be evaluated based on the used material models.

### 5.2.2.1 Rankine-Fracturing Model for Concrete Cracking

For concrete cracking the software use the Rankine criterion:

$$F_{i}^{f} = \sigma_{ii}^{\prime t} - f_{ti}^{\prime} \leq 0 \tag{5.8}$$

In this case strains and stresses are converted into the material directions, therefore when the rotated crack model is adopted, it corresponds to the principal directions, and when the fixed crack model is used, it corresponds to the principal directions at the onset of cracking. In the preceding formulation $f_{ti}^{'}$ identifies the tensile strain in the direction *i* and $\sigma_{ii}^{'t}$ is the trial stress that is computed by elastic predictor.

$$\sigma_{ii}^{\prime t} = \sigma_{ii}^{\prime n-1} + E_{ijkl}\Delta\varepsilon_{kl}^{\prime} \tag{5.8}$$

When the trial stress does not satisfy, the increment of fracturing strain in direction *i* can be computed using the assumption that the final stress state must satisfy.

$$F_{i}^{f} = \sigma_{ii}^{\prime n} - f_{ti}^{\prime} = \sigma_{ii}^{\prime t} - E_{ijkl}\Delta\varepsilon_{kl}^{\prime f} - f_{ti}^{\prime} = 0 \tag{5.9}$$

If we assume that the increment of fracturing strain is normal to the failure surface, and that always only the failure surface is being checked, the last equation can be simplified, and after substitution, a formula for the increment of the fracturing multiplier $\lambda$ has the following form.

$$\Delta\lambda = \frac{\sigma_{ii}'^{t} - f_t'(w_k^{max})}{E_{kkkk}} \tag{5.10}$$

Where $w_k^{max}$ is

$$w_k^{max} = L_t\left(\acute{\varepsilon}_{kk}'^{f} + \Delta\lambda\right) \tag{5.11}$$

This equation (5.11) must be solved by iterations considering that for softening materials the value of current tensile strength $f_t'(w_k^{max})$ is a function of the crack opening *w,* where it is computed from the total value of fracturing strain $\varepsilon_{kk}'^{f}$ in direction *k,* plus the current increment of fracturing strain $\Delta\lambda$, and this sum is multiplied by the characteristic length $L_t$. The characteristic length as a crack band size is calculated as a size of the element projected into the crack direction, Figure (5.7). This approach is satisfactory for low order linear elements.

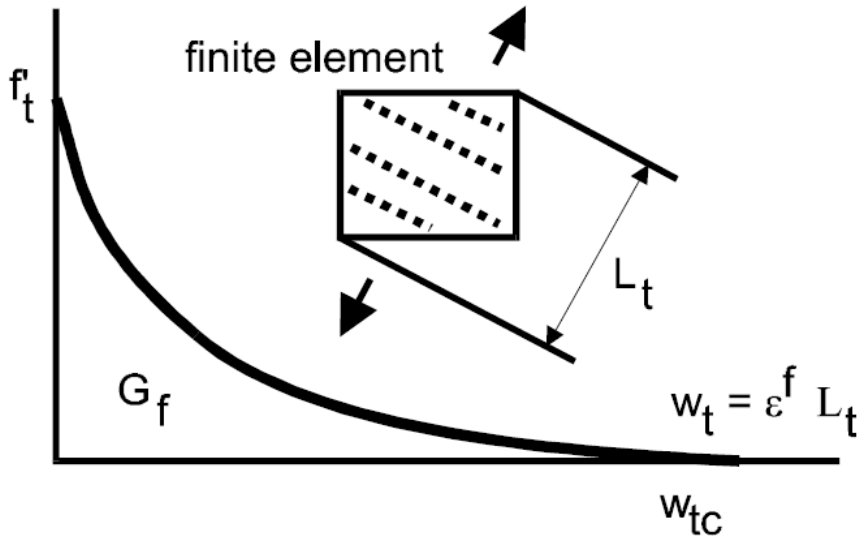


*Figure 5.7:Tensile softening and characteristic length*

The tensile strength $f_t'(w_k^{max})$ can be expanded into a Taylor series that this iteration scheme converges as long as:

$$\left|\frac{\partial f_t'(w_k^{max})}{\partial w}\right| < \frac{E_{kkkk}}{L_t} \tag{5.12}$$

When snap back is observed in the stress-strain relationship, the equation (5.12) is violated for softening materials. This event can happen when large finite elements are used. The snap back on the constitutive level cannot be captured in the standard displacement based finite element method. This means that the critical region, with snap back on the softening curve, will be skipped in a real calculation, which physically means, that the energy dissipated by the system will be over estimated. This is of course undesirable, and finite elements small should be used.

The total fracturing strain $\acute{\varepsilon}_{ij}^{\prime f}$, which corresponds to the maximal fracturing strain reached during the loading process is different than the current fracturing strain $\varepsilon_{ij}^{\prime f}$, which can be smaller due to crack closure.

Shear strength of a cracked concrete is calculated using the Modified Compression Field Theory of VECHIO and COLLINS (1986).

$$\sigma_{ij} \leq \frac{0.18\sqrt{f_c'}}{0.31 + \frac{24w}{a_g + 16}} \tag{5.13}$$

Where $f_c'$ is the compressive strength in MPa, $a_g$ is the maximum aggregate size in mm and *w* is the maximum crack width in mm at the given location. This model is activated by specifying the maximum aggregate size $a_g$ otherwise the default behavior is used where the shear stress on a crack surface cannot exceed the tensile strength.

#### 5.2.2.2 Plasticity Model for Concrete Crushing

In the plastic model the stress state is computed using the predictor-corrector formula.

$$\sigma_{ij} = \sigma_{ij}^{t} - \sigma_{ij}^{p} \tag{5.14}$$

Where the plastic corrector $\sigma_{ij}^{p}$ is computed directly from the yield function by the return mapping algorithm.

$$F^{p}\left(\sigma_{ij}^{t} - \sigma_{ij}^{p}\right) = F^{p}\left(\sigma_{ij}^{t} - \Delta\lambda l_{ij}\right) = 0 \tag{5.15}$$

In the preceding formulation the difficult aspect is the definition of the return direction $l_{ij}$. The failure surface used in the current version is from Menétrey-Willam.

$$F_{3p}^{p} = \left[\sqrt{15}\frac{\rho}{f_c'}\right] + m\left[\frac{\rho}{\sqrt{6}f_c'}r(\theta, e) + \frac{\xi}{\sqrt{3}f_c'}\right] - c = 0 \tag{5.16}$$

Where

$$m = 3\frac{f'^{2}_{c} - f'^{2}_{t}}{f'_{c}f'_{t}}\frac{e}{e+1} \tag{5.17}$$

And

$$r(\theta, e) = \frac{4(1-e^2)\cos^2\theta + (2e-1)^2}{2(1-e^2)\cos\theta + (2e-1)[4(1-e^2)\cos^2\theta + 5e^2 - 4e]^{\frac{1}{2}}} \tag{5.18}$$

In the equations (5.16) $f'_c$ and $f'_t$ is compressive strength and tensile strength respectively and (ξ,ρ,θ) are Heigh-Vestergaard coordinates. Parameter *e* defines the

roundness of the failure surface. Its value is from 0.5 in cases where the failure surface has sharp corners, from 1 if it's fully circular around the hydrostatic axis.

Depending on the value of strain hardening/softening parameter, the position of failure surface can move. The strain hardening is based on the equivalent plastic strain, which is calculated according to the following formula

$$\Delta\varepsilon_{eq}^{p} = min\left(\Delta\varepsilon_{ij}^{p}\right) \tag{5.19}$$

In this surface the hardening/softening is controlled by the parameter *c,* which evolves during the the yielding/crushing process by the following relationship:

$$c = \left(\frac{f'_c\left(\varepsilon_{ij}^{p}\right)}{f'_c}\right) \tag{5.20}$$

The $f'_c\left(\varepsilon_{ij}^{p}\right)$ represents the hardening/softening law which is based on the uniaxial compressive test. The law is shown in Figure 5.8, where the softening curve is linear and the elliptical ascending part is given by the following formula:

$$\sigma = f_{co} + (f_c - f_{co})\sqrt{1 - \left(\frac{\varepsilon_c - \varepsilon_{eq}^{p}}{\varepsilon_c}\right)^2} \tag{5.21}$$

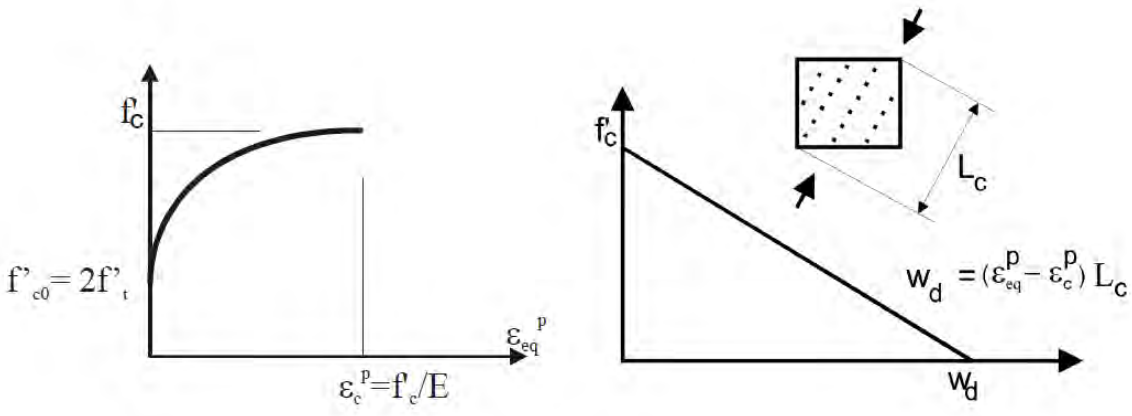


*Figure 5.8:Compressive hardening/softening and compressive characteristic length. Based on experimental observations by VAN MIER*

The law on the ascending and descending branch is based on strain and displacements

respectively, where the mesh has objectivity into the finite element solution. The shape is based on the work of VAN MIER. The value of $f'_{co}$ is a input parameter in the beginning of nonlinear behavior as well as the value of plastic strain at compressive strength $\varepsilon_c^p$. The parameter $f'_{co}$ should be selected prudently because it is important to ensure that the fracture and plastic surfaces intersect each other in all material stages. On the descending curve, the length scale parameter $L_c$ transforms the equivalent plastic strain into displacements. This parameter is defined through the crak band parameter in the fracture model, and it corresponds to the projection of element size into the direction of minimal principal stresses.

In the constitutive model, the plastic potential is given by the following formula:

$$G^P(\sigma_{ij}) = \beta \frac{1}{\sqrt{3}} I_1 + \sqrt{2J_2} \tag{5.22}$$

The parameter $\beta$ is needed to determine the return direction. When $\beta < 0$ it means that the material is being compacted during crushing, when $\beta > 0$ the material is dilating instead. If $\beta = 0$ the material volume is preserved. Considering that the plastic flow is not perpendicular to the failure surface, usually the plastic model is non-associated.

Figure 5.9 shows the predictor-corrector approach used in the return mapping algorithm for the plastic model. To simulate hardening and softening behavior, the failure surface moves along the hydrostatic axis during the corrector phase of the algorithm. At the origin of the Haigh-Vestergaard coordinate system there is an apex of final failure surface. The Secant method is used to determine the stress on the surface, which satisfies the yield condition and also the hardening/softening law.

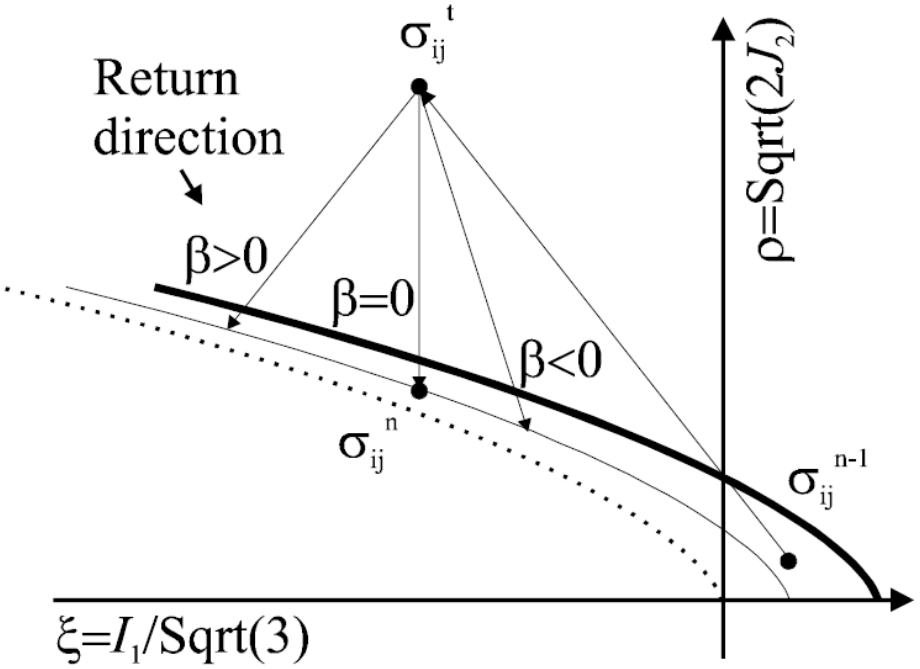


:

*Figure 5.9: Plastic predictor-corrector algorithm.*

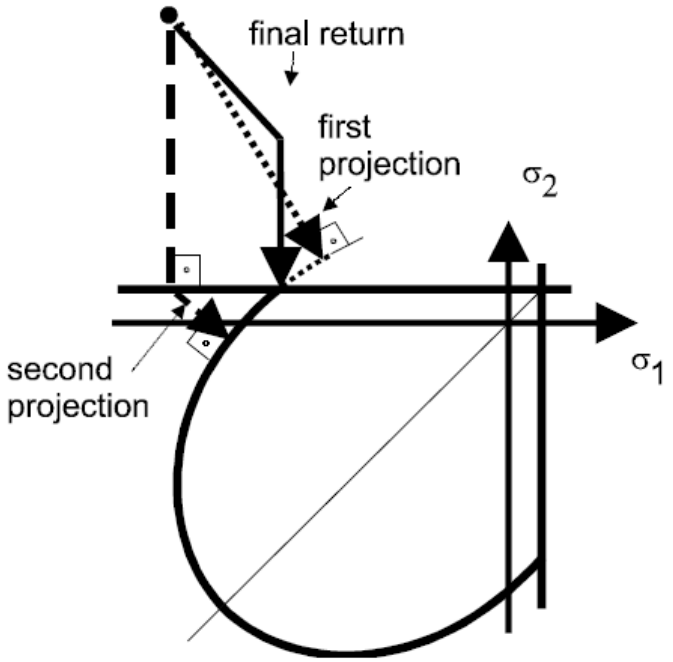


*Figure 5.10: Schematic description of the iterative process. For clarity shown in two dimensions*

#### 5.2.2.3 Combination of Plasticity and Fracture model

The two preceding models are combined into a single model such that plasticity is used for concrete crushing and the Rankine fracture model for cracking. This model is declared as a simultaneous solution of the two following inequalities.

$$F^p\left(\sigma_{ij}^{n-1} + E_{ijkl}\left(\Delta\varepsilon_{kl} - \Delta\varepsilon_{kl}^f - \Delta\varepsilon_{kl}^p\right)\right) \leq 0 \tag{5.23}$$

$$F^f\left(\sigma_{ij}^{n-1} + E_{ijkl}\left(\Delta\varepsilon_{kl} - \Delta\varepsilon_{kl}^p - \Delta\varepsilon_{kl}^f\right)\right) \leq 0 \tag{5.24}$$

The first inequality is used to define the increase of plastic deformation $\Delta\varepsilon_{kl}^p$, while the second is used to define the increase of deformation of cracking $\Delta\varepsilon_{kl}^f$.

Figure 5.10 shows the algorithm for the combination of plastic and fracture models. When both surfaces are activated, the behavior is quite similar to the multi-surface plasticity (SIMO et al. 1988).

Contrary to the multi-surface plasticity algorithm covers all loading regimes regimes including physical changes such as for instance crack closure. At present, it is developed for only two interacting models, and its extension to multiple models is not straightforward.

To describe the behavior of a concrete material correctly, it is necessary to consider two additional interactions between the two models. The first one is that after concrete crushing the tensile strength should decrease as well, and the second one is that compressive strength should also decrease when cracking occurs in the perpendicular direction (VECHIO and COLLINS 1986). The name of this theory is compression field and it is used to explain the shear failure of concrete beams and walls.

The first interaction is resolved by adding the equivalent plastic strain to the maximal fracturing strain in the fracture model to automatically increase the tensile damage based on the compressive damage. The fracturing strains have to satisfy the following condition

$$\varepsilon'^{f}_{kk} \geq \frac{f'_t}{f'_c}\varepsilon^{p}_{eq} \tag{5.25}$$

Collins proposed the formula (5.26) for the compressive strength reduction

$$\sigma_c = r_c f'_c \tag{5.26}$$

Where

$$r_c = \frac{1}{0.8 + 170\varepsilon_1},\ r_c^{lim} \leq r_c \leq 1.0 \tag{5.27}$$

Where $\varepsilon_1$ is the tensile strain in the crack.

### 5.2.3 Variants of the Fracture Plastic Model

In ATENA there are some variants of the fracture plastic model with the following differences: *CC3DCementitious* assumes linear response up to the point when the failure envelope is reached, both in tension and compression. In this case there is no hardening regime in Figure 5.8. Contrary to it, the material *CC3DNonLinCementitious* assumes a hardening regime before the compressive strength is reached. It uses a total formulation for the fracturing part of the model. A material equivalent to *CC3DNonLinCementitious,* where the incremental formulation is used, is *CC3DNonLinCementitious2*. This material can be used in creep calculations or when it is necessary to change material properties during the analysis. The material that allows definition of history evolution laws is *CC3DNonLinCementitious2Variable.*

The material *CC3DNonLinCementitious2User* allows for user defined laws for selected material laws such as: diagrams for tensile and softening behavior, shear retention factor and the effect of lateral compression on tensile strength.

Similarly to the SBETA material, the Cementitious material family offers the choice of fixed and rotated crack models. The fixed crack material parameter determines at which maximum residual tensile stress level the crack direction gets fixed. In other words, 0.0 means fully rotated crack model (as 0 in SBETA), 1.0 means fixed crack model (as 1 in SBETA), values between 0.0 and 1.0 determine the crack direction locking level, e.g., 0.7 fixes the crack direction as soon it opens so far that the softening law drops to 0.7 times the initial tensile strength.

### 5.2.4 Modelling of cracks in concrete

Figure 5.11 shows the process of crack formation can be divided into three stages. The uncracked stage is before a tensile strength is reached. The crack formation takes place in the process zone of a potential crack with decreasing tensile stress on a crack face due to a bridging effect. Finally, after a complete release of the stress, the crack opening continues without the stress.

The crack width *w* is calculated as a total crack opening displacement within the crack band.

$$w = \varepsilon_{cr} L_t' \tag{5.28}$$

where $\varepsilon_{cr}$ is the crack opening strain, which is equal to the strain normal to the crack direction in the cracked state after the complete stress release.

The tension failure of concrete is characterized by a gradual growth of cracks, which join together and eventually disconnect larger parts of the structure. It is usually assumed that cracking formation is a brittle process and that the strength in tension loading direction abruptly goes to zero after such cracks have formed

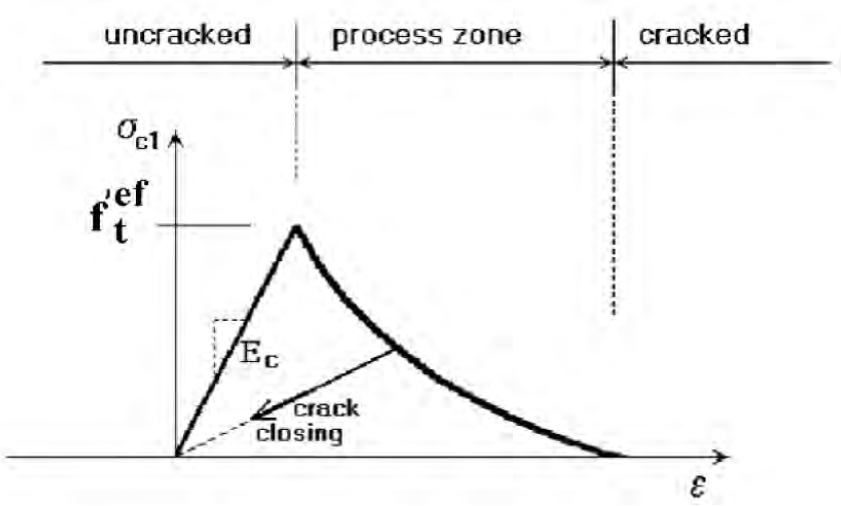


*Figure 5.11:Stages of crack opening*

Therefore, the formation of cracks is undoubtedly one of the most important non-linear phenomenons, which governs the behavior of the concrete structures. In the finite element analysis of concrete structures, two principally different approaches have been employed for crack modelling. These are discrete crack modeling and smeared crack modeling.

The discrete approach is physically attractive but this approach suffers from a few drawbacks, such as**,** employing a continuous change in nodal connectivity, which does not fit in the nature of finite element displacement method; the crack is considered to follow a predefined path along the element edges and excessive computational efforts are required. The second approach is the smeared crack approach. In this approach the cracks are assumed to be smeared out in a continuous fashion.

Within the smeared concept two options are available for crack models: the fixed crack model and the rotated crack model. In both models the crack is formed when the principal stress exceeds the tensile strength. It is assumed that the cracks are uniformly distributed within the material volume. This is reflected in the constitutive model by an introduction of orthotropy.

### 5.2.5 Fixed Crack Model

In the fixed crack model (CERVENKA 1985, DARWIN 1974) the crack direction is given by the principal stress direction at the moment of the crack initiation. During further loading this direction is fixed and represents the material axis of the orthotropy. After cracking the orthotropy is introduced, but in the uncracked concrete the principal stress and strain directions coincide for the isotropy assumption in the concrete component. The weak material axis *m1* is normal to the crack direction, the strong axis *m2* is parallel with the cracks.

Figure 5.12 shows a shear stress on the crack face because the principal strain axes $\varepsilon_1$ and $\varepsilon_2$ rotate and need not to coincide with the axes of the orthotropy $m_1$ and $m_2$. The stress components $\sigma_{c1}$ and $\sigma_{c2}$ denote, respectively, the normal stresses and parallel to the crack plane and, due to shear stress, they are not the principal stresses.

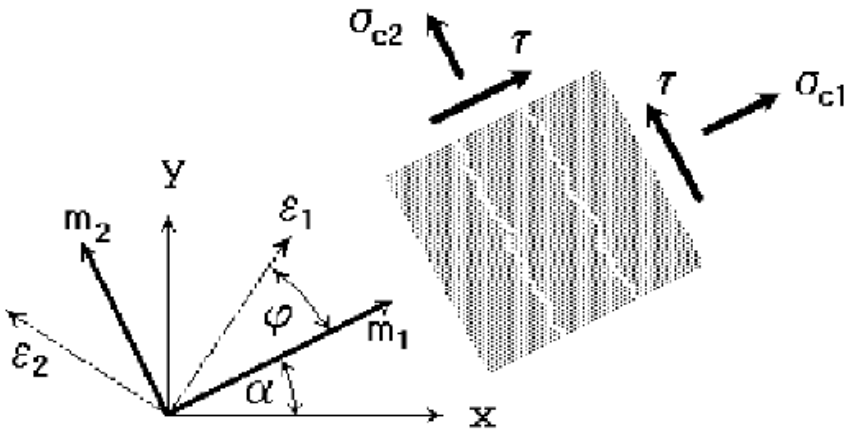


*Figure 5.12: Fixed crack model. Stress and strain state*

### 5.2.6 Rotated Crack Model

In the rotated crack model the direction of the principal stress coincides with the direction of the principal strain. Thus, no shear strain occurs on the crack plane and only two normal stress components must be defined, as shown in Figure 5.13.

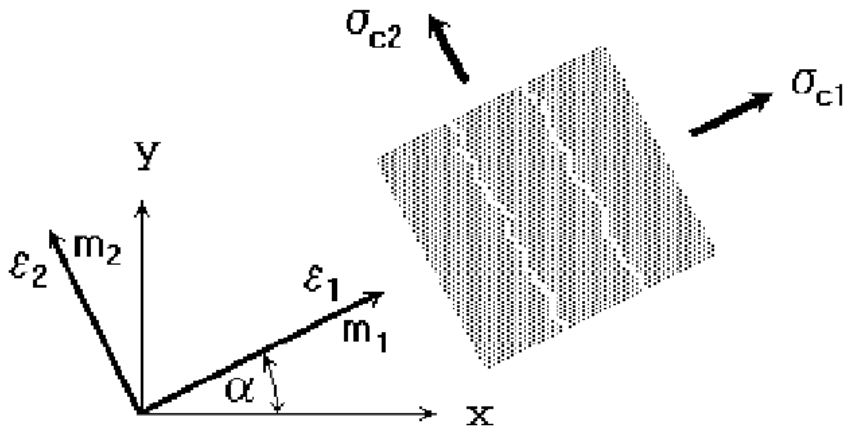


*Figure 5.13: Rotated crack model. Stress and strain state*

If the principal strain axes rotate during the loading the direction of the cracks rotate, too. In order to ensure the co-axiality of the principal strain axes with the material axes the tangent shear modulus *Gt* is calculated according to CRISFIELD 1989 as

$$G_t = \frac{\sigma_{c1} - \sigma_{c2}}{2(\varepsilon_1 - \varepsilon_2)} \tag{5.29}$$

### 5.2.7 Interface material model

To create the finite element model it was necessary to use the interface material model between specimen and frame, in fact the interface material model can be used to simulate contact between two materials. The interface material is based on Mohr-

Coulomb criterion with tension cut off. The constitutive relation for a general three-dimensional case is given in terms of tractions on interface planes and relative sliding and opening displacements

$$\begin{Bmatrix}\tau_1\\ \tau_2\\ \sigma\end{Bmatrix} = \begin{bmatrix}K_{tt} & 0 & 0\\ 0 & K_{tt} & 0\\ 0 & 0 & K_{nn}\end{bmatrix}\begin{Bmatrix}\Delta v_1\\ \Delta v_2\\ \Delta u\end{Bmatrix} \tag{5.30}$$

The initial failure surface corresponds to Mohr-Coulomb condition (5.31) with ellipsoid in tension regime. After stresses violate this condition, this surface collapses to a residual surface which corresponds to dry friction.

$$|\tau| \le c - \sigma \cdot \phi, \sigma \le 0 \tag{5.31}$$

$$\tau = \tau_0\sqrt{\frac{(\sigma-\sigma_c)^2}{(f_t-\sigma_c)^2}}, \qquad \tau_0 = \frac{c}{\sqrt{1-\frac{\sigma_c^2}{(f_t-\sigma_c)^2}}}, \quad \sigma_c = -\frac{f_t^2}{c-2f_t\phi}, \ 0<\sigma<f_t$$

$$\tau = 0, \qquad \sigma > f_t \tag{5.32}$$

In tension the failure criterion is replaced by an ellipsoid, which intersect the normal stress axis at the value of *t f* with the vertical tangent and the shear axis is intersected at the value of c (i.e. cohesion) with the tangent equivalent to –ϕ. The parameters for the interface model cannot be defined arbitrarily; there is certain dependence of some parameters on the others. When defining the interface parameters, the following rules should be observed

$$f_t < \frac{c}{\phi}, \qquad f_t < c \tag{5.33}$$

$$c > 0, \qquad f_t > 0, \qquad \phi > 0 \tag{5.34}$$

It is recommended that parameters $f_t, c$ and $\phi$ are always greater than zero. In cases when no cohesion or no tensile strength is required, some very small values should be prescribed.

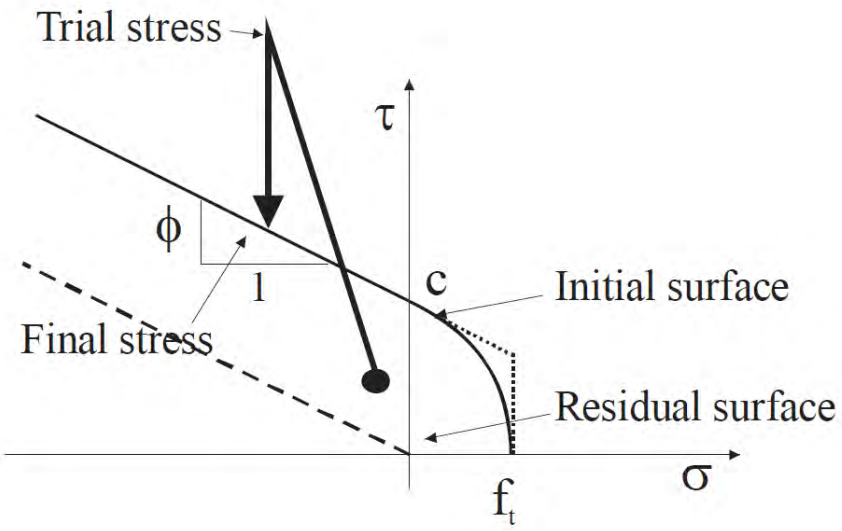


*Figure 5.14:Failure surface for interface elements*

For the three-dimensional case $\tau$ in Fig. 5.15 and equation (5.35) is calculated as:

$$\tau = \sqrt{\tau_1 + \tau_2} \tag{5.35}$$

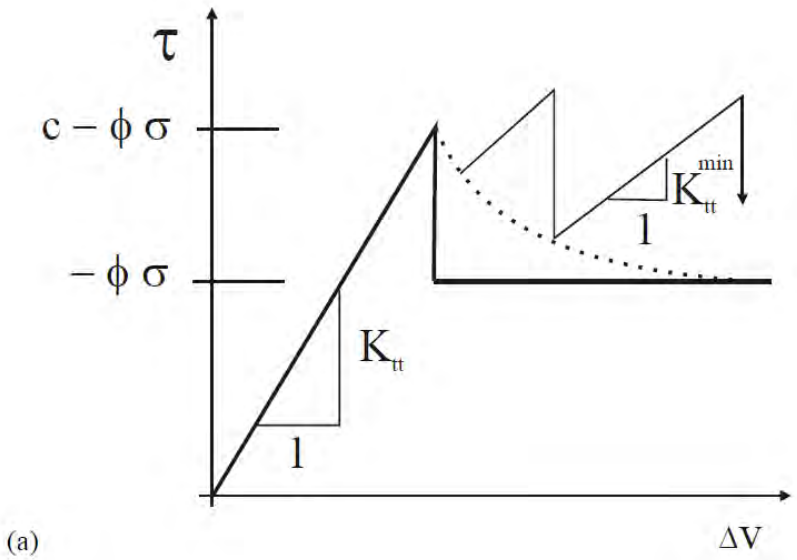


*Figure 5.15: Typical interface model behavior in shear*

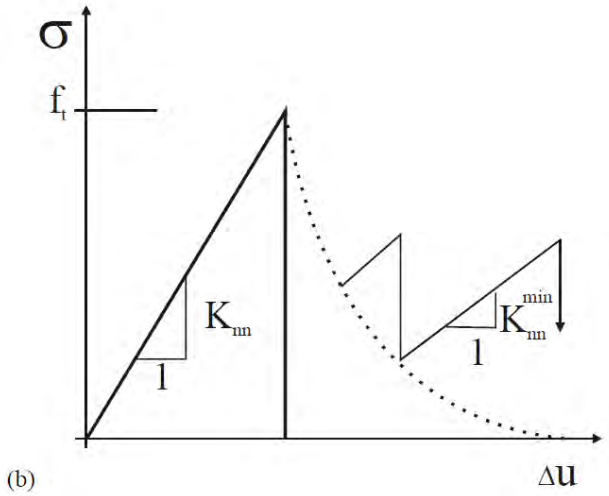


*Figure 5.16:Typical interface model behavior in tension*

The initial elastic normal is indicated with $K_{nn}$ and the shear stiffness with $K_{tt}$. When the thickness interfaces is zero, the value of these stiffnesses correspond to a high penalty number. It is recommended not to use extremely high values as this may result in numerical instabilities and to estimate the stiffness value it is advised to use the following formulas

$$K_{nn} = \frac{E}{t}, \qquad K_{tt} = \frac{G}{t} \tag{5.36}$$

where $E$ and $G$ is minimal elastic modulus and shear modulus respectively of the surrounding material and $t$ is the width of the interface zone. Its value can be selected either on the basis of the reality. $t$ can be estimated as a dimension, which can be considered negligible with respect to the structural size.

The Figure 5.15 and figure 5.16 also show $K_{nn}^{min}$ and $K_{tt}^{min}$ these are two additional stiffness values that need to be specified in the ATENA input. . They are used only for numerical purposes after the failure of the element in order to preserve the positive definiteness of the global system of equations. Theoretically, after the interface failure the interface stiffness should be zero, which would mean that the global stiffness will become indefinite. These minimal stiffnesses should be about 0.001 times the initial ones.

## 5.3 Finite elements in ATENA

The available elements in ATENA can be divided into three groups: plane elements for 2D, 3D and axisymmetric analysis, solid 3D elements and special elements, which comprises elements for modeling external cable, springs, gaps etc. This Thesis will explain only the element used.

For the most part all elements implemented in ATENA are constructed using isoparametric formulation with linear and/or quadratic interpolation functions. The isoparametric formulation belongs to the "classic" element formulations because this method, due to the fact that it is a versatile and general approach with no hidden difficulties and, also very important, these elements and formulation are easy to understand. This is very important particularly in nonlinear analysis. A big advantage of these elements is that their interpolation $h_i(r,s,t)$ functions are constructed in hierarchical manner.

Although the concept of hierarchical elements was described for plane quadrilateral elements, in ATENA it applies for plane triangular elements, 3D bricks, tetrahedral and wedge elements too. There is always a set of basic interpolation function that can be extended by any "higher" interpolation function.

Apart from interpolation functions finite element properties depend strongly on the numerical integration scheme used to integrate element stiffness matrix, element nodal forces etc. In Atena, the majority of elements are integrated by the Gauss integration scheme that ensures $n(n-1)$ order accuracy, where $n$ is the degree of the polynomial used to approximate the integrated function.

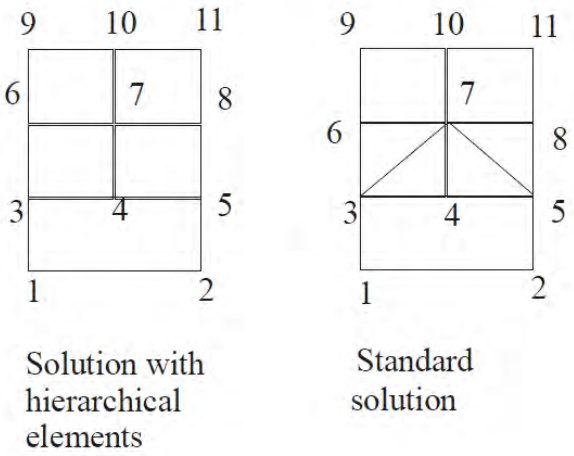


*Figure 5.17:Change of finite element mesh density*

### 5.3.1 3D Solid Elements

3D solid brick element has three degrees of freedom at each node: translations in the nodal x, y and z directions. This is an isoparametric element integrated by Gauss integration at integration points. This element is capable of plastic deformation, cracking in three orthogonal directions, and crushing. The most important aspect of this element is the treatment of non-linear material properties. To create the FEM model two kinds of finite element were used, the first one is a tetrahedral element

called CCIsoTetra with 4 to 10 nodes, see Figure 5.18, and the second is a brick element called CCIsoBrick with 8 to 20 nodes, see Figure 5.19.

To reproduce the unconfined compression the interface element to model a contact between two surfaces needs to be used. The finite element used is CCIsoGap<xxxxxx>. The string in < > describes present element nodes. The elements are derived from the corresponding isoparametric elements, it uses the same geometry and nodal. Geometry of the supported gap elements is depicted in Figure 5.20.

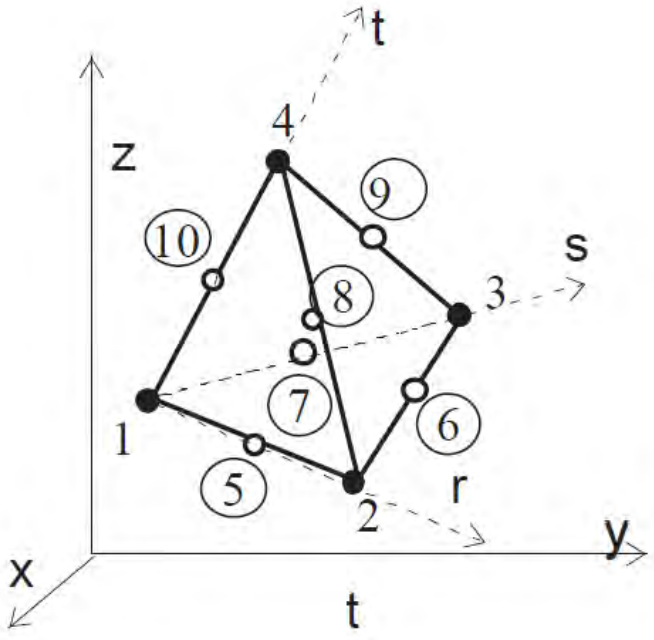


*Fifure 5.18 : Geometry of CCIsoTetra elements*

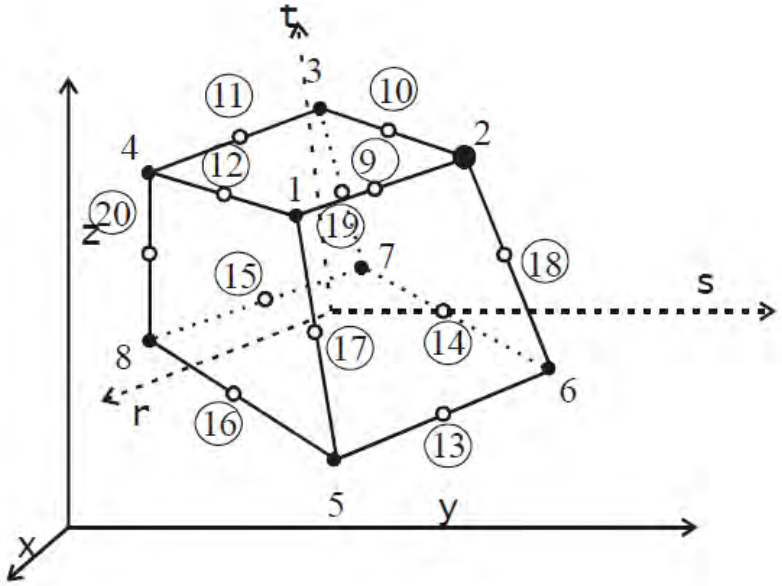


*Figure 5.19:Geometry of CCIsoBrick elements*

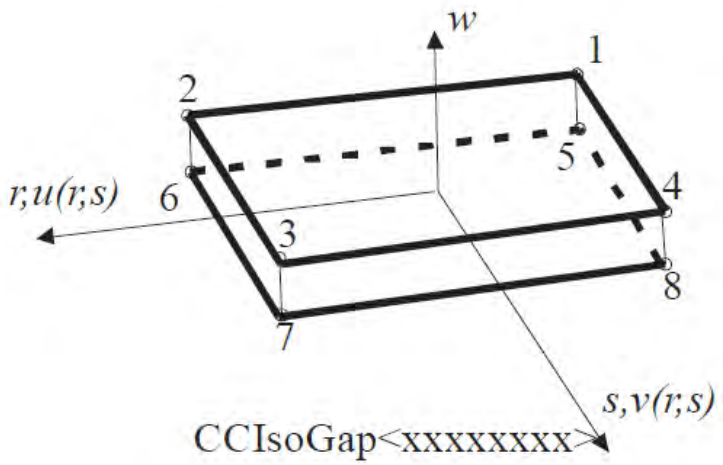


*Figure5.20:CCIsoGap elements*

The interface is defined by surfaces each located on the opposite side of interface. In the original geometry, the interface surfaces can share the same position, or they can be separated by a small distance. In this case we speak about the interface with nonzero thickness.

## 5.4 Nonlinear analysis in ATENA

Structural response of elements can be simulated by nonlinear finite element analysis. This is a general approach based on principles of mechanics and should provide an objective tool for all types of geometry, material properties and loading. Such simulations have been recently used to supplement experimental investigations, where the value of experimental data has been significantly increased. This approach has provided a tool more general than simple design formulas, which are usually valid for limited ranges of parameters. The goal of this application for complex nonlinear analysis is proposed at the development of new technical solutions and special loading types and investigation of failure cases.

An algorithm for nonlinear analysis is based on three basic parts: Finite element technique, constitutive model and nonlinear solution methods. The constitutive model is the most important object, because it decides the materials behavior, and therefore is treated more extensively here. Two of the most important effects to be included in the constitutive model of concrete are tensile fracturing and compressive confinement. Several constitutive models covering these effects are implemented in the computer code ATENA

ATENA is a nonlinear finite element analysis program that specializes in the modeling and computer simulation of concrete behavior. The program was developed by Cervenka Consulting. The program consists of two primary components. The first one is the solution core which houses the 2D and 3D continuum models, the element, material, and solution libraries and the second one is the user interface. ATENA is capable of calculating load carrying capacity, push-over analysis, crack widths, accurate deflections and areas of concrete crushing.

Non-linear analysis can be classified according to a type of non-linear behavior. Where the deformation is relatively small, for example, in common reinforced concrete structures, not only the non-linear materials behavior needs to be considered but also the low tensile strength of concrete. In the case that the

deformation is significant, but still small, the constitutive equations are linear but the complete form of the geometric equations, including quadratic terms has to be employed. The most accurate and general approach uses non-linear, both material and geometric, equations. In this case it is not possible to apply the total value of load immediately but it is necessary to integrate it in time increment or loading increment.

Considering the deformed shape, there are two possibilities for formulating the general structural behavior, the *Lagrange formulation* and the *Euler formulation.* The first one is ordinarily used to calculate civil engineering structures, and its formulation evaluates the behavior of infinitesimal particles of volume $dV$, which depend on the loading level applied and the deformations. The Euler formulation is used where there are material flows. For structural analysis the Lagrange formulation is more suitable, and can be divided into two forms. The Total Lagrangian formulation writes the governing equations in respect to the undeformed original configuration at time $t=0$, whereas the updated Lagrangian formulation refer to the most recent deformed configuration at time $t$. ATENA currently uses the latter one.

Usually, for a common analysis of a structure, many small load increments have to be applied. We call the start of the load increment $t$, where its structural state is known, and the $t+\Delta t$ the end of the load. For each increment an iterative solution procedure returns a structural response at the end of the increment. To research the final level of loading, this procedure is repeated as many times as needed.

The most common method applied to introduce the equations that govern the problem is the principle of virtual work in its different form. Using this procedure it is possible to derive several different variation principles. This method is general for linear analysis, but unfortunately doesn't always work in nonlinear analysis. The principle of virtual displacement is used in ATENA. The stress and strain tensor used in nonlinear analysis is symmetric.

All expressions of geometric and constitutive equations were derived independently of the structural shape or regarding the finite element used. Atena implements some types of element finite.
There are plane elements for 2D, 3D and axisymmetric analysis, and solid 3D elements and special elements. The majority of elements implemented in ATENA are constructed using isoparametric formulation with linear or quadratic interpolation functions and are also principally integrated by Gauss integration scheme.

### 5.4.1 Solution of nonlinear equation

A major advantage of ATENA is the simpler way of solving the non-linear structural behaviour through finite element method and its incremental loading criteria. Different methods are available in ATENA for solving non-linear equations such as, linear method, Newton-Raphson Method, Modified Newton-Raphson method and Arc Length methods.

These methods need to be able to solve a set of linear algebraic equation in the form

$$A\underline{x} = \underline{b} \tag{5.37}$$

where A, $\underline{x}$, $\underline{b}$ stands for a global structural matrix and vectors of unknown variables and R.H.S. of the problem, respectively. Newton-Raphson Method and Modified Newton-Raphson Method are more commonly used methods. In the present study, Newton-Raphson method is used for solving the simultaneous equations. It is an iterative process of solving the non-linear equations.

One approach to non-linear solutions is to divide the load into a series of load increments. The load increments can be applied either over several load steps or over several sub steps within a load step. At the completion of each incremental

solution, the program adjusts the stiffness matrix to reflect the nonlinear changes in structural stiffness before proceeding to the next load increment.

The ATENA program overcomes this difficulty by using Full Newton-Raphson method, or Modified Newton-Raphson method, which drive the solution to equilibrium convergence (within some tolerance limit) at the end of each load increment.

Using the concept of incremental step by step analysis in Full Newton-Raphson method the following set of nonlinear equations is obtained:

$$K\left(\underline{p}\right)\Delta\underline{p} = \underline{q} - f\left(\underline{p}\right) \tag{5.38}$$

Where:

$\underline{q}$ is the vector of total applied joint loads

$f\left(\underline{p}\right)$ is the vector of internal joint forces

$\Delta\underline{p}$ is the deformation increment due to loading increment

$\underline{p}$ are the deformations of structure prior to load increment

$K\left(\underline{p}\right)$ ) is the stiffness matrix, relating loading increments to deformation increments.

The set of nonlinear equations shown in Eq. (5.38) represents out-of-balance forces during a load increment, that is the total load level after applying the loading increment minus internal forces at the end of the previous load step. For the most part the stiffness matrix is deformation dependent, that is a function of $p$ , but this is usually neglected within a load increment in order to preserve linearity. In this case the stiffness matrix is calculated based on the value of $p$ pertaining to the level prior to the load increment.

Before each solution, the Newton-Raphson method evaluates the out-of -balance load vector, which is the difference between the restoring, forces (the loads corresponding to the element stresses) and the applied loads. The program then

performs a linear solution, using the out-of -balance loads, and checks for convergence. If convergence criteria are not satisfied, the out-of-balance load vector is re-evaluated, the stiffness matrix is updated, and a new solution is obtained. This iterative procedure continues until the problem converges.
The set of equations (5.39) is nonlinear because of the non-linear properties of the internal forces:

$$f\left(k\underline{p}\right) \neq kf\left(\underline{p}\right) \tag{5.39}$$

and non-linearity in the stiffness matrix

$$K\left(\underline{p}\right) \neq K\left(\underline{p} + \Delta\underline{p}\right) \tag{5.40}$$

where *k* is an arbitrary constant.

The set of equations represents the mathematical description of structural behavior during one step of the solution. Rewriting equations (5.40) for the *i-th* iteration within a distinct loading increment we obtain:

$$K\left(\underline{p}_{i-1}\right)\Delta\underline{p_i} = \underline{q} - f\left(\underline{p}_{i-1}\right) \tag{5.41}$$

All the quantities for the (*i-1)*-th iteration have already been calculated during previous solution steps. Now we solve for $\underline{p_i}$ at load level *q* using:

$$p_i = \underline{p}_{i-1} + \Delta\underline{p_i} \tag{5.42}$$

As pointed out earlier, equation (5.42) is nonlinear and therefore it is necessary to iterate until some convergence criterion is satisfied.

The concept of solution nonlinear equation set by Full Newton-Raphson method is depicted in Figure 5.21.

Therefore, the most time consuming part of the Full Newton-Raphson method solution is the re-calculation of the stiffness matrix $K\left(\underline{p}_{i-1}\right)$ at each iteration. In many cases this is not necessary and we can use matrix $K\left(\underline{p}_0\right)$ from the first iteration of the step.

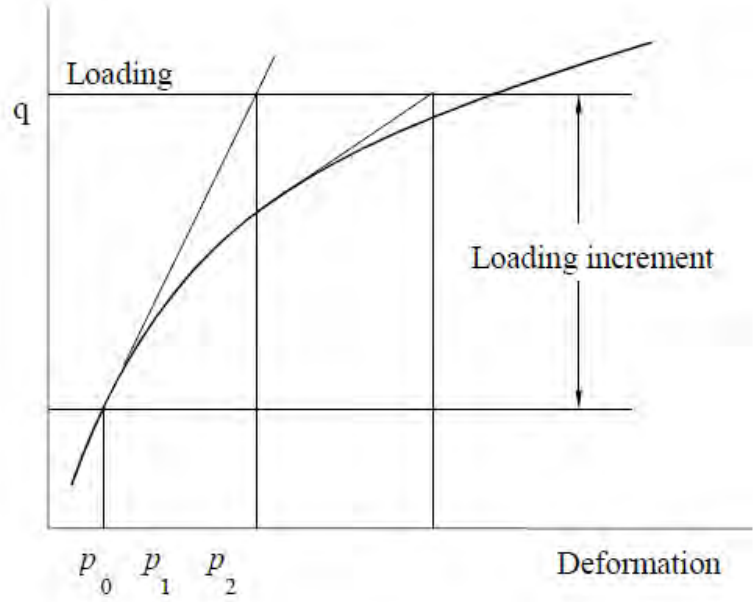


*Figure 5.21:Full Newton-Raphson method*

This is the basic idea of the so-called Modified Newton-Raphson method. It produces very significant time saving, but on the other hand, it also exhibits worse convergence of the solution procedure. The simplification adopted in the Modified Newton-Raphson method can be mathematically expressed by:

$$K\left(\underline{p}_{i-1}\right) \cong K\left(\underline{p}_0\right) \tag{5.43}$$

The modified Newton-Raphson method is shown in Figure 5.22. Comparing Figure 5.21 and Figure 5.22 it is apparent that the Modified Newton-Raphson method

converges more slowly than the original Full Newton-Raphson method. On the other hand a single iteration costs less computing time, because it is necessary to assemble and eliminate the stiffness matrix only once. In practice a careful balance of the two methods is usually adopted in order to produce the best performance for a particular case. Usually, it is recommended to start a solution with the original Newton-Raphson method and later, i.e. near extreme points, switch to the modified procedure to avoid divergence.

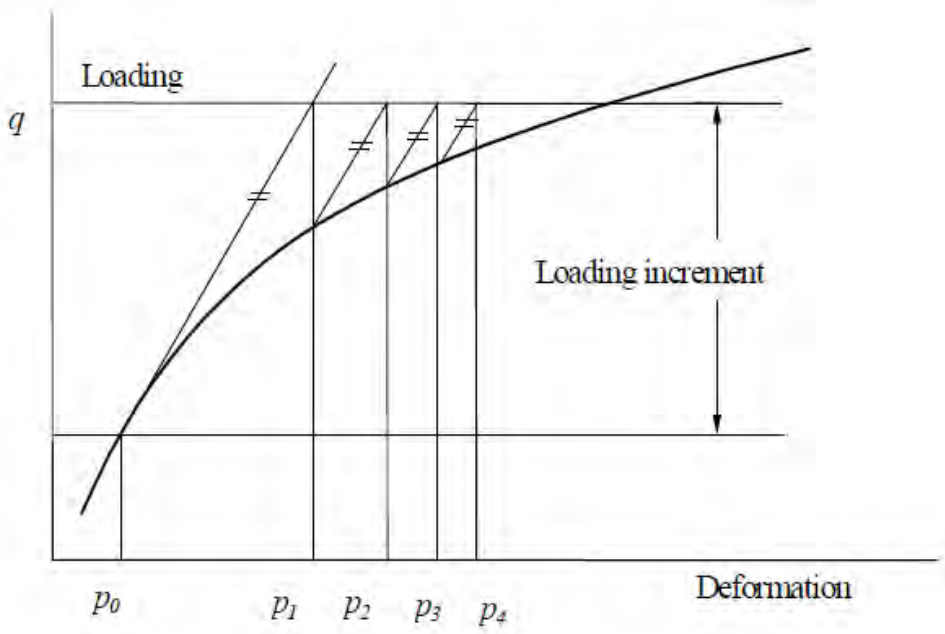


*Figure 5.22:Modified Newton-Raphson method*

# Chapter 6

# CREATION OF THE FEM MODELS

The models reproduced can be parted in two groups. The numerous group is about the three-point bending tests, where it was necessary to produce four different modes for each beam size, and for each size there are four or five different notch depths. In the other group a cube model for unconfined compression was produced.

The creation of the models was done with ATENA 3D Graphical User Interface, which is a part of the ATENA program system. The program, which is determined for nonlinear finite element analysis of structures, offers tools specially designed for computer simulation of concrete structural behavior. The ATENA program system consists of a solution core and several user interfaces. The solution core offers capabilities for a variety of structural analysis tasks.

ATENA 3D program is designed for 3D nonlinear analysis of solids with special tools for concrete structures in this case.

The program has three main functions:

1. Pre-processing. Input of geometrical objects (concrete and interfaces.), loading and boundary conditions, meshing and solution parameters.
2. Analysis. It was possible a real time monitoring of results during calculations
3. Post-processing. It was utilized for graphical and numerical results

ATENA recognizes two models, geometrical and numerical. Data of these models are treated strictly separately. *Geometrical model* represents dimensions, properties and loading. It consists of an assembly of macro elements (solids). Macro elements are connected by contacts. Each macro element is an independent object defined by joints, lines and surfaces. Thus on a contact of neighboring macro elements there are

double surfaces. This provision assures that each object is independent of the others. All interaction between the macro elements is provided by contacts. Geometrical model is completed by defining loading (load cases and load history) and construction cases.

*The Numerical model* is generated based on the geometrical model and represents a numerical approximation of the structural analysis problem. The Numerical model is a result of discretization made by the finite element method. The tool mesh generator was used to generate meshes automatically. As a consequence of independent macro elements the finite element meshes were made independently for each macro element. Thus, when two macro elements are connected as neighboring objects, there are two surfaces belonging to each object on the contact.

In succession the basic steps used to define a complete geometrical, and then a finite element model for non-linear analysis will be explained. The purpose of the geometrical model is to describe the geometry of the structure, its material properties and boundary conditions.

## 6.1 Three point bending tests

The three point-bending test is composed of four different sizes, where the parameters that change are the height and length, whereas the thickness is always the same. Each size also has four or five different notch depths, the mesh is therefore different for each model.

The analytical model for the finite element analysis was created during the pre-processing with the initial help of the fully automated mesh generator. The geometrical model is composed of three-dimensional solid regions called “macro-elements”. To reproduce the three point bending test it was necessary to create the concrete beam, that represents a macro-element, and the support. There are three, one positioned on the top of the beam, and the other two below, near to the corner.

Each macro-element is defined separately, and is composed of joints, lines and surfaces. In ATENA 3D each macro-element has its own joints, lines and surfaces. This means that no joint, line or surface can be shared by two macro-elements.

Macro-element definition started with the creation of geometrical joints. These joints are later connected into boundary lines. The subsequent step is the creation of surfaces. They are composed of the previously defined lines. When two macro-elements touch each other, the program automatically detects this condition and creates contacts at the appropriate locations.

After examination of the user interface layout, it was possible to start with the definition of the geometrical model of the analyzed structure. The next step was the definition of material groups and material properties. For the current problem, it was necessary to define two material types: one elastic material for the steel plates at support and loading points and concrete material for the beam. For the support *3D elastic isotropic* was used and for concrete *3D Nonlinear cementitiuos 2* was used. The material characteristics of the support are shown in the following table (6.1). The characteristics of the concrete will be shown later.

| ***3D elastic isotropic*** | |
|---|---|
| *Elastic modulus E* | 200 [GPa] |
| Poisson's ratio ν | 0.3 |
| Material density ρ | 0.0023 [M/l$^3$] |
| *Coef. of thermal expansion* | 0.000012 [l/T] |

*Table 6.1:characteristics of the steel support*

After the material type of the concrete was inserted, ATENA asks for the cube strength of the concrete, and starting from that, the software generates the default values of material parameters. $f_{cu}$= 31MPa was inserted, the same as what was specified from the experiment data tests. After that, it was possible to change all the properties of the concrete, such as the basic properties, the tensile and compressive properties, and the miscellaneous properties.

Next step in the Input data preparation was the definition of problem geometry. The geometry was created by defining individual solid regions. The first task was to define the concrete beam and subsequently the steel plates for loading and supports was created. Each macro-element has its own set of joints, lines and surfaces. Every macro-element was created with the simplest approach. This method defines individual joints and then connects them to lines, which are later connected to form surfaces. Surfaces can be used directly to define a solid or the extrusion feature can be used to create a new solid by extruding a surface along a predefined vector.

When macro-elements were defined for modeling the loading and supporting steel plates, it was necessary to consider some aspects. In nonlinear analysis it is often necessary to avoid any unrealistic stress concentration, as this may cause premature failure or cracking in these locations. If the support conditions or loads are applied at single nodes, this may create strong stress concentrations affecting the analysis results. It should be considered that in most cases such a stress concentration very seldom exists in reality as the supports or loads are usually applied over a certain area and never at single points. This is also the case in the current problem, which corresponds to an experimental setup, where loading and supports were realized using small steel plates.

After the definition of macro-elements was completed it was possible to proceed to the next step in the definition of the numerical model that is the automatic mesh generation. Each macro-element was meshed independently. Many attempts regarding mesh generation were done to search for the best response of the software.

There are three main options for the macro-element mesh generation. It was possible to create a structured mesh that consists of only brick elements. Such a method is possible only for macro-elements that have six boundary surfaces. An important factor is to set the mesh generation parameters. The finite element mesh quality has a very important influence on the quality of the analysis results, the speed, and memory requirements. Refining only the important parts can save a lot of processor time and disk space. The global default mesh size was changed many times, and it

was decided to intensify the area near the notch. At the beginning for the lateral area the value of 1 was used and for central area 0.4 was used. The result of this operation is shown in Figure 6.1, Figure 6.2 and Figure 6.3.

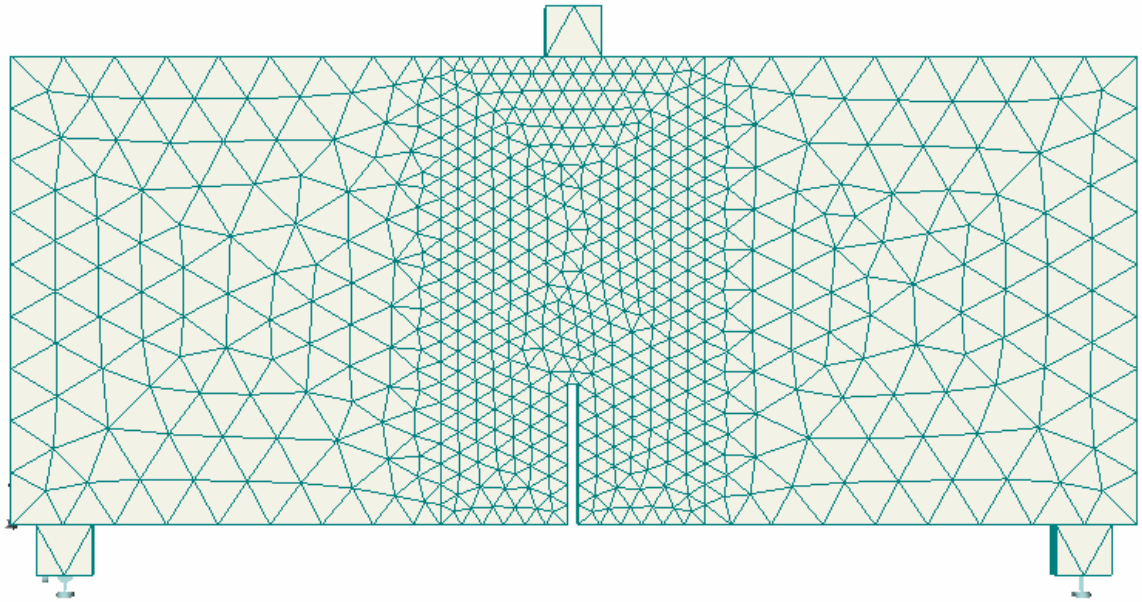

*Figure 6.1: Front view of Beam C with notch α=30%*

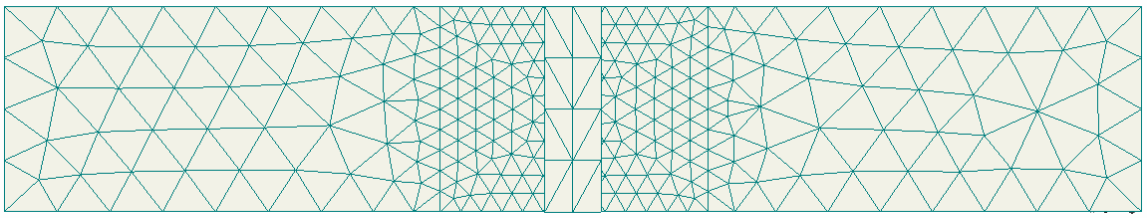

*Figure 6.2: top view of Beam C with notch α=30%*

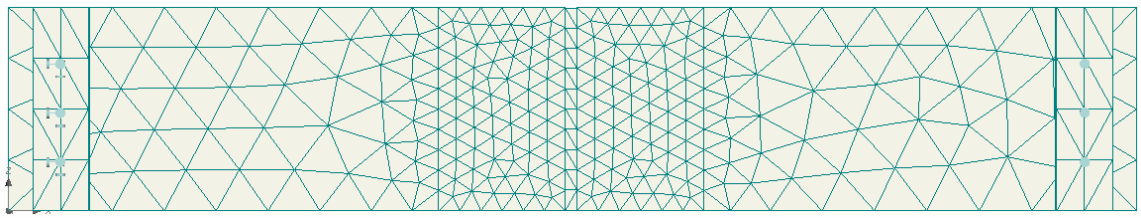

*Figure 6.3: bottom view of Beam C with notch α=30%*

It was possible to select what kind of elements are to be generated for which macro-elements: linear or quadratic. Linear elements are low order elements with nodes at each element corner. Quadratic elements usually have additional nodes on each element edge. Some quadratic elements may have even nodes in the middle of element sides or inside the element.

Even though the linear tetrahedral elements are generally not recommended for stress analysis, they can be used in this case for modeling the steel plates, since an accurate modeling of stresses and deformations in these areas is not as important as the modeling of the concrete beam itself.

In this case, linear elements were used and for the steel plates the tetrahedral elements had to be used. In the case of contacts, it was possible to enforce compatible meshes on both sides of the contact. In general cases, ATENA supports contacts with incompatible meshes, but this feature should not be used if it is important to properly model stresses and deformation in the contact area. In the analyzed case, the contact regions between concrete beam and steel plates should not have a great influence on the beam behavior, so it is not necessary to enforce the full mesh compatibility on the two contacts.

Due to this assumption, it is also possible to mesh the beam with brick elements and the plates with tetras. This greatly simplifies the model definition, but it is necessary to understand that this will result in certain incompatibilities in the displacement field on these contacts. In this case, it is not a big problem, since in reality the connection among the steel plates and concrete would also not be perfect.

### 6.1.1 Supports and Actions

The next step in creating the model is to describe the definition of supports and loads for this problem. The analyzed beam is supported at the bottom steel plate in the vertical direction. The beam is loaded at the top steel plate. We are interested in

determining the maximal load-carrying capacity of the beam, which means we want to also be able to trace the structural response in the post-peak regime.

The easiest method to accomplish this is by loading the beam by prescribed displacements at the top steel plate. It is also possible to apply the loading by vertical forces, which will be increased in each load step. In order to be able to go into post-peak, advanced non-linear strategies such as Newton-Raphson method solution was necessary. The first load cases were defined, and then they were combined together to form a loading history for an analyzed structure. In ATENA each loading step then represents a loading increment, which is added to the previous loading history.

For this problem, two load cases are needed: one containing the vertical and horizontal supports, and one with the prescribed deformations at the top steel plate. The choice of how to secure the beam is very important because this may change the results and thus obtain different solutions more or less close to the real solution. The purpose is to try to bind the specimen in question in order to reproduce, as much as possible, the real constrain used in laboratory.

It was decided to constrain the beam with the static scheme support-support, as you can see in the picture (6.4) the left steel plate was bound in the x and y direction to play the zip tie. We could choose two different options for entry: tying the knots of the lower steel or tying the central line of the steel plate entirely. The second option considered fairer and more similar to the real situation was chosen.

It was necessary for this support to also be fixed in the *z* direction in order to prevent any rigid body displacements. To reproduce the simple constraint support, the right steel plate was bound only in the y direction. In this way a loaded beam support-support was reproduced.

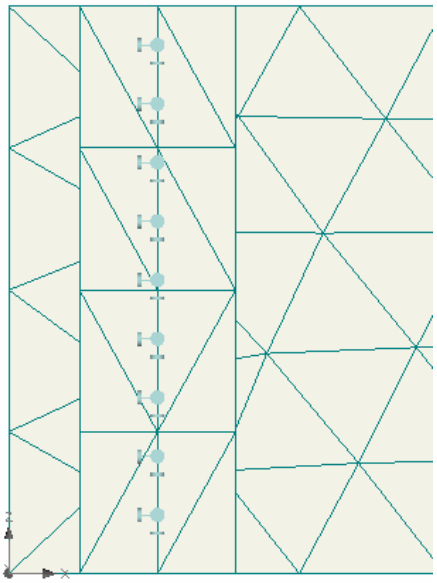

*Figure 6.4: Constraint at the bottom, fixed in all direction*

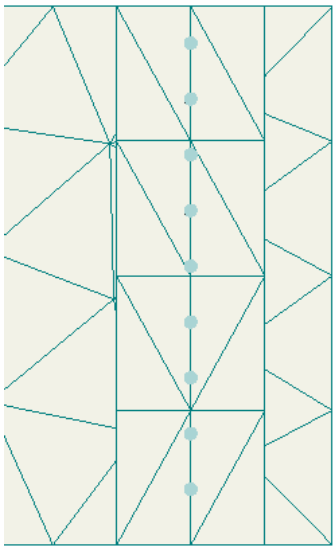

*Figure 6.5: Constraint at the bottom, fixed in y direction*

It was decided to apply the prescribed displacement to a line at the top steel plate. It was necessary to sum all the reactions at these nodes in order to obtain the total loading force. In this way, it is possible to have a more precise value of the loading force as we could monitor the reaction force at each node. Added together, they are directly equivalent to the total of the loading force necessary to break the beam.

### 6.1.2 Loading History and Solution Parameters

The next step describes the definition of loading history for the analysis of the beam. The loading history consists of load steps. Each load step is defined as a combination of load cases, which has been defined previously. Each load step also contains a definition of solution parameters, which define solution methods that are to be used during the load steps. Analysis steps define loading history for solution, there are some rules to consider for the load steps.

Load steps are incremental. This means that values of loadings applied in the current step are added to the loading applied in previous load steps. Total loading in a step is a sum of all loading in the entire load history up to, and including this step. Another important rule is that loading need not be proportional and loading history is unique. In a non-proportional load history the sequence of loading is important. A change of load sequence may produce different results. Superposition of stress states is not admissible in nonlinear analysis.

ATENA 3D contains a standard set of solution parameters. This section defines methods and parameters for solution of nonlinear equations. Two default sets can be chosen, Standard Newton-Raphson method and Standard arc-length method. The solution method used was Newton-Raphson. It was possible to set up many parameters of this method. Newton-Raphson method keeps the load increment unchanged and iterates displacements until equilibrium is satisfied within the given tolerance. This means that this method should be used in cases when load values must be exactly met..

After that, it was possible to prescribe the loading history for the given problem. The objective was to keep increasing the load up to failure. Very often before an analysis is started it is difficult to estimate the required loading level that would lead to failure. The maximal load level however, can be often estimated either by simple hand calculation or by performing an initial analysis with a very small load level.

Then from the resulting stresses it is possible to estimate how much the load must be increased to fail the structure.

In this case, it is known from the experimental results that the beam should fail at the deflection of about 0.003 m. In load case 2 a prescribed displacement of -0.0001 mm was defined. This means that approximately 50 load steps would be needed to reach the failure. It required many steps because it was also necessary to know the behavior after pick.

For each analysis step, it was necessary to select the load cases, which should be applied, solution parameters and a multiplier that was used to scale all forces or prescribed displacements for the given step.

### 6.1.3 Monitoring Points

Monitoring points serve to monitor results of calculation during analysis. Monitoring points have similar meanings as measuring gauges in laboratory experiments.

During non-linear analysis it is useful to monitor forces, displacements or stresses in the model. The monitored data can provide important information about the state of the structure. For instance from monitoring of applied forces or reactions, it is possible to determine if the maximal load was reached or not.

There are two kinds of monitoring points, in nodes and in integration points. In nodes the following can be monitored: external forces, reactions and displacements. In integration points the following can be monitored: stress, strain, temperature, initial stress and strain, body forces, crack attributes. Monitored data can be listed in printed output, exported and used for subsequent data processing, graphs, etc.

There are two monitor Point types studied in this analysis. The first type was used to obtain the forces developed in the specimen due to the predetermined deformation in

sets summit. In fact, these monitor Points were positioned immediately below the top of the steel plate as shown in figure (6.6). Figure (6.7) shows the longitudinal arrangement of these points instead, where one was positioned for each node, so for about 5. In this manner, the force for each node was obtained and by summing all 5 we also obtained the total force acting on the specimen

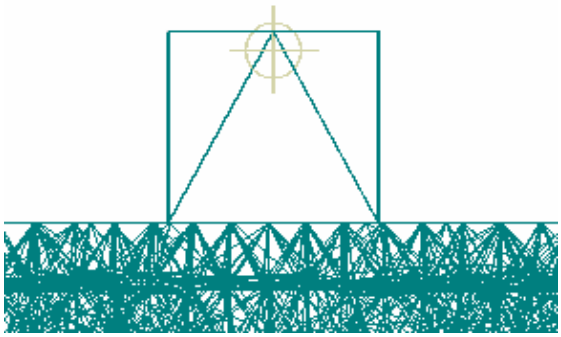

*Figure 6.6:Front view of  Monitor Points below the top of the steel plate*

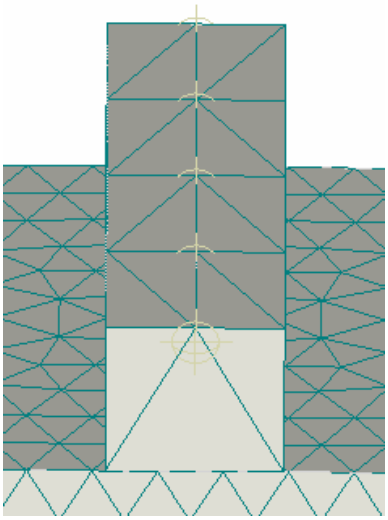

*Figure 6.7:Top view of  Monitor Points below the top of the steel plate*

The second type of monitor point was used to obtain the displacement between the two sides of the notch. As is shown in figure (6.8) per side 5 monitor points were positioned. Each monitor point on one side is exactly in front of the other on the opposite side.

In this way, it is possible to derive the opening for each step that the notch undergoes by comparing the displacements of the points. The obtained value of the opening will later be used in the formula (7.4) to get the strain.

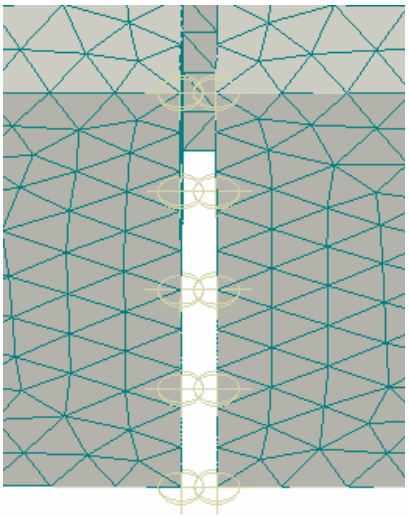

*Figure 6.7:bottom view of Monitor Points in the notch*

## 6.2 Unconfined compression tests

To create the model of the unconfined compression, all the general rules utilized for the creation of the three-point bending beam were used. The size of cubes considerate are 40x40mm and 150x150mm.

Also the analytical model for this finite element analysis was created during the pre-processing with the help initially of the fully automated mesh generator. To reproduce the unconfined compression test it was necessary to create a cube that represents a unique macro-element. The second macro-element created was the steel plate up and down the cube. In this model there is another problem with the creation of the simulation, because an important factor to evaluate is the contact between the two materials. These contacts can be modified to simulate perfect connection, gaps or other interface types. The incorrect evaluation of this value can produce wrong

results. To study this, ATENA offers an interface material model, where by changing the value of the parameters it is possible to decide which kind of contact to use. The interface material model used is *CC3Dinterface*. For its calibration, there are seven parameters that can be set. These parameters are discussed in chapter 7.

The first step was the definition of the geometrical model of the analyzed structure. The cube started with the creation of geometrical joints. These joints were connected into boundary lines and later the surfaces were created.

The material used for the unconfined compression were obviously the same as those used for the three-point bending tests. *3D elastic isotropic* for steel plate and *3D Nonlinear cementitiuos 2* for the concrete.

All the procedures regarding the setting of material model were done in the same way as the three-point bending tests. After the definition of macro-elements was completed it was possible to proceed to the next step in the definition of the numerical model that is the automatic mesh generation. Each macro-element was meshed independently.

Considering the cube shape, it was easy to generate the mesh, using brick elements. The important thing to choose is the size of the ele1ments. For an accurate result this cannot be too wide or too small, because the model will become too busy in regards to the memory requirements. After some attempts 3.3 mm was chosen for the element. The result of this operation is shown in Figure (6.8).

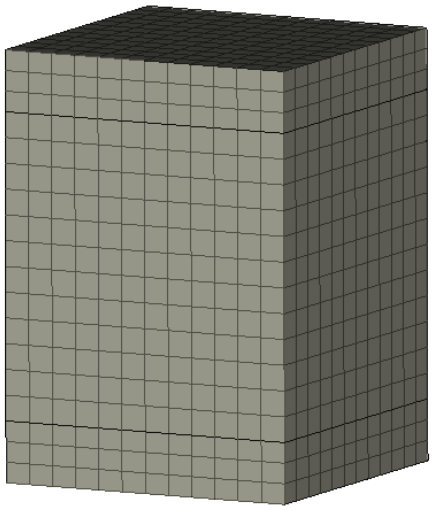

*Figure 6.8: Model of Cube 40x40mm*

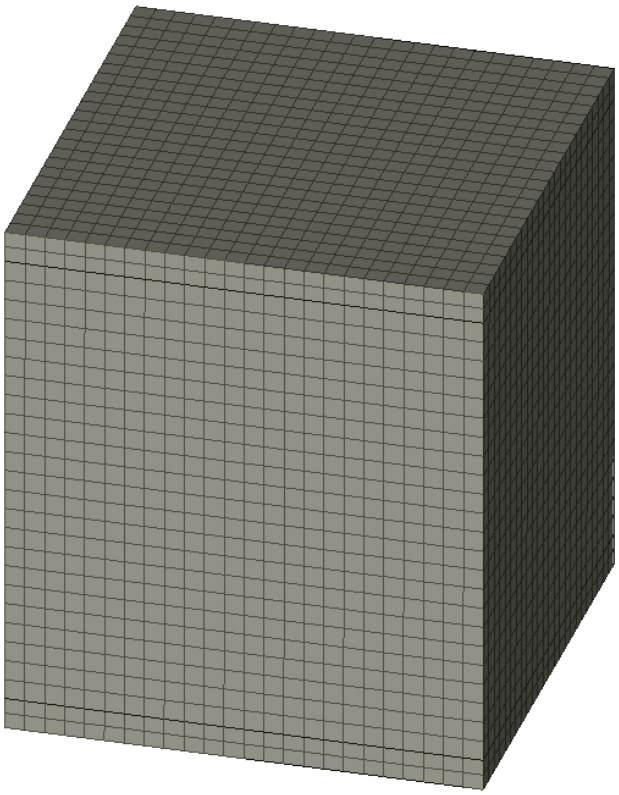

*Figure 6.9: Model of Cube 150x150mm*

.As in the three-point bending model the next step is to describe the definition of loading history for the analysis of the cube. The values of the parameters that can be decided for setting the Newton-Rapson method were almost the same as in the three point bending tests. In the beginning the prescribed deformation given was – 0.0001 m.

There are two monitoring points necessary for this simulation. One on the top, to get the reactions, and one on the bottom, to get the shortening of the specimen. The steps used initially was eighty, and its result enought.

## 6.3 ATENA studio

After the creation of the first three-point bending model, it was necessary to accelerate the creation process of the models, as four different models needed to be produced for each size, due to the different notches evaluated. There are four sizes considered, eighteen models were therefore needed in total. For this reason it was decided to use ATENA studio, which is a part of the ATENA program system. Thanks to this section of the software it was faster to produce these eighteen models. The basic description of the ATENA studio is shown in the following sections.

The ATENA Studio is simple and has an intuitive user interface for ATENA solution core. It is a unified environment for all analysis types. The program has two main modules. Runtime module where a real time monitoring of results during calculations is made possible and Post-processor module where there is access to a wide range of graphical and numerical results. Calculation or post-processing phases are processed separately by these program modules by opening a corresponding window. By switching the programs, ATENA replaces one program module with another and all data related to the specific task, if available, are also loaded.

ATENA recognizes two models, geometrical and numerical. Data from these models are treated strictly separately. *Geometrical model* represents dimensions, properties

and loading. It consists of an assembly of macro-elements (solids). Macro-elements may be connected by contacts. Each macro-element is an independent object defined by joints lines and surfaces. Geometrical model is supplemented by the definition of load cases, load history and construction cases. The current version of the ATENA Studio does not support the definition of the geometrical model, it operates strictly on the numerical model, which is created from the geometric model using a suitable pre-processor.

The *Numerical model* is generated based on a geometrical model and represents a numerical approximation of the structural analysis problem. The Numerical model is a result of discretisation made by the finite element method. The mesh generator in ATENA makes it possible to generate meshes automatically for solid and reinforcing objects. The data of a new task must be imported from an input file. It can be produced by ATENA interface in other programs. The input can be edited after its import but not after executing command Runtime.

The creation of each input file was done with support of MATLAB. Inside the input file there is all the information to create the model. ATENA input commands were used to produce the input file. They are used to define finite element model, to specify the loading history and to activate the finite element non-linear analysis.

The main function of Runtime module is to control calculation progress and to monitor intermediate results. During the process it is possible to monitor some useful graphics in the diagram window. The main graphics convergence criteria, which are of the greatest importance in nonlinear analysis, because they indicate solution accuracy. These are evaluated and shown automatically and need not be defined by the user. If desired, other results like forces, displacements, stresses can be defined in the input file by the user. Four solution errors serve to check the following criteria: displacement increment, normalized residual force, absolute residual force, energy dissipation. The load-displacement diagram is a useful tool to illustrate the response of a structure.

When the analysis is completed ATENA post-processing can be started. In this section it is possible to check all the results by the main window and see the graphics that can be done. There are several advanced processing options that can calculate average, or min. max. Values for the specified output request.

ATENA studio produces an output file where there are the values that were decided to be shown in the creation of the input file.

In the following are shown the model generate from ATENA Studio, for each size there are four or five different notch depth

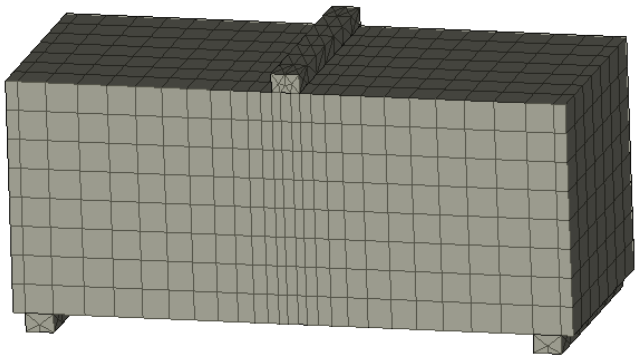

*Figure 6.10: Beam D, 40x40x96mm, without notch.*

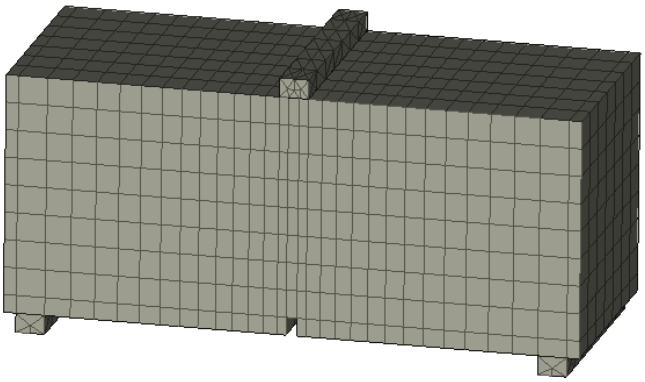

*Figure 6.11: Beam D, 40x40x96mm, notch depth α=7,5%*

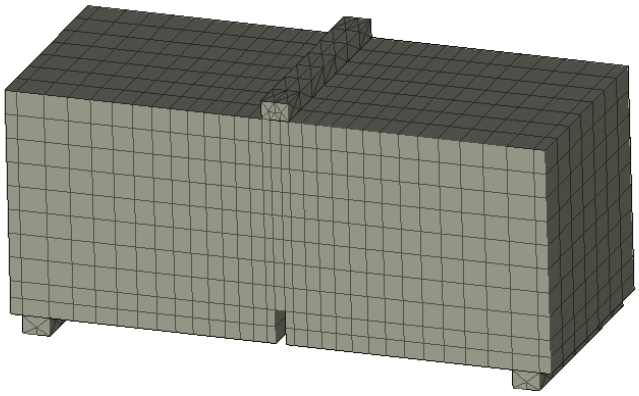

*Figure 6.12: Beam D, 40x40x96mm, notch depth α=15%*

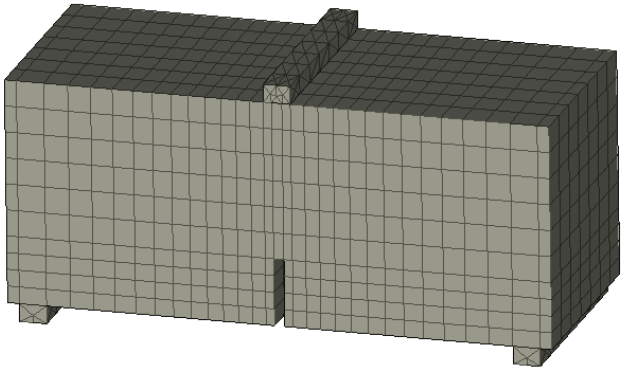

*Figure 6.13: Beam D, 40x40x96mm, notch depth α=30%*

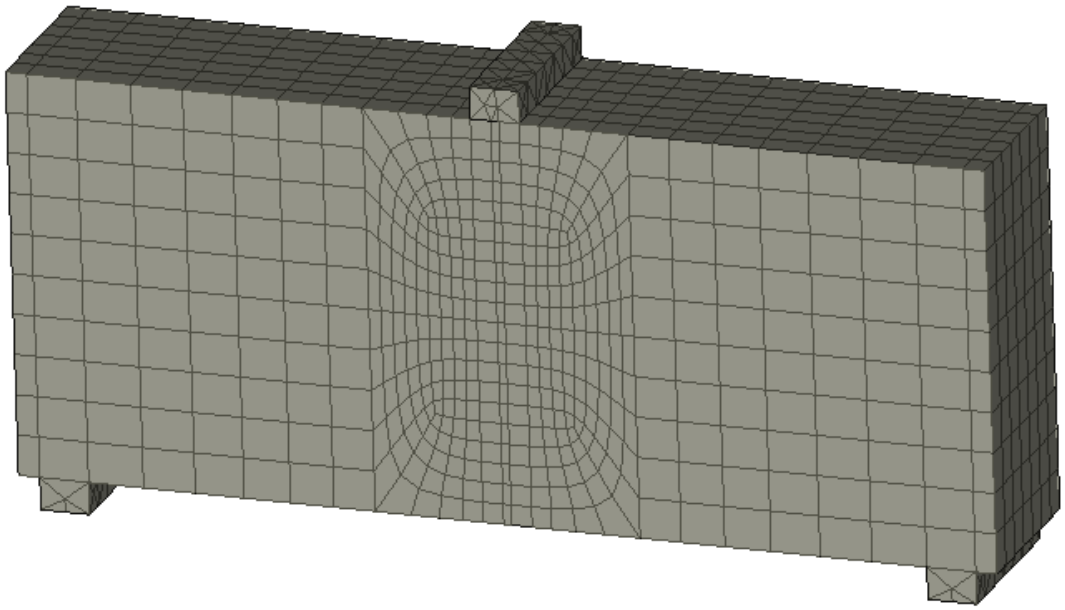

*Figure 6.14: Beam C, 40x93x223mm, without notch.*

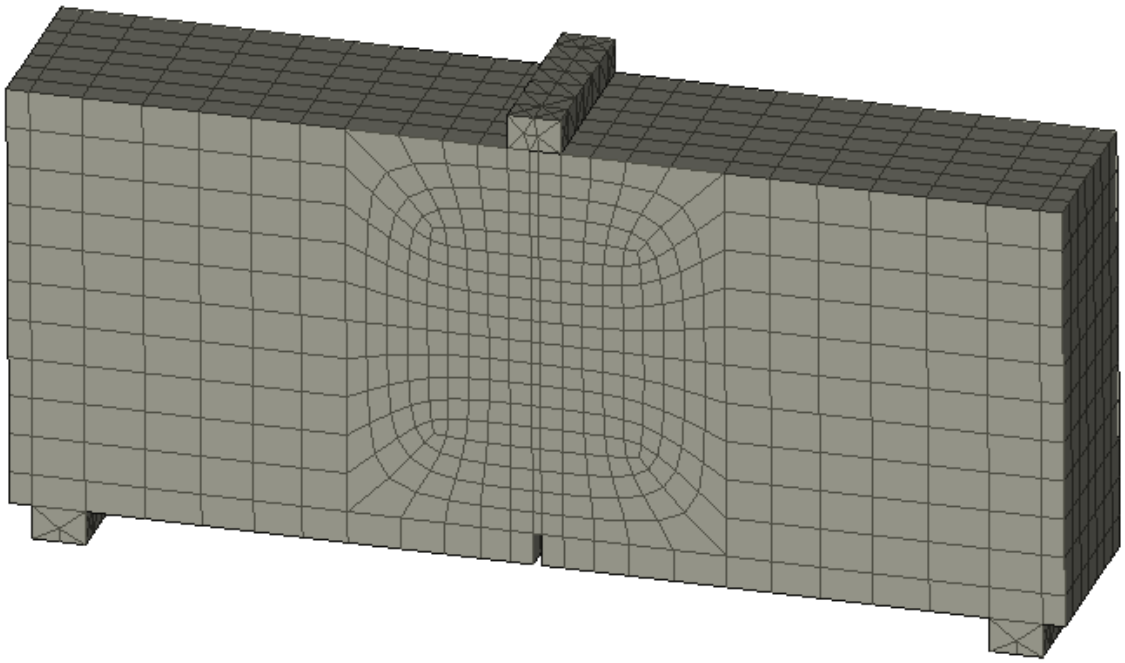

*Figure 6.15: Beam C, 40x93x223mm, notch depth α=7.5%.*

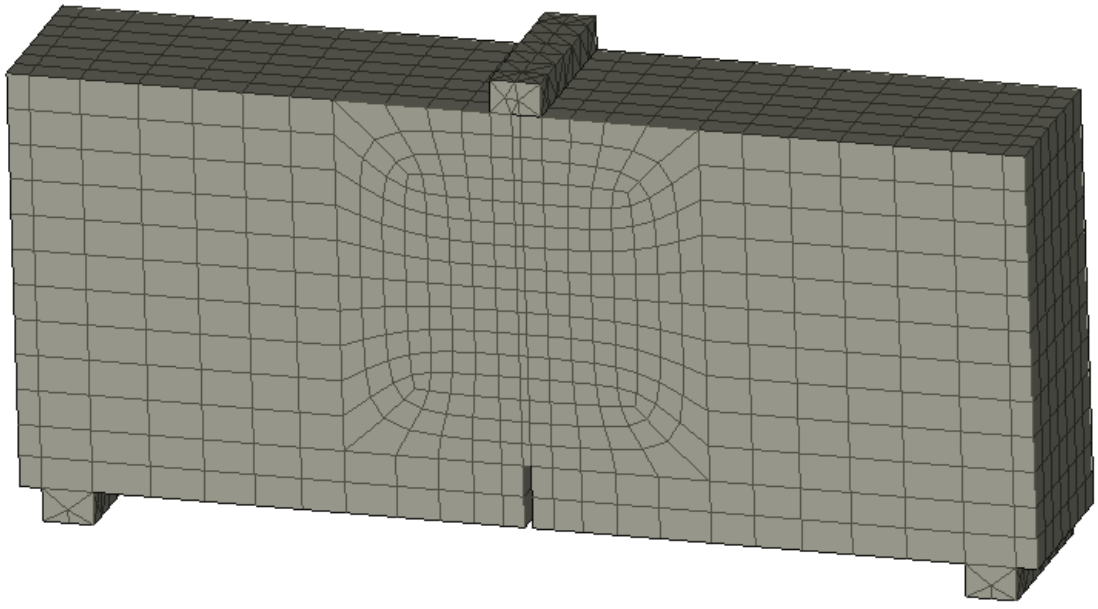

*Figure 6.16: Beam C, 40x93x223mm, notch depth α=15%.*

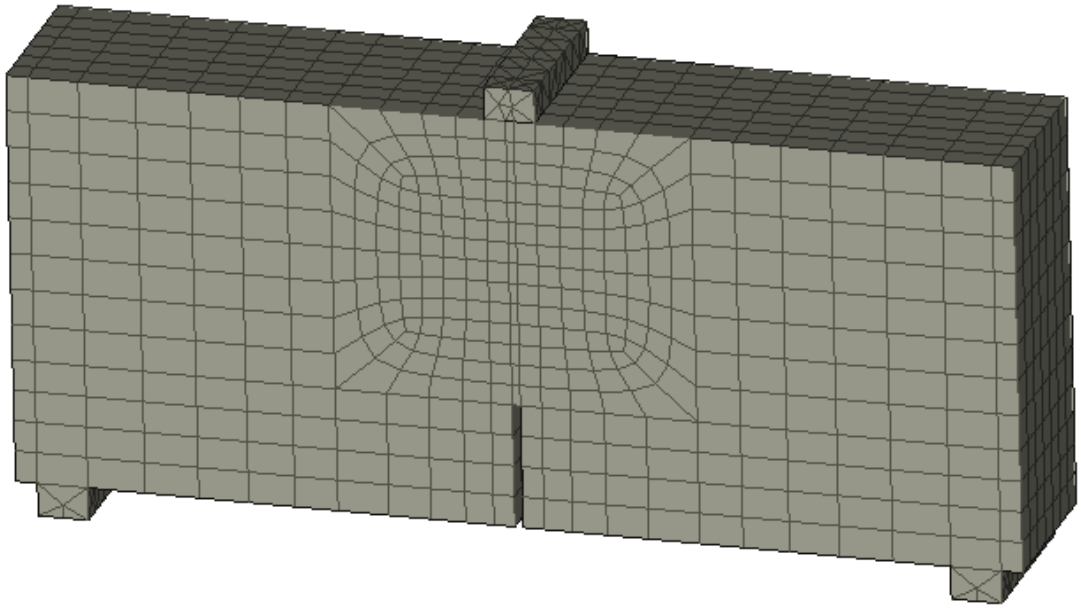

*Figure 6.16: Beam C, 40x93x223mm, notch depth α=30%.*

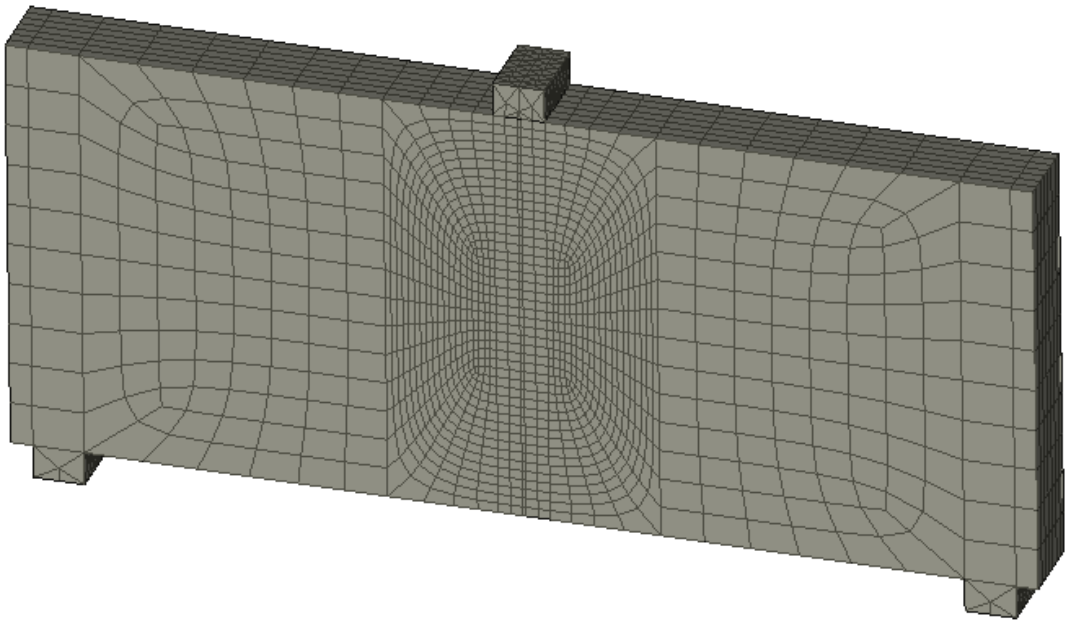

*Figure 6.17: Beam B, 40x215x517mm, without notch.*

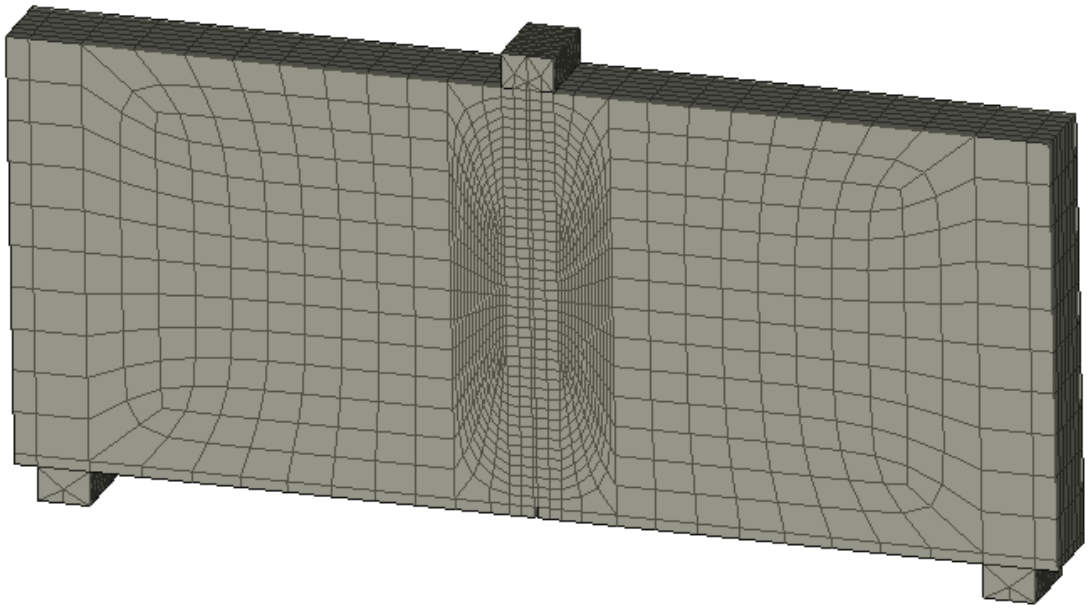

*Figure 6.18: Beam B, 40x215x517mm, notch depth α=2.5%*

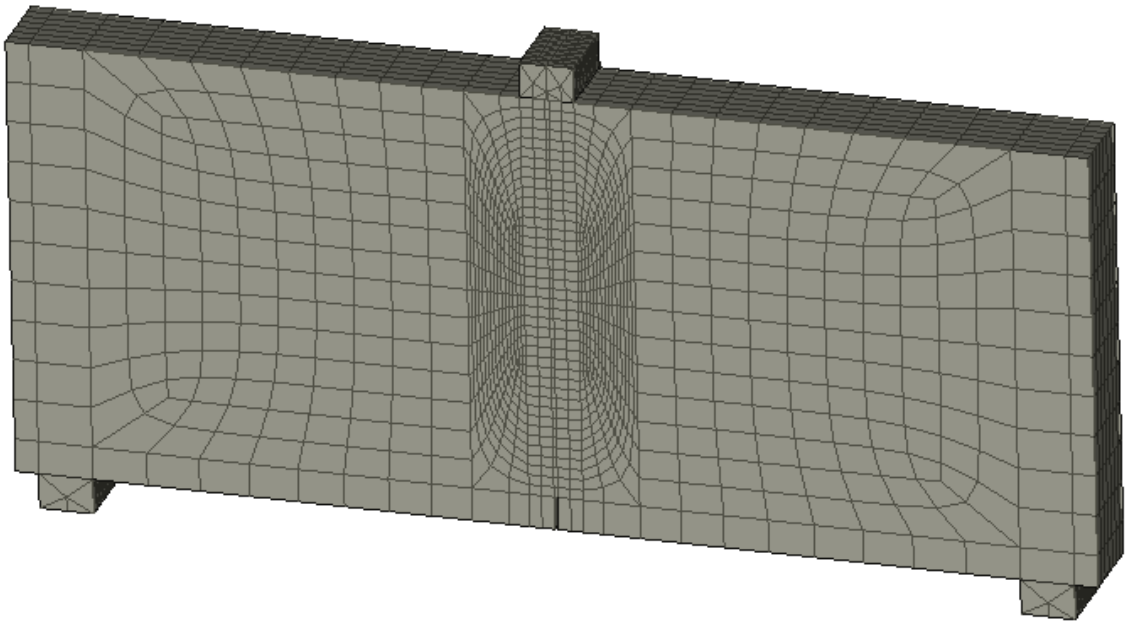

*Figure 6.19: Beam B, 40x215x517mm, notch depth α=7.5%*

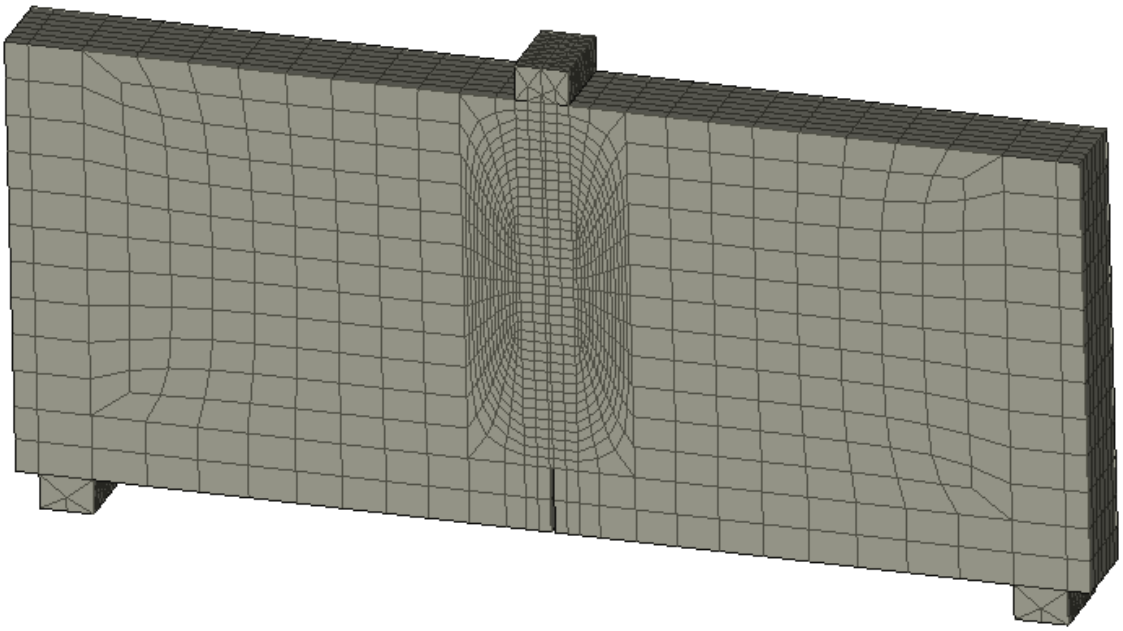

*Figure 6.20: Beam B, 40x215x517mm, notch depth α=15%*

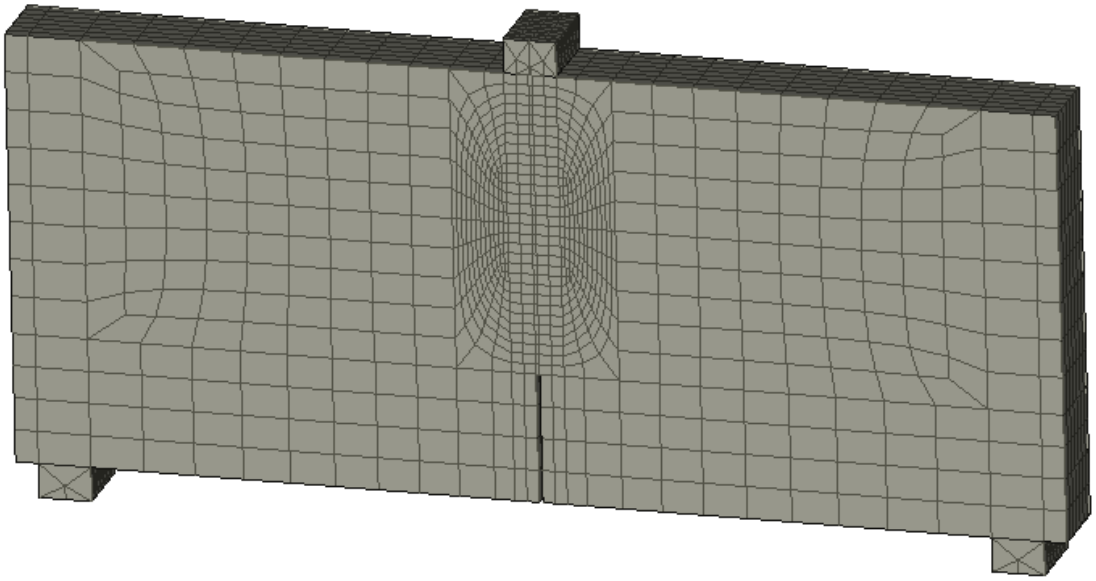

*Figure 6.21: Beam B, 40x215x517mm, notch depth α=30%*

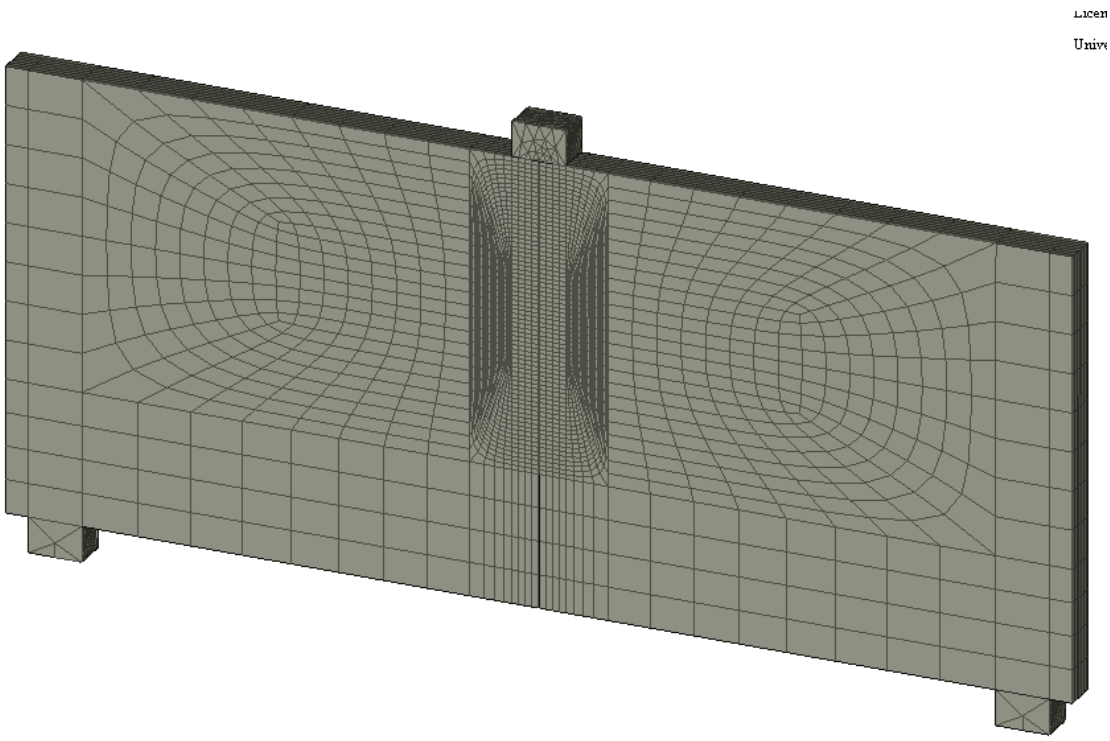

*Figure 6.21: Beam A, 40x500x1200mm, notch depth α=30%*

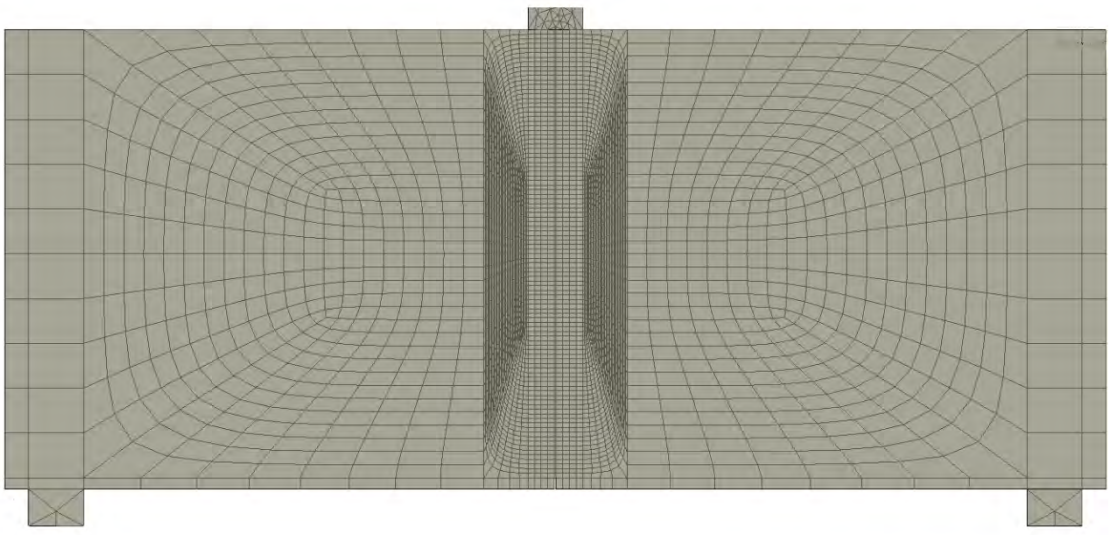

*Figure 6.21: Beam A, 40x500x1200mm, without notch.*

# Chapter 7

# MATERIAL MODEL CALIBRATION

## 7.1 Creation of graphics.

The objective of this research is to compare the curves found through the experimental data, done in the laboratory, with the curve obtained through the nonlinear analysis of the analytical model.

The first objective of the calibration is to create the graphics which will later they will be compared with the other graphics. The diagrams are nominal stress $\sigma_N$ versus nominal strain $\varepsilon_N$ with the first one in the ordinate and the second one in the abscissa. When the process of nonlinear analysis is finished, ATENA returns an output file with the results of what was required in the input file. The data necessary for reaching the graphics was obtained by *Microsoft Excel*. The procedure is identical for both the tests. The output file was opened in Microsoft Excel and the formula to obtain the data necessary to draw the graphics was reproduced. The graphics were drawn by the program *Grapher 8.* It is a specific program for drawing the graphics. The method to compare the two curves is very simple, it consists of putting the founded curve on top of the curve that is already known

### 7.1.1 Unconfined compression test

The output file of unconfined compression returns two values for each step. The first one is a reaction, that represents the force applied on the step in question, and the second one is a displacement, that represents the shortening of the specimen. After arranging the values in a table, it was possible to obtain the curves sought. The

formula (7.1) obtains the values of nominal stress, where *k* is a coefficient equal to one, *D* is the mean of the specimen dimension in the respective axis, and *F* is the Force obtained from the output file.

$$\sigma_N = \frac{kF}{D^2} \tag{7.1}$$

To obtain the nominal stress the formula (7.2) was applied, where *D* is always the dimension of the specimen and *u* is the shortening of the specimen.

$$\varepsilon_N = \frac{u}{D} \tag{7.2}$$

Both the formulas were applied for each step, in this way the values for the curve nominal stress-nominal strain to compare with the curve nominal stress-nominal strain reached from the experimental were found.

### 7.1.2 Three-point bending test

The output file from the three-point bending returns two different kinds of values. The prescribed deformation along the thickness was put on the top of the beam, precisely above the steel plate. Figure (7.1) shows how on the top of the steel plate there are 8 nodes. For each node the output file returns one value of the reaction that represents the force employed in the step in question. Summing each value we find the total force for each step.

After that, thanks to the formula (7.3) it is possible to find the nominal stress used in the graphics.

$$\sigma_N = \frac{6F(1-\xi)\xi l}{WD^2} \tag{7.3}$$

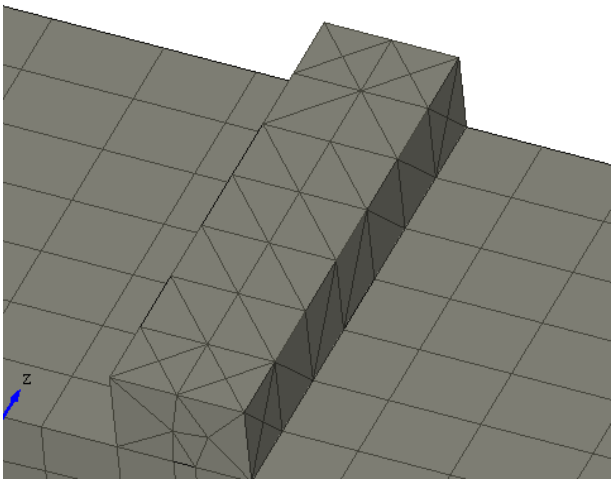


*Figure 7.1: Top of steel plate*

$F$ represents the sum of the force on each node, $\xi$ is the ratio of $x$ and $l$ and represents the eccentricity of the application of the force. $W$ and $D$ are the thickness and the height, respectively.

To obtain the displacement the procedure is a bit more complex. It is necessary to know the opening between two sides of the notch.

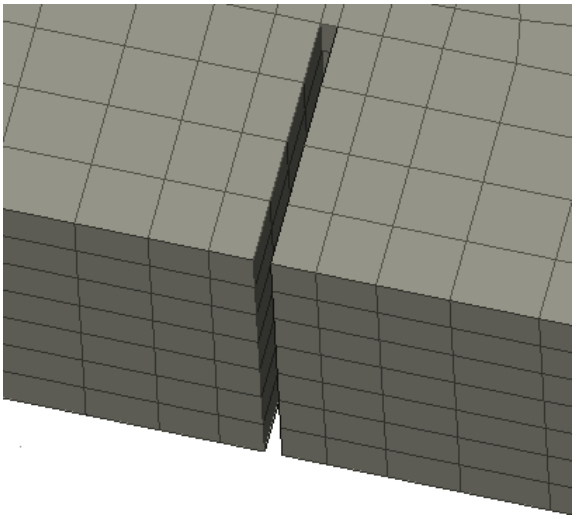

*Figure 7.2: Bottom of beam, notch depth*

Considering there are 8 nodes for each side along the thickness of the specimen, the output file returns eight values of the displacement for each side. Summing each

value with the value of the node in front of the node considered, and taking the average of these eight values finds the opening of the notch. It was done for each step and the result of this operation was used in the formula (7.4) to obtain the nominal strain.

$$\varepsilon_N = \begin{cases} \frac{\beta u}{g} \; for & \alpha = 0 \\ \frac{u}{D} \; for & \alpha > 0 \end{cases} \tag{7.4}$$

In the previous formula for α=0 , $g$ is the gauge length and $\beta$ is a correction factor to explain the linear moment distribution between the extensometer feet with spacing $g$ by converting the average measured strain to peak strain in mid-span.

## 7.2 Numerical calibration

Modeling of a structure with a nonlinear analysis usually involves multiple choices of constitutive relationships and modeling approaches. The variety of the choices demonstrates the versatility of the tools, but, at the same time, it can greatly complicate the validation procedure, because each combination of constitutive relationships and modeling approaches will usually produce different predictions.

To understand the meaning of the Calibration, it is important to define the meaning of *Computation model,* that can be definite like a specific non linear analysis with the selected behavioral model, constitutive relationships, and modeling approach.

This definition is especially useful when a specific set of constitutive relationships and modeling approaches is determined *a priori.* Since it would be hardly feasible to consider all possible combinations to draw conclusions about a nonlinear analysis, the first step in the model validation procedure should be *model calibration.* It is possible definite as "The process of adjusting numerical or physical modeling parameters in the computational model for the purpose of improving agreement with experimental data."

It is important to note that the model calibration is not the process of finding the modeling parameters which give the best agreement with experimental data of structural level, but, it is the process to find parameters which are most suitable values in basic material level. Therefore, the calibration of material models is the task of model developers or researchers.

In the experimental observations and model predictions, the specimens are identified by their own parameters. Usually, computational models use only selected parameters of which the effects are considered to be significant in defining physical behavior out of all available parameters from experiments

In this study, the definition of calibration refers to the *selection* and *tuning* of material property relationships and the model adjustments that are often made to obtain a good fit between the measured and predicted overall-response of a laboratory test structure were not made. It was possible to select the most appropriate set of material models, but to modify the details of selected material models was not allowed. In ATENA, the freedom is limited by the program itself.

The responses of the proposed model are dependent upon several parameters, including three material parameters, i.e., the uniaxial compressive strength $f_c$, the (macroscopic) initial tangent modulus $E$ as well as the (initial) Poisson's ratio ν and other dimensionless parameters defined on the fracture-plastic constitutive model.

For the calibration of that material model, several parameters were studied, each one has a specific position in the behavior of concrete. For each parameters the most suitable value was found.

.The calibration of this material model is a repetitive process that consists in setting the parameters in the input file, and once obtained the curve for the specimen in question, compare it with the curve obtained from experimental data, and then assess which parameters will be changed in the research of the most suitable value for each of these.

Not being able to calibrate the material model for each laboratory test, it was necessary to choose a small number of tests to be calibrated and subsequently the validation on the other remaining tests was made. In the selection of tests to calibrate, the most appropriate in terms of size and also based on the solution that each specimen provides must be considered.

Therefore it was decided the calibration of the model would be done on one kind of specimen for the three point bending test and unconfined compression test. The specimens chosen are *beam C* with the characteristic shown in the table (7.1) and the cube 40x40 mm.

Once suitable values of the parameters regarding the three-point bending curve were found, the next step was setting the curve regarding the unconfined compression of the cube. In this time a repetitive process was started that consisted of proceeding from the unconfined compression curve to three-point bending curve. It was necessary to do it in that way because the purpuse is to find the best values for both tests, the best matching curve, as similar as possible to the experimental data curve. Therefore, when a good curve was found for the three-point bending test but an unsuitable unconfined compression curve with the same value, it was necessary to come back to three-point bending test and change the value again to be able to find a more suitable match.

| ***Specimen C** (mm)* | |
|---|---|
| *Thickness,W* | 40.0 |
| *Height,D* | 92.8 |
| *Length,L* | 223 |
| *Span,l* | 202 |
| *Gauge length,g* | 12.7 |
| *Loading block width,w* | 11 |
| *Loading block height,h* | 10 |

*Table 7.1:Beam C, characteristic.*

The first step was to analyze and study the curve of the three point bending test and later examine the unconfined compression. The calibration of these tests can't be done separately because these two tests are interrelated to each other and the parameters used on one tests have to be verified in the other test. In this way it is possible to find the best value combination for each test.

After reproducing the curve, it was put on top of the experimental test curve to compare them.

In the beginning, for the first attempt, the values of the parameters given by the program ATENA were used, having used the specific compressive strength $f'_c$ =31Mpa.

The default values from ATENA are shown in the table (7.2) and the curve found is shown in the figure (7.3).

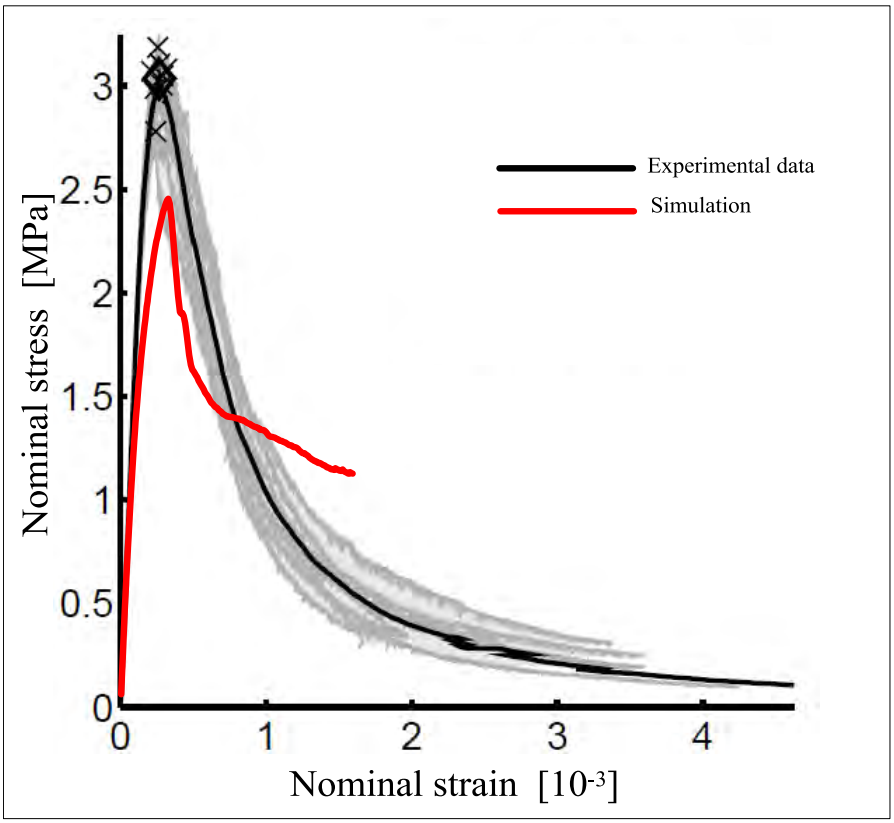


Figure 7.3: Curve obtained with *3D Nonlinear cementitiuos 2 default values*

| *3D Nonlinear cementitiuos 2* | | |
|---|---|---|
| Material type | Units | |
| *BASIC* | | |
| Elastic modulus $E_C$ [Gpa] | [Gpa] | 30.73 |
| Poisson's ratio | | 0.172 |
| Compressive strength $f_c$ | [Mpa] | -26.35 |
| Tensile strength $f_t$ | [Mpa] | 2.368 |
| *TENSILE* | | |
| Fracture energy $G_f$ | [MN/m] | 5.921E-05 |
| *MISCELLANEOUS* | | |
| Fixed crack model coefficiet | | 1 |
| Fail.surface excentricy | | 0.52 |
| Specific material weight ρ | [MN/m$^3$] | 2.300E-02 |
| Coefficiet of termal expanzion α | [1/K] | 1.200E-05 |
| Multipler for the plastic flow dir β | | 0.0 |
| *SHEAR* | | |
| Crack shear Stiff. Factor $S_F$ | | 20 |
| Aggregate size | [m] | 0.01 |
| *COMPRESSIVE* | | |
| Critical compressive displacement $W_d$ | [m] | -5.00E-4 |
| Plastic strain at compressive strength $\varepsilon_{cp}$ | | -8.574E-04 |
| Reduction of comp. strength due to cracks $r_{c,lim}$ | | 0.2 |

*Table 7.2:Default value of 3D Nonlinear cementitiuos 2*

It was noted that the value of Elastic modulus *E* is lesser than the value advised from the experimental test. ATENA uses the formula (7.5) to calculate the Elastic modulus, for the experimental tests the formula (2.1) was used instead.

$$E = (6000 - 15.5R_{cu})\sqrt{R_{cu}}\frac{f_F}{f_l^2} \tag{7.5}$$

In this way the tensile strength $f_t$ and the compressive strength $f_c$, calculated with (7.6) and (7.7) respectively, also have lower values.

$$f_t = 024{R_{cu}}^{2/3}\frac{f_F}{f_l^2} \tag{7.6}$$

$$f_c = -30\frac{f_F}{f_l^2} \tag{7.7}$$

The curve found with these values is totally incorrect. The pick of the crack is very low compared with the pick from the experimental data, there is about 0.5 MPa of nominal stress difference between the two curves. For both curves the nominal strain of the pick is the same

After that, the real process of the calibration was started, with the goal to find the best value for each parameter and research the more suitable curve. The research for the best value is not an easy process, because often the parameters are connected to each other and changing one, changes another. The first thing to understand is how the curve changes when adjusting the value for each parameter. Many attempts for researching the best value for each parameter were done.

Every parameter has a different influence on the curve. In this chapter every effect for each parameter will be shown, however to bring some important examples, in the three point bending, the tensile strength  defines the peak, the fracture energy and the parameter $\beta$ define the slope of the post-peak curve, the Elastic modulus changes the degree level of the peak . For the unconfined compression other significant examples are the influence of the compression strength that defines the peak, and the parameter $w_d$ (Critical compressive displacement) that defines the slope of the post-peak.

In the following each parameter and it's correlations will be studied. The calibration procedure has been done in the following way: first we analyzed the behavior of the curve for the three-point bending and then we verified if the decisions made were also correct for the unconfined compression. If not, we turned back and changed

again the value of the parameters for the three-point bending and then rechecked on the unconfined compression.

Once we found good values for the three-point bending, we went to set values for the parameters in the unconfined compression and then performed the same procedure done before and it occurred that the values used in unconfined compression are also good for the three point bending. This process took a long time because a lot of attempts had to be performed to search for the most suitable values for both tests.

During this calibration process, the influence that each parameter has in the two tests analyzed has been studied, understanding how the curves change and looking for correlations between the various parameters and between the two tests.

Studying the parameters it was noticed that some are correlated. For the three point bending the $\beta$ and $G_f$ parameters are correlated and hence the difficulty is to find the best pairing in order to obtain a curve as close as possible to the one obtained from the experimental data. These two parameters are also very influential in the unconfined compression, and in this chapter their influence to this test will also be shown.

After many attempts two principal ways to follow with two different matches of the parameters were found. The first one is with $G_f = 9.5\text{x}10^{-5}$ [MN/m] and $\beta = -0.09$ called *curve A* and the second one with $G_f = 9.0\text{x}10^{-5}$ [MN/m] and $\beta = -0.09$ called *curve B*. Therefore the problem now was to find the best fitting values for each curve and decide which one is suitable. Through the unconfined compression It was tried some time and it was see that the curve B needs value of compression strength higher that the curve A. For each curve was found the exact value for having a correct peak. For the curve A the result was -43 MPa and for curve B was -46 MPa. Seeing the characteristic of this batch of concrete it was noticed the value of the curve B is more suitable. In table (7.3) the values used for each parameter for the curve A and the curve B are shown.

| *3D Nonlinear cementitiuos 2* | | *Curve A* | *Curve B* |
|---|---|---|---|
| Material type | Units | | |
| *BASIC* | | | |
| Elastic modulus $E_C$ [Gpa] | [Gpa] | 41.29 | 41.29 |
| Poisson's ratio | | 0.172 | 0.172 |
| Compressive strength $f_c$ | [Mpa] | -43.00 | -46.00 |
| Tensile strength $f_t$ | [Mpa] | 3.00 | 3.00 |
| *TENSILE* | | | |
| Fracture energy $G_f$ | [MN/m] | 9.50E-05 | 9.00E-05 |
| *MISCELLANEOUS* | | | |
| Fixed crack model coefficiet | | 1 | 1 |
| Fail.surface excentricy | | 0.52 | 0.52 |
| Specific material weight ρ | [$MN/m^3$] | 2.300E-02 | 2.300E-02 |
| Coefficiet of termal expanzion α | [1/K] | 1.200E-05 | 1.200E-05 |
| Multipler for the plastic flow dir β | | -0.09 | -0.20 |
| *SHEAR* | | | |
| Crack shear Stiff. Factor $S_F$ | | 20 | 20 |
| Aggregate size | [m] | 0.01 | 0.01 |
| *COMPRESSIVE* | | | |
| Critical compressive displacement $W_d$ | [m] | -1.500E-5 | -1.700E-5 |
| Plastic strain at compressive strength $\varepsilon_{cp}$ | | -8.574E-04 | -8.574E-04 |
| Reduction of comp. strength due to cracks $r_{c,lim}$ | | 0.2 | 0.2 |

*Table 7.3:Values used for curve A and curve B*

Figure (7.4) shows the difference between the curves A and B in the three-point bending and figure (7.5) shows the difference between these two curves for the unconfined compression. Analyzing the difference between the two curves in the three-point bending, it can be noticed, how for both curves, the peak coincides with the curve obtained from experimental data, this is because both have practically a value of identical tensile strength, which is the parameter that determines the position of the peak.

Looking instead at the trend of the curve in the post-peak, we note how the curve A is closer to the curve obtained by experimental data and this is due to the fact that for curve A we used higher values of β and $G_f$ than those used in the curve B.

Another important difference between the two curves is the difference of the value used for the compression strength. This parameter is also strongly connected with the β parameter. You can observe this correlation in the unconfined compression, where, for a higher value of compressive strength (in absolute value, whereas the compressive strength is negative) we need a lower β value. In fact, looking at the difference between curve A and B in the unconfined compression, one can notice that the peak is almost the same although the values of the compressive strength are different.

This is precisely due to coupling with the value β just described. Always looking at the graph between the difference of the curves in unconfined compression one can notice how for the two curves the post-peak behavior is different. In this test, the post-peak behavior is governed by the parameter WD where by doing a series of tests it was found that lower values tend to increase the slope of the curve. However, we should be careful because here too, the coupling takes over with other parameters and however if the values WD are too high there is a risk that the analysis does not converge and stops before. Between the two curves the values WD are very similar differing only by a value equal to 0.2, however, it can be seen for the curve B that the inclination of the latter is more accentuated and better compared to the 'inclination of the curve A which tends to enlarge in post-peak and shortly after stops due to problems of convergence of the solution.

The next step was to decide which of the two is the best way to perform validation. This choice should be made considering also the results from experimental data. A first consideration that can be made is that the curve B is better because it has a higher value of compressive strength and therefore similar to values found from experimental data.

One consideration that must be to the detriment of curve B is that it has a low value of the parameter β, and this parameter is difficult to calibrate and would therefore need more tests to determine it. In fact, in this calibration, it would be better not to modify or change this parameter too much. Regarding the value of the fracture

energy $G_f$, curve A would be more appropriate because it is closer to the value of 96.94 obtained from experimental data as in fact it can be seen from the graph in figure (7.4) where curve A is closer to the curve obtained from experimental data. To obtain a correct decision in the choice between curve A and curve B some proof of validation was also made and tuning of parameters in the three-point bending but with a different dimension.

The size that was considered is the beam D. After a careful analysis and a series of validation tests for other types of samples as well, it was decided that the values of curve B are more correct and better reflect the results obtained with experimental data.

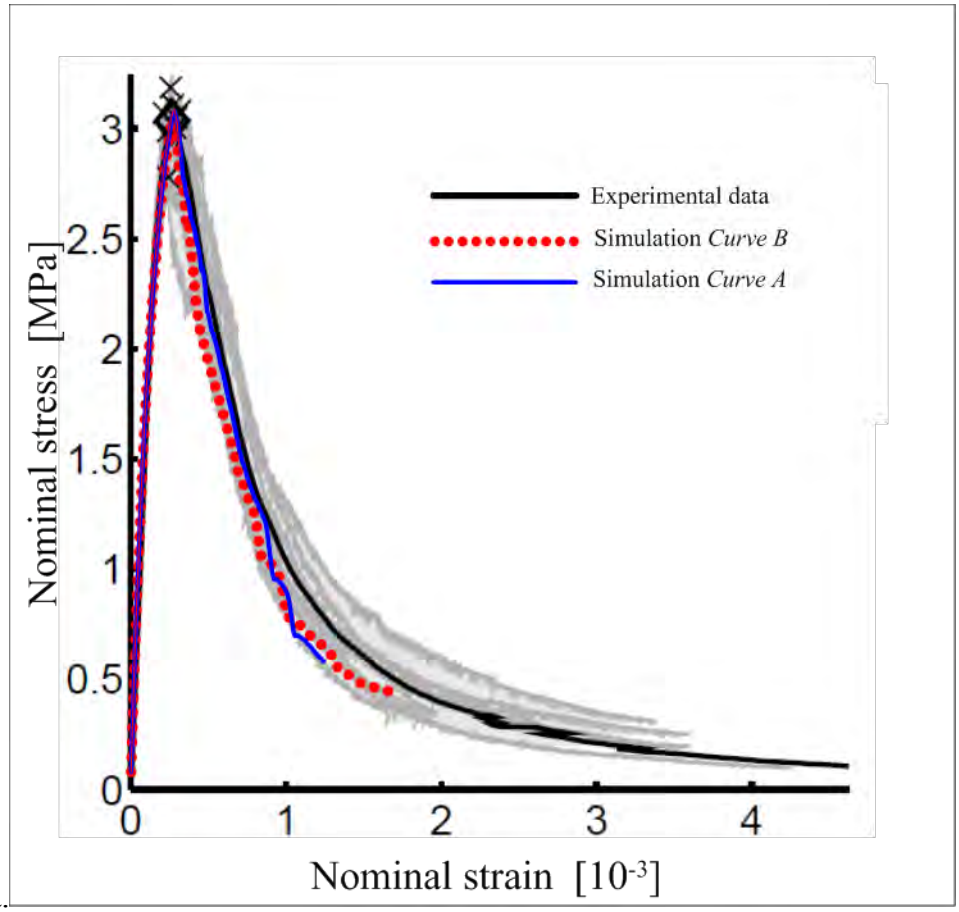


*Figure 7.4: Curve A and Curve B differences in three-point bending test*

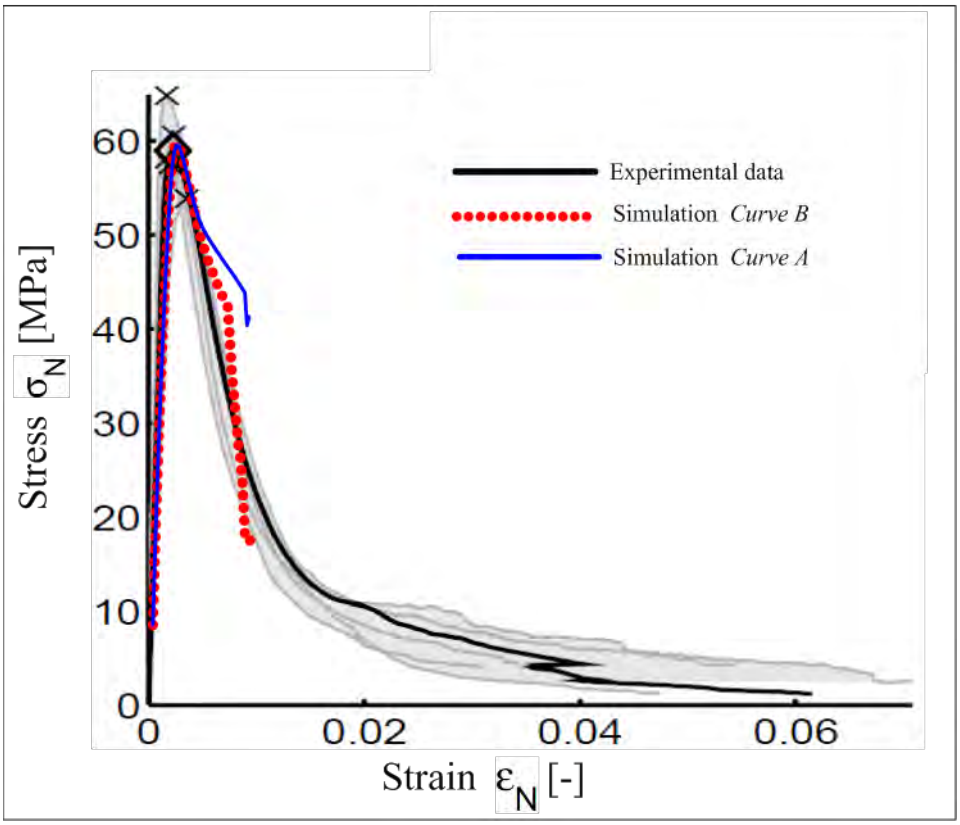


*Figure 7.5: Curve A and Curve B differences in unconfined compression test*

## 7.3 Parameters analysis

Throughout the calibration, a parametric analysis for each parameter considered was carried out in order to understand how each one influenced the shape of the curve. To better understand the calibration done, in this chapter this parametric analysis will be shown and each parameter will be assessed individually.

The correlation between the various parameters will also be shown. For each parameter, its influence both in the case of three-point bending and for the unconfined compression will be shown. The comparison between the different values for each parameter will be carried out on curve B, determined as the best possible solution after a careful calibration.

### 7.3.1 Elastic modulus

The first parameter studied was the *Elastic modulus E.* The modulus of elasticity of concrete is a function of the modulus of elasticity of the aggregates and the cement matrix and their relative proportions. The modulus of elasticity of concrete is relatively constant at low stress levels but starts decreasing at higher stress levels as matrix cracking develops. It is a very important mechanical parameter reflecting the ability of the concrete to deform elastically

The elastic modulus is a property of a material which tells how much tension is needed to make it a little bit longer or shorter. Normal concrete mixture has an E-modulus of 25-30 Gpa Please note that the higher the E-module, the higher peak stresses will become, Which means that the higher the E-module in concrete, the sooner cracks will appear. If you get a really weak E-module, it will bend more. It this case the Elastic modulus is higher, because from the experimental test for the three point bending used, the value is 41,129 Gpa.

Figure (7.6) shows the difference of the curves with the different Elastic modulus. In this picture the default parameters given from ATENA and the same parameters but with the Elastic modulus changed are compared. It shows how changing one parameter, the curve doesn't change so much, but it is possible to see how the pick is moved up. The reason is the influence of the Elastic modulus, where greater values raise the pick of the curve.

It is also important to differentiate *elastic hardening* from *plastic hardening*. *Elastic hardening* corresponds to the stiffening of the material due to the closure of porosity, which corresponds to an increase of the elastic modulus of concrete experimentally.

The knowledge of the modulus of high-strength concrete is very important in avoiding excessive deformation, providing satisfactory serviceability and achieving the most cost-effective designs. The next step was to keep the same value of the Elastic modulus and research the best suitable values for the other parameters.

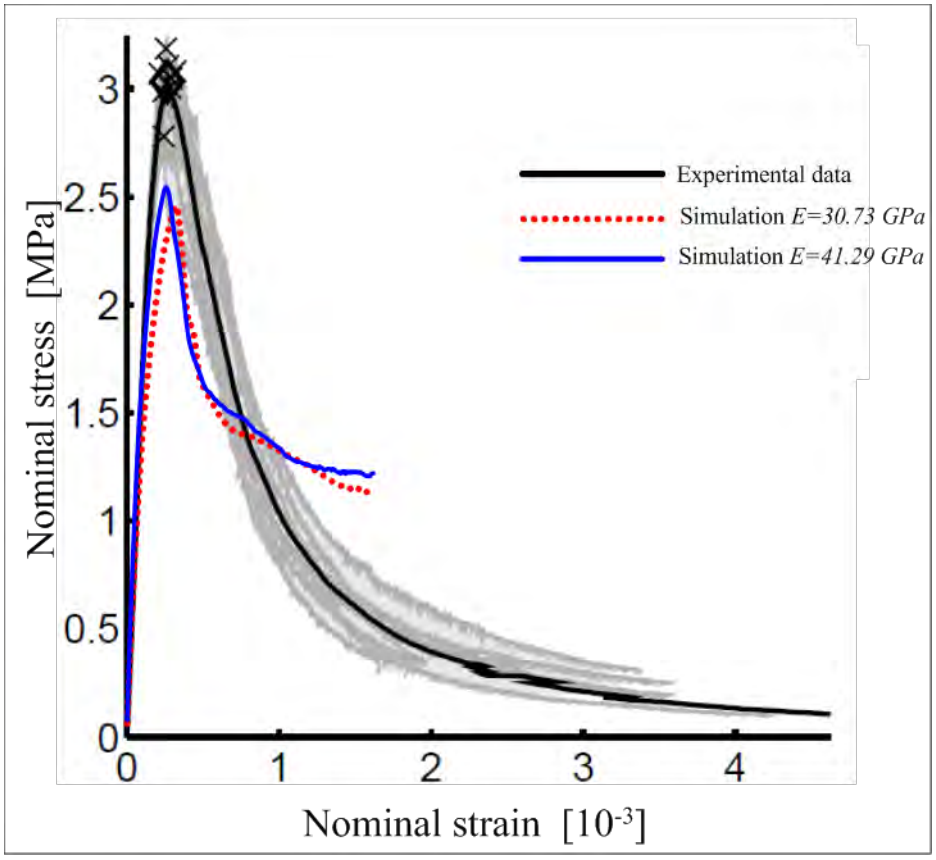


*Figure 7.6: Three-point bending test, different values of Elastic modulus.*

### 7.3.2 Tensile strength

The next parameter studied was the tensile strength. It is one of the basic and important properties of the concrete. It is one of the most significant parameters for the three-point bending because it helps to define the exact point of the pick. The tensile strength of normal concrete may vary within a wide range depending, among other parameters, on the shape and surface texture of the aggregate. The concrete is not usually expected to resist the direct tension because of its low tensile strength and brittle nature. However, the determination of tensile strength of concrete is necessary to determine the load at which the concrete members may crack. Although concrete is not normally designed to resist direct tension, the knowledge of tensile strength is used to estimate the load under which cracking will develop. This is due to its influence on the formation of cracks and its propagation to the

tension side of reinforced concrete flexural member. In most cases member behavior changes upon cracking. So tension strength of concrete is also considered in proportioning concrete member.

Tensile strength can be estimated from the compressive strength using the following equation:

$$f_t = k_t(f_c)^n \tag{7.7}$$

Where $k_t$ and $n$ are two coefficients. Some studies suggest the value $n$ = 0.57. Coefficient $k_t$ depends only on the nature of the aggregate and has to be calibrated using known results. It varies from about 0.35 for limestone aggregates to 0.45 for flints or basalts, on sealed specimens. For some specimens cured in water, coefficient $k_t$ slightly increases.

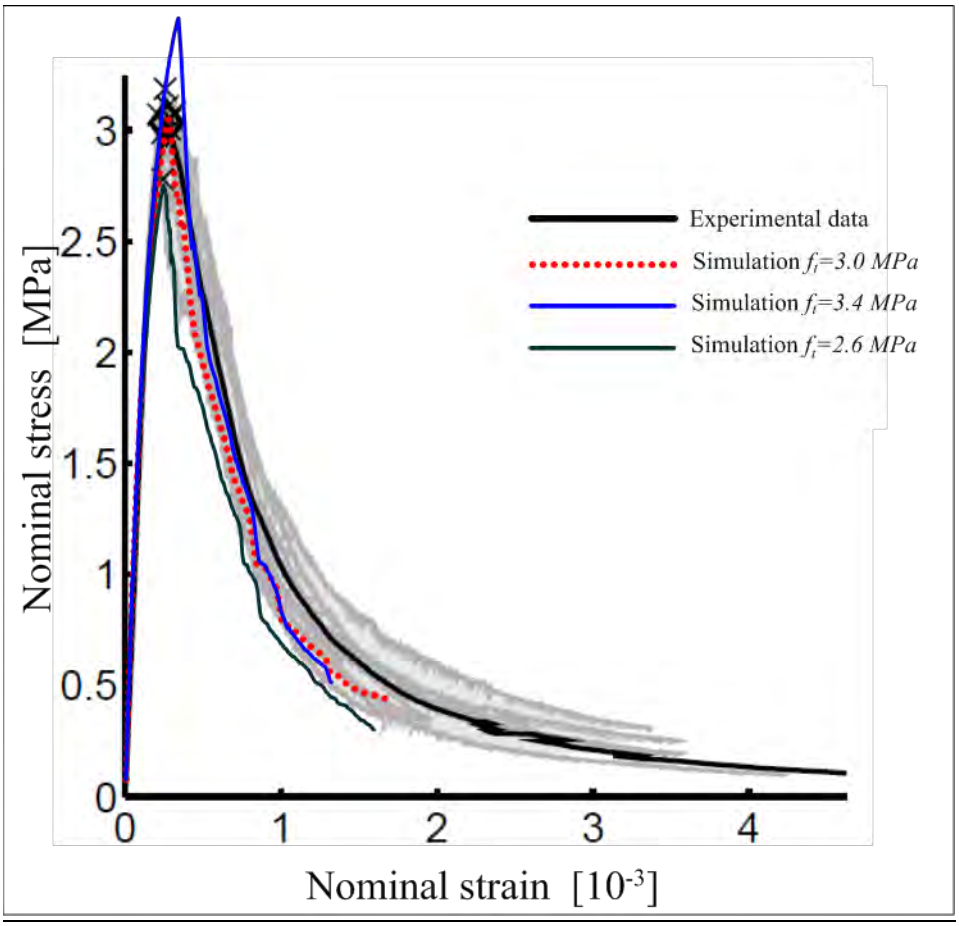


*Figure 7.7: Three-point bending test, different values of Tensile strength.*

The ratio between tensile strength and compressive strength is an important material property of concrete. The value of this ratio is required for some applications. the ultimate strain value in uniaxial tension is expressed in terms of this strength ratio. The tensile strength of concrete is relatively low, about 10 to 15% of the compressive, occasionally 20%.

The default value of tensile strength given from ATENA is very low if compared with the Elastic modulus obtained from the experimental data. This aspect brings the thought that the real value is higher. Therefore for the Calibration of these parameters higher values were researched and after some attempts it was found that a suitable value is around 3 MPa. To understand how the value of the tensile strength changes the curve, especially the peak, in Figure 7.7 three curves with three different values of it are shown. It is possible to see how for high values of tensile strength the peak is higher, this means that for breaking the specimen a greater force is needed.

### 7.3.3 Fracture energy

Another important parameter to trace the curve stress-strain is the *fracture energy* $G_f$. The fracture energy is defined as the amount of energy necessary to create one unit of area of a crack. It is a material property and does not depend on the size of structure. This can be well understood from the definition that it is defined for a unit area and thus influence of size is removed. Fracture energy can be expressed as the sum of surface creation energy and surface separation energy. Fracture energy is found to be increasing as we approach crack tip. Fracture energy is a function of displacement and not strain. Fracture energy deserves prime role in determining ultimate stress at crack tip. The area under the curve represents the amount of energy that is consumed by the crack when it grows through the beam (corrections have to be made for the energy supplied by the weight of the beam). ATENA calculates the fracture energy with the formula (7.8).

$$G_f = 0.000025 f_t \tag{7.8}$$

During the experimental data two kinds of fracture energy were found. The initial fracture energy, with the value of 51.87 N/m and the total fracture energy with the value of 96.94 N/m. the second value could have errors and the calibration also needs to find a suitable value for it. After the exact point of the pick is found, some attempts were done changing the value of fracture energy for searching the post-peak curve that follows the curve given from the experimental data as much as possible.

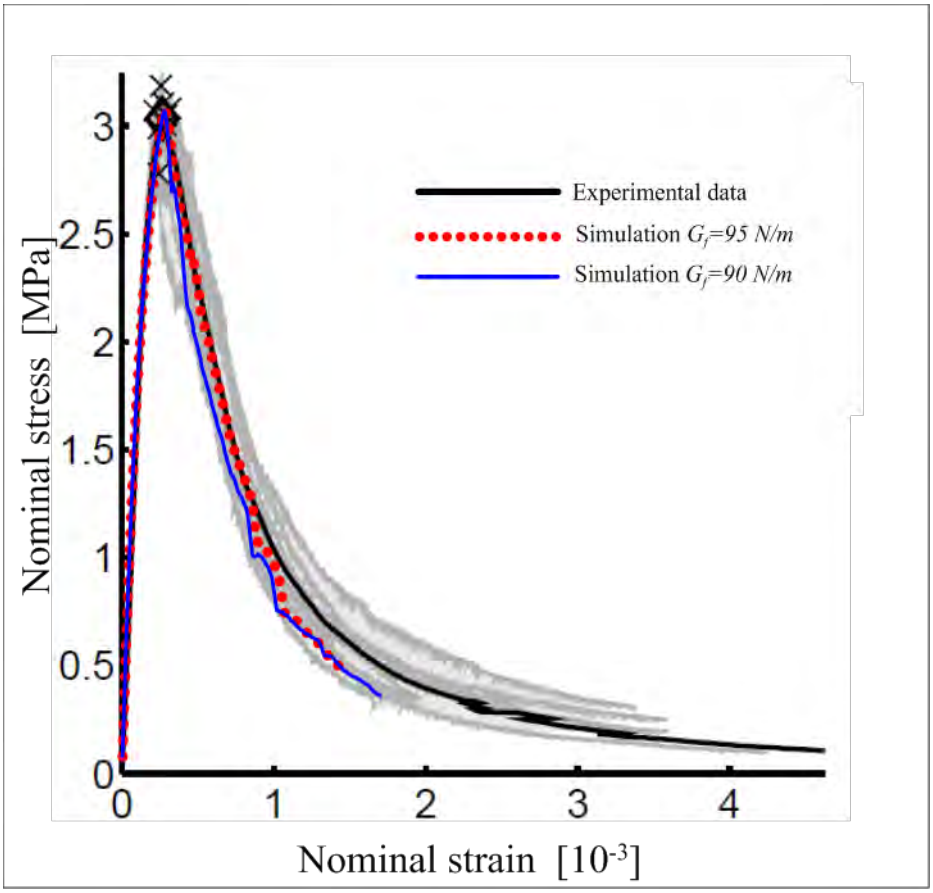


*Figure 7.8: Three-point bending test, different values of Fracture energy*

### 7.3.4 Multiplier for the direction of the plastic flow

A parameter useful for obtaining the right slope of the curve is $\beta$. It represents the multiplier for the direction of the plastic flow. The calibration of this parameter is very difficult because it needs a specific experiment to predict the right value. The plastic potential controls the plastic flow, and uses a model parameter, which for positive values means volume expansion and for negative material compaction during the compressive crushing.

When $\beta < 0$ it means that the material is being compacted during crushing, when $\beta > 0$ the material is dilating instead. If $\beta = 0$ the material volume is preserved. In the Figure7.9 it is possible to see how $\beta$ influences the trend curve. If it uses 0.0 the slope curve is wrong, it is too high and using values below -0.25 the execution was killed due to violation of the step divergence criteria. After some attempts were made it was noticed that the suitable value is between -0.1 to -0.2, and the choice also depends on the other parameter. The $\beta$ parameter is correlated with the fracture energy. For high values of $G_f$ (around 9.50E-05), $\beta$ has to be about -0.1 to keep the slope of the post-peak curve similar to the experimental data curve, instead for smaller values of $G_f$ the value of $\beta$ has to be -0.2.

The analysis was conducted for several combinations of $\beta$ and $G_f$. the best matching parameter sets were $\beta$= -0.2 and $G_f$ = 9.0E-05.

The parameter $\beta$ is also very influential in the unconfined compression. As you can see in fig (7.9) for a higher value of $\beta$, the peak tends to move upward with a stress of about 10 MPa higher than the optimum value that the peak should have. In this chart, it can also be noticed how, after the peak the curve with a greater value of $\beta$ tends to expand more and have greater strain.

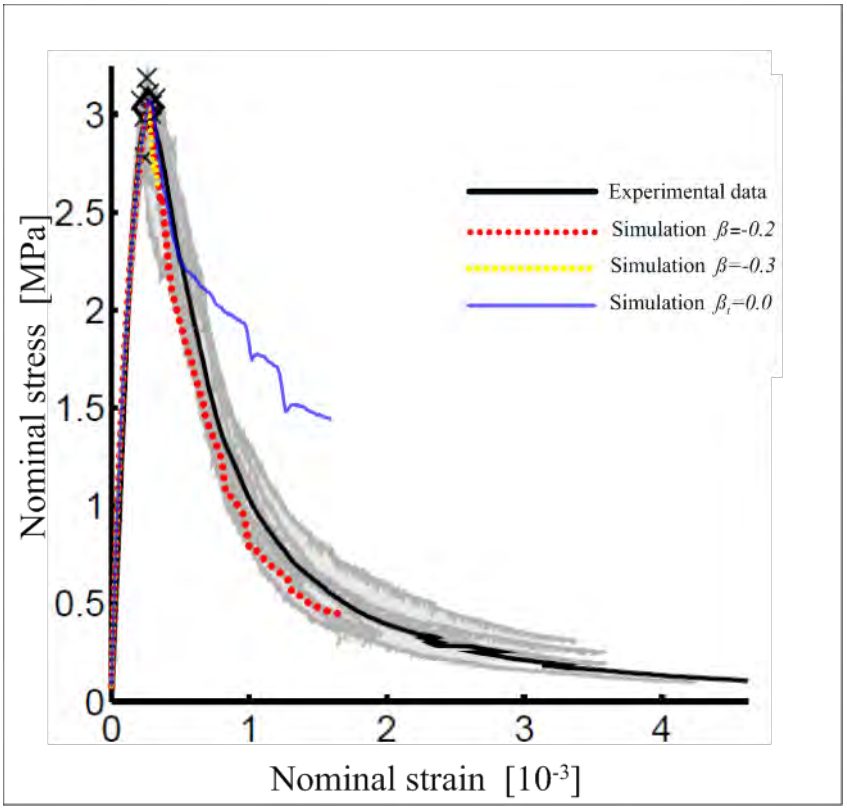


*Figure 7.9: Three-point bending test, different values of β parameter.*

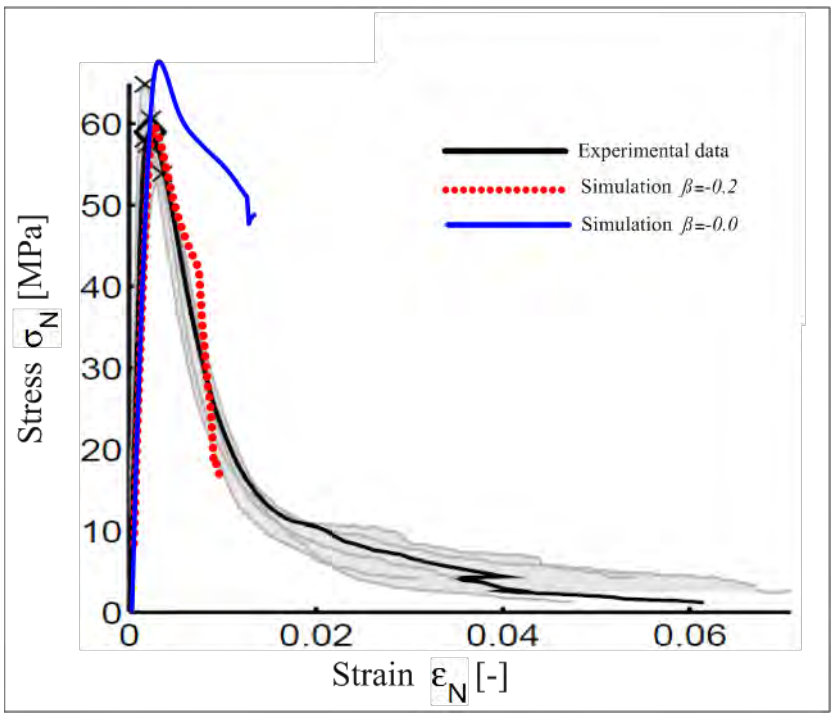


*Figure 7.10: Unconfined compression test, different values of β parameter.*

### 7.3.5 Compressive strength

The more important parameter of this curve is the compressive strength. Compressive strength of concrete is the utmost important which gives an idea about all the characteristics of concrete. There are many factors which control concrete compressive strength. Concrete mix proportioning, aggregate quality, aggregate gradation, type of cement, mixing and placing method, concrete curing and curing temperature and the most important one is the water cement ratio. Water cement (W/C) ratio has a critical impact on concrete strength characteristics. A minimum amount of water is necessary for proper chemical reaction in the concrete and extra amount of water increases the workability and reduces strength.

By this single test one can judge whether Concreting has been done properly or not. For the cube test one type of specimen cubes was analyzed, with the size 40x40 cm.

The compressive strength is measured by breaking cube concrete specimens in a compression-testing machine. The compressive strength is calculated from the failure load divided by the cross-sectional area resisting the load and reported in units of megapascals (MPa). Compressive strength test results are primarily used to determine that the concrete mixture as delivered meets the requirements of the specified strength, $f'_c$, in the job specification.

The first problem that arises in the calibration of this test was the determination of compressive strength. To understand how influential the compressive strength is in the unconfined compression, in figure (7.10) three curves with three different values of the compressive strength are shown. Seeing it, it is possible to understand how the position of the peak changes, while for higher values of compression strength it has higher values of nominal stress.

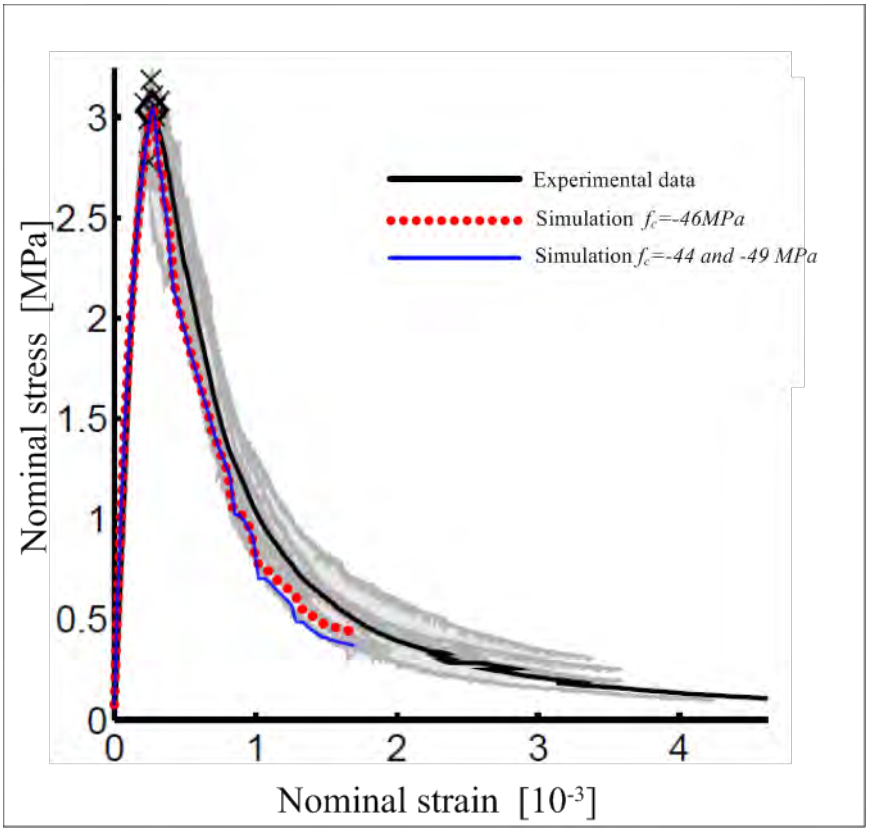


*Figure 7.11: Three-point bending test, different values of compressive strength*

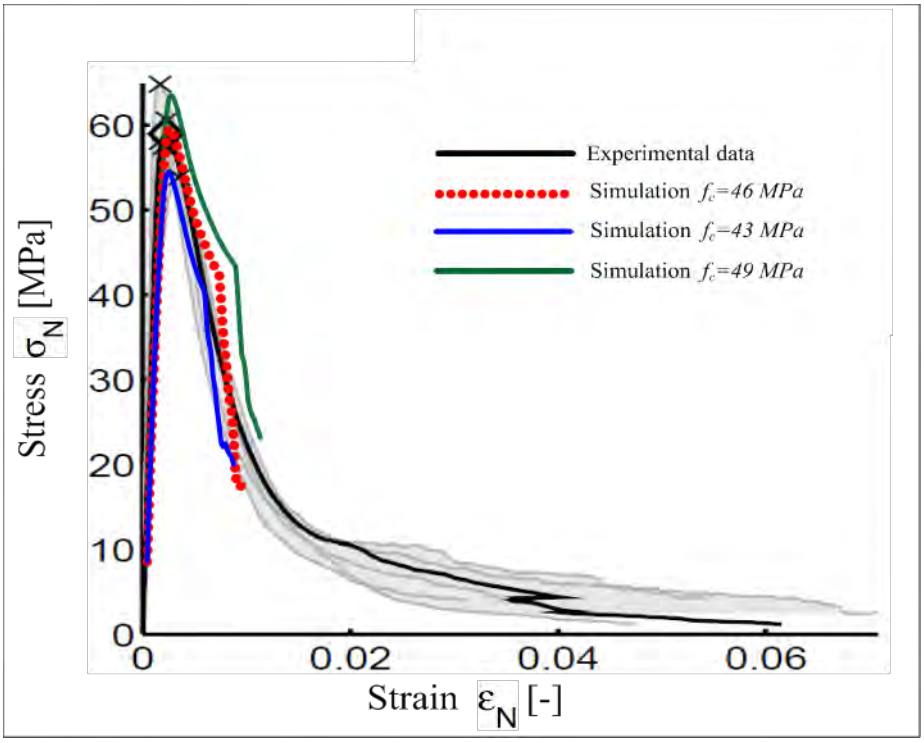


*Figure 7.12: Three-point bending test, different values of compressive strengt*

### 7.3.6 Critical compressive displacement

In unconfined compression, there is another parameter that governs the trend of the curve, this is the critical compressive displacement $W_D$ which has a strong influence in the trend of the post-peak curve but at the same time also affects the point of its peak. As shown in figure (7.11) for lower values of $W_D$, after the peak curve tends to widen and not to follow the right trend that it should have. Always to lower values, the formation of the peak occurs for higher values of stress, although not by much.

It is noted that this parameter is practically irrelevant in the three-point bending test.

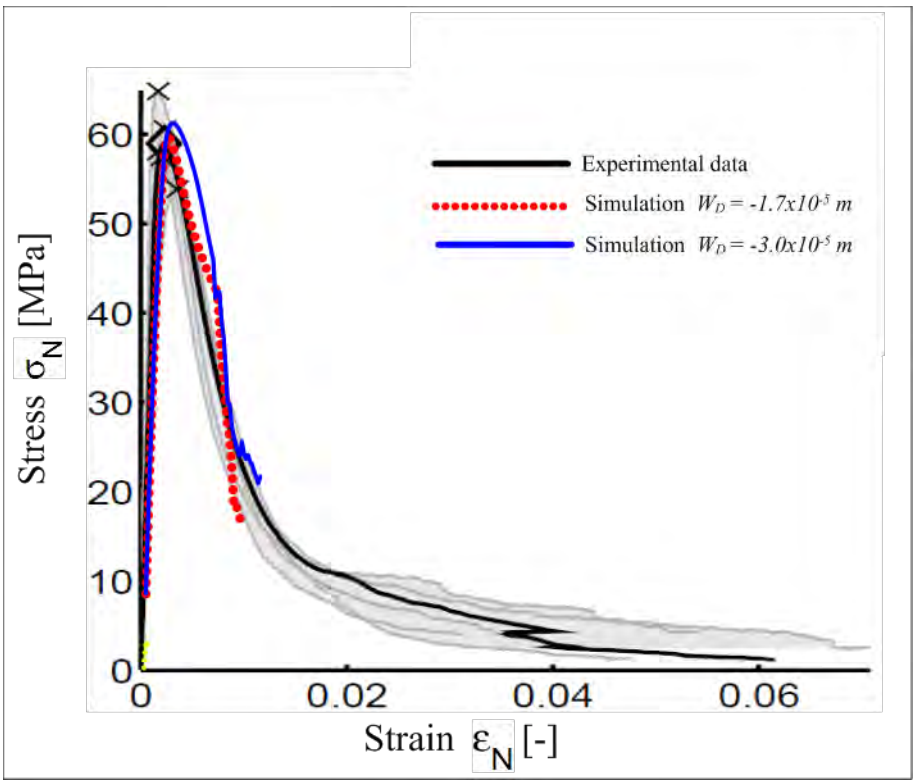


*Figure 7.13: Unconfined compression test, different values of $W_D$ parameter.*

# Chapter 8

# MATERIAL MODEL VALIDATION

In the validation procedure, the reality of interest is represented in terms of experimental data "A validation experiment is conducted for the primary purpose of determining the validity of a computational model.

During the last two decades, several organizations and research communities developed and proposed terminology and general concepts for model verification and validation.

A lot of the time the term *validation is* correlated with the term *verification.* These two terms have been used with ambiguous definitions among researchers and practitioners. Some disciplines have developed definitions for V&V, and the definitions by PCT60 of ASME (2006) are clear and useful:

*Verification:* "The process of determining that a model implementation accurately represents the underlying mathematical model and its solution, the essence of specifications for the simulation"

*Validation:* "The process of determining the degree to which a model is an accurate representation of the real world from the perspective of the intended uses of the model."

The objects of Validation and verification are the real world entity (concrete structure under experiment), the conceptual model for behavior (Fracture–Plastic Constitutive Model), and the computational tool (ATENA). Software verification is the evaluation of the accuracy obtained when the conceptual model is implemented in the computational tool. Conceptual model validation assesses the appropriateness

of the model to predict the real world entity's behavior. Validation utilizes physical testing to assess the suitability of the computational tool for predicting the behavior of the real world entity. These three Validation and verification activities require computer programming, modeling, analysis and experimentation.

Another important term is validation metrics. According to ASME (2006):

*Validation metrics:* "mathematical measures used to assess the accuracy of the simulation results with respect to experimental data. These metrics can take the form of an error norm or a statistical test between response features from the computational model and corresponding features from the experimental data."

The first step of any validation procedure is the identification and classification of the uncertainties. The possible sources of uncertainty associated with the model validation activity are listed below:

- Random nature of basic variables, such as the uncertain material properties.
- Measurement errors in experimental observations, such as noise in measurement apparatus, and errors from indirect measurements.
- Uncertain estimation of parameters of probabilistic distribution of basic variables.
- Inexact form or selection of basic variables in the computational or conceptual model.
- Statistical uncertainty by assumption on the probabilistic distribution of model outcome.
- Uncertainty of derived random variables from basic random variables, such as tensile strength of concrete derived from compressive strength.

Ideally, all uncertainties should be included in the model validation procedure for precise assessment of accuracy of model prediction. However, since the importance of each uncertainty varies according to the characteristics of physical phenomena

and corresponding computational models and experiments, not all types of uncertainties are included in the model validation procedures of current practice.

A probabilistic approach for model validation gives the level of agreement between experimental data and model prediction by the evaluation of confidence interval of experimental observation expressed in nonlinear regression model.

This approach estimates the accuracy of computational models by a comparison of deterministic model prediction with the estimated mean of experimental data. By this comparison, it is possible to provide a statistical measure of quantitative agreement between computational models and the experimental data.

In order to build up the validation, some fundamental assumptions were made in this approach. First, input variables were assumed to be measured the same as the experimental measurement. The variance of experimental observation coming from the model parameter uncertainty can be assumed to be negligible, and thus the variance analysis by propagation uncertainty becomes unnecessary. The expected value of a computational model is the model prediction at the mean values of model parameters. No variance is assumed in model prediction. Second, the experimental observation has uncertainty coming from measurement error. This uncertainty results in the uncertain location of the true mean of the experimental data.

In building a validation procedure for a specific computational model, the initial step should be to understand the model and the associated potential sources of uncertainties.

A computational model was selected to illustrate the proposed procedure, namely Fracture–Plastic Constitutive Model. This model incorporates several refined material models for structural concrete. The ATENA programs have tractable pre- and post-processors, and they can thus be used immediately in design offices.

In the model validation, it is often necessary to compare structural behaviors which are essential to evaluating the capability of the tools but difficult to be quantified.

For the model validation procedure to be more comprehensive and to avoid misleading, such aspects should be included in the model validation procedure. Among other such difficulties to quantify behaviors, this study deals with the aspects associated with cracking and failure modes to illustrate the importance of the qualitative comparison in the model validation. Cracking is one of the most important characteristics of structural concrete behavior; it is difficult to model individual cracks numerically because of the randomness of the locations and structural softening.

Another essential capability of nonlinear analysis to be evaluated is their ability to predict modes. In the design of concrete structure, not only accurate prediction of failure strength but also correct prediction of failure mode is essentially important because it is usually related to the ductility of failure. In general, a design goal is to ensure ductile failures to avoid unpredictable brittle failures. Therefore, if a computational tool fails to predict the mode of failure, it is unlikely to be a as a proper design tool. However, since the decision of the failure mode frequently involves the identification of the order of damage of materials, it is also difficult to quantify the failure mode, and thus qualitative comparison would be a better choice.

Since the beam is unreinforced, it may be expected that failure occurs at relatively low levels of load and reactions in supports. Thus, it may directly specify concentrated supports and loads, without a danger that these would cause local compressive crushing. The first objective is to trace the load-displacement curve up to the post-failure softening regime, and later, employing the exact formulas it is possible to reach stress-strain curve.

To this end, it may prescribe loading in terms of forces and use the arc-length method, which automatically changes the sign of load increment once a peak is attained. Alternatively, it may control displacement. Since displacement will keep on increasing even after the beam fails, we can employ either the Newton-Raphson method or the arc-length method. Due to its better stability, we opt for the Newton-Raphson solution method. Note that, for large or brittle beams, a snap-back behavior

may occur, in which case both displacement and force increments at the loading point change their sign upon failure. In such a situation, the arc-length solution is the only applicable method.

To speed up convergence of the solution, the full Newton-Raphson method was employed, with tangent stiffness updated in each iteration. To automatically adjust the speed of analysis according to the nonlinearity of the response, the line search method was utilized.

## 8.1 Three-point bending tests of beam C

The first valid dimension is the beam C. (93x40mm) having made the calibration on the beam with notch α = 30%, remained to validate the three remaining beams, the two with notch α =15% and α = 7.5% respectively and the un-notch beam. In figure you can see how for the un-notch beam the peak value is much lower than the one obtained through laboratory tests, and is in the rank of about a little less than 2 MPa.

We can say that the peak value is not in total agreement with the peak obtained in the laboratory and this will also be true for the other specimens without notch. Attempting to evaluate the performance of the post-peak curves obtained by the numerical computation, we note that this follows the curve obtained in the laboratory quite well even though the final part tends to rise and this suggests too high a fracture energy $G_f$ .

The beam C validation with the notch α = 7.5% is shown in Figure 8.2. Even in this case it can be noted how the peak is incorrect even if closer than the results obtained in the un-notch beam. In this case the peak is about 1 MPa lower than the one obtained through laboratory tests. The trend of the curve after the peak in this case is not the best, because the slope of the curve tends to grow significantly in the final part and does not reflect the seeking trend.

The validation of the beam c with notch α = 15%, shown in figure (8.3) is definitely the best of the beam C 's group. This is certainly due to this type of beam being very close to the beam calibrated, and having the same size but changing only the depth of the notch. This can be noted also when comparing how the curve with notch α = 30% obtained from calibration shows a trend very similar to the one obtained by the validation. Both the curves in fact follow the respective curves obtained from laboratory tests just below their progress.

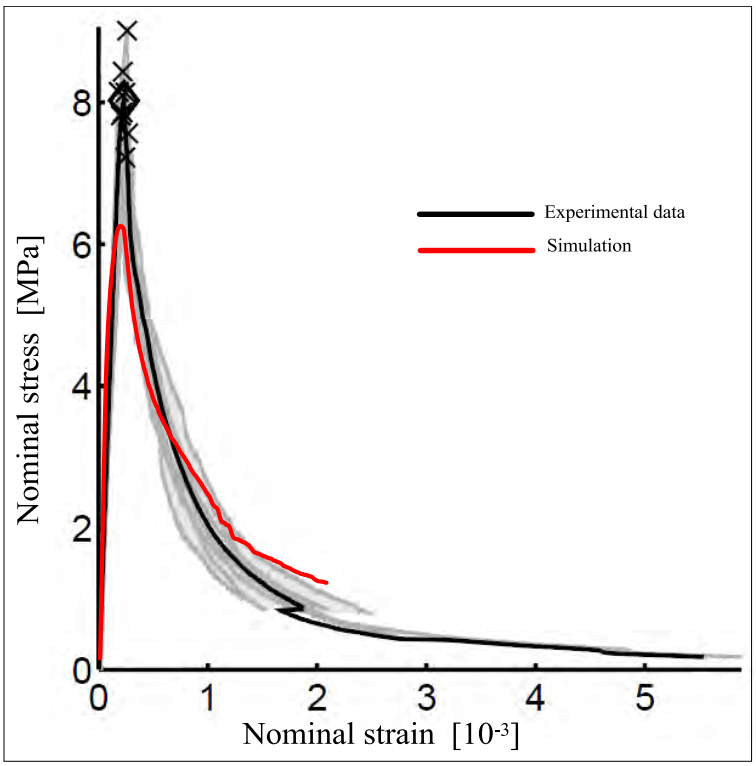


*Figure 8.1: Beam C, without notch, comparison between Simulation-Experimental data*

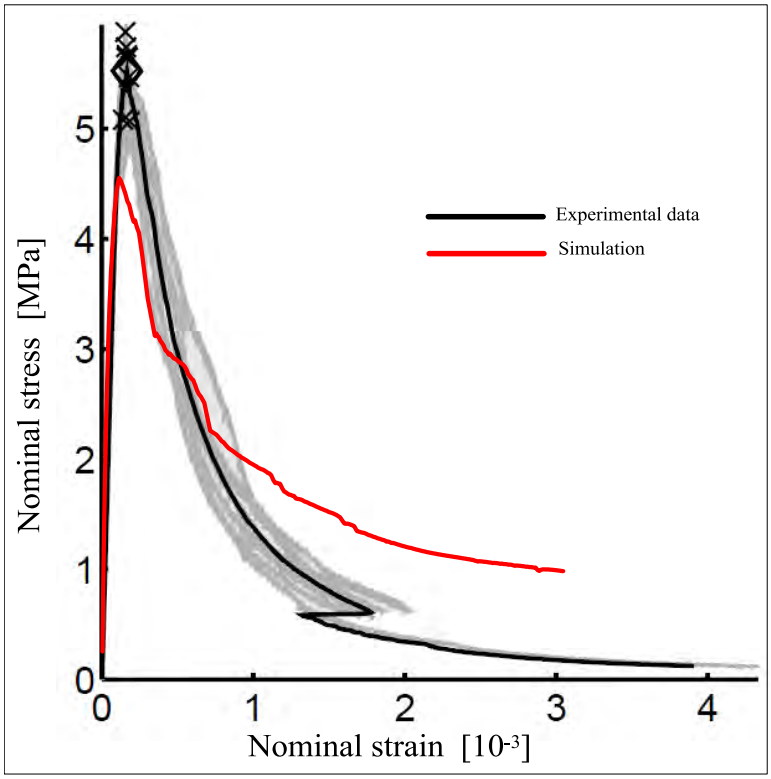


*Figure 8.2: Beam C, notch depth α=7.5%, comparison between Simulation-Experimental data*

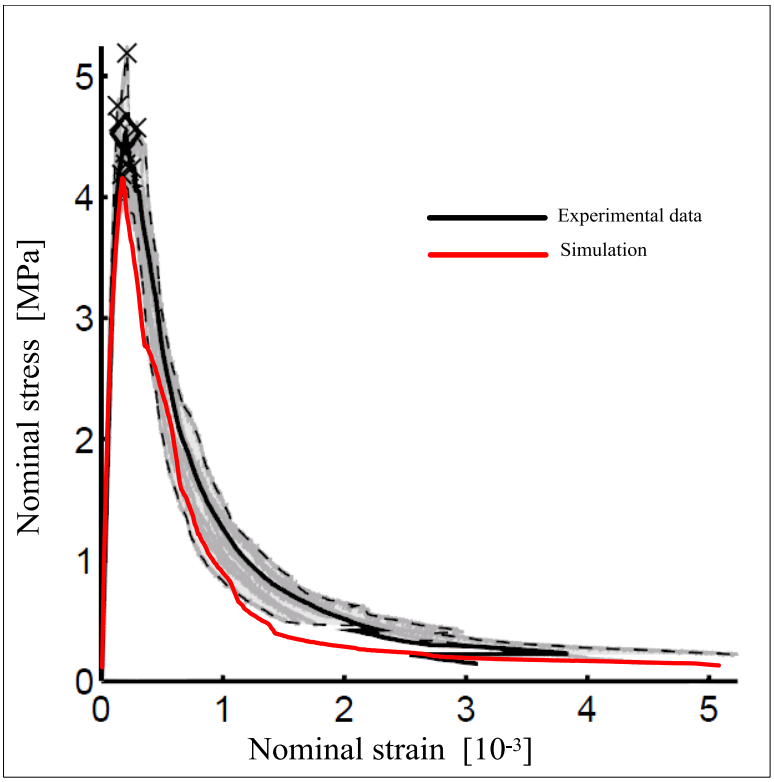


*Figure 8.3: Beam C, notch depth α=15%, comparison between Simulation-Experimental data*

## 8.2 Three-point bending tests of beam D

The second dimension of the validated beam is Beam D. This is the smallest among all of the beams and it is the one that has shown better results. In figure (8.4) is shown the beam D without notch, which has a peak value lower than about 1 MPa and the softening branch is lower than the compared Curve. For Beam D with notch $\alpha = 7.5\%$ (figure 8.5) the peak value obtained is the closest to the real one, differing only by 0.5 MPa. For the softening branch you can make the same considerations as in the previous case, even if the curve obtained numerically approaches a bit more the one obtained from experimental data.

The curve relating to the beam D with notch $\alpha = 15\%$, shown in figure (8.6) is definitely the best between the curves of the Beam group D. This curve is practically in full agreement with the one obtained by experimental data, having a lower peak of only 0.3Mpa and having the post-peak trend identical to the curve to compare with. This result would be expected for the Beam with notch $\alpha = 30\%$.

This can be interpreted as an early sign of the problem related to different sizes that will be noticed more and more when increasing the size of the specimens. The beam with notch $\alpha = 30\%$ is shown in figure (8.7). In this case the peak is exactly the same for the stress and the one obtained by experimental data, while it can be noted that the origin of the peak in this case was carried out with a slightly greater strain, and in fact this reflected in the softening branch where the curve appears to have a minor slope to the one compared with. This is the only case in which there is a situation of that kind.

Analyzing the validation of the beam Group D in his complexity, it can be seen that in the growth of the notch the value of the peak is getting closer and closer to the real value, reaching the optimal value for the beam with notch $\alpha = 30\%$. The same consideration can be done for the softening branch where it can be noted that the curve is always more in agreement with the one obtained by the experimental data when increasing the notch.

These observations find their explanation in the fact that the calibration was done on a specimen with a notch α = 30%, so, going closer and closer to this type of specimen we note a greater similarity between the two curves to compare.

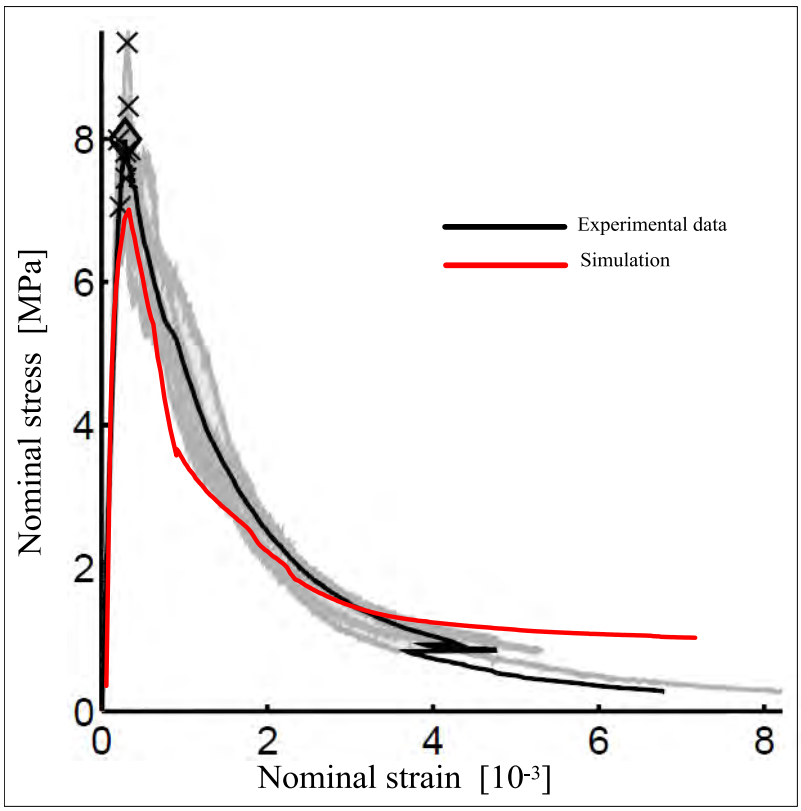


*Figure 8.4: Beam D, without notch, comparison between Simulation-Experimental data*

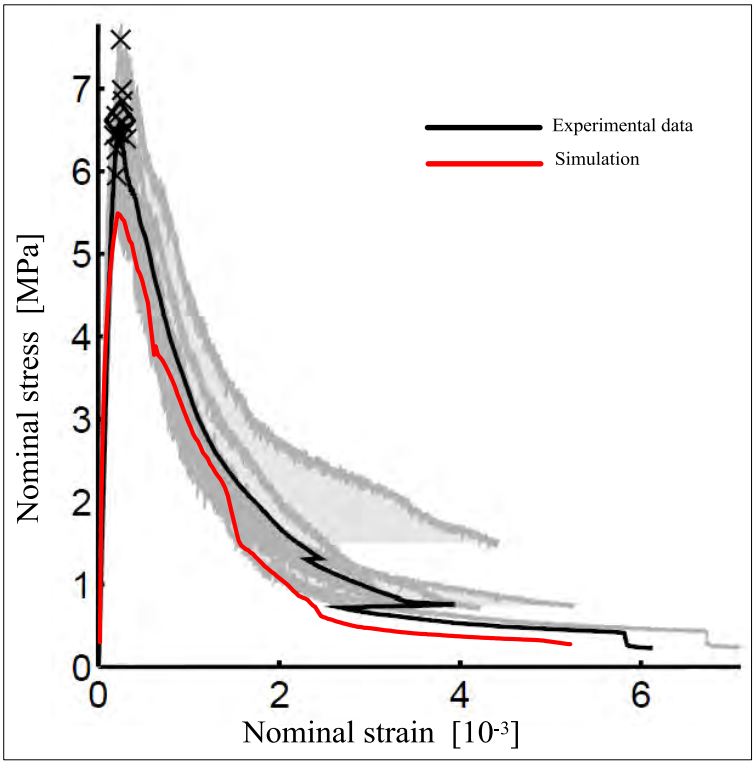


*Figure 8.5: Beam D, notch depth α=7.5%, comparison between Simulation-Experimental data*

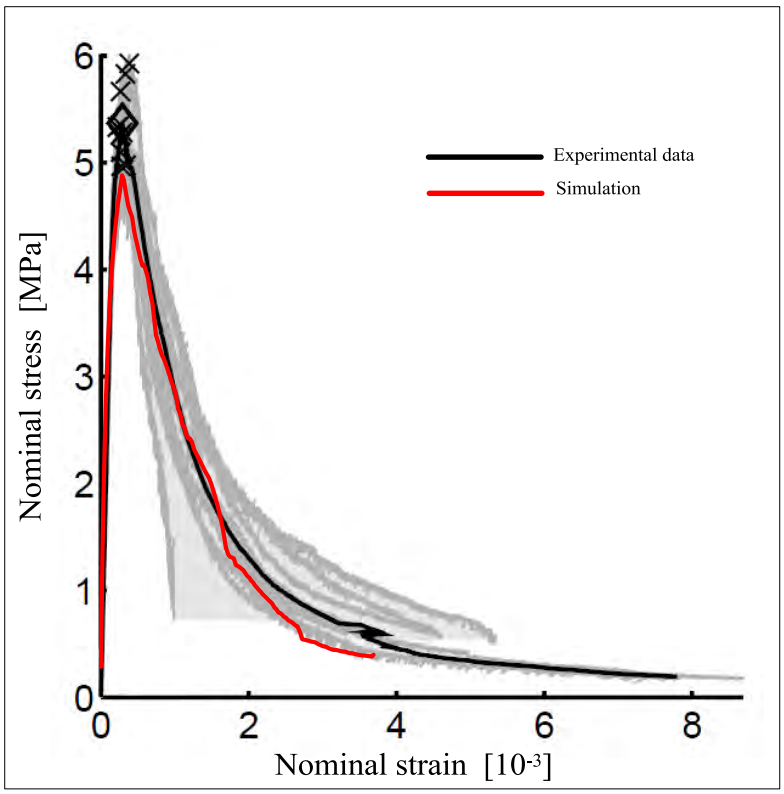


*Figure 8.6: Beam D, notch depth α=15%, comparison between Simulation-Experimental data*

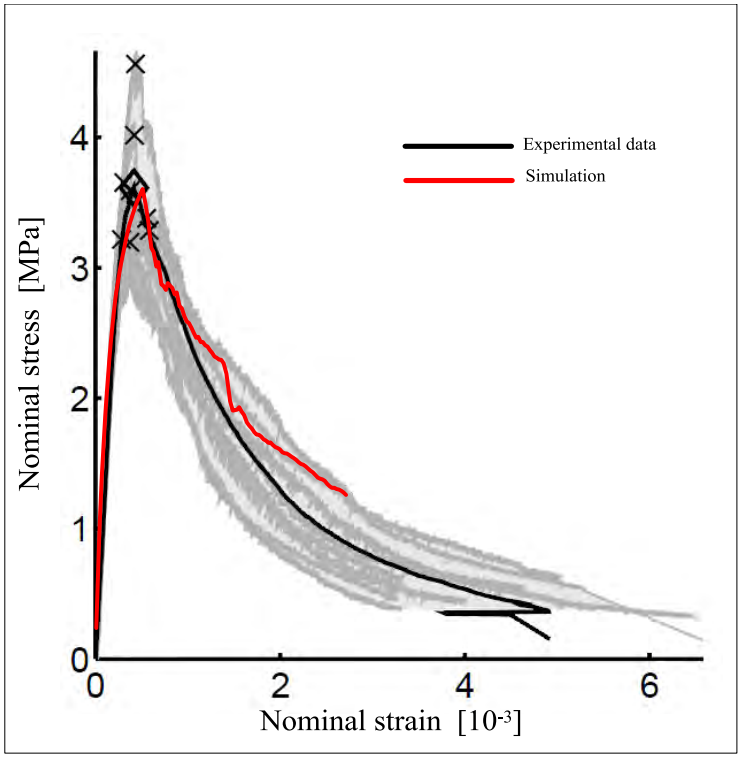


*Figure 8.7: Beam D, notch depth α=30%, comparison between Simulation-Experimental data*

## 8.3 Three-point bending tests of beam B

.The third group validated was the beam B. In this group instead of the usual 4 different notches if it has one more, this is because the specimen size begins to change a lot, having a size far greater than the beam used for the calibration. In fact, as can be seen in the figures that represent the validation for this group of beam, it has values not entirely in agreement with the curves obtained through experimental date. In fig (8.8) is shown the case without notch, where it can be noticed, as in previous cases without notch, a lower peak of about 2 MPa and a softening branch that reflects only part of the right trend. A problem encountered in making the nonlinear analysis of these large specimens is that often the program was not orientated to the problem. (Convergence criteria not satisfied. The execution is killed two to violation of the step divergence criteria).

To solve this problem we choose to decrease the size of the step reducing the prescribe deformation. In this way it was possible to hold up multiple values for each simulation.

In figure (8.9) and (8.10) are shown cases regarding the validation of the Beam B with notches $\alpha = 2.5\%$ and $\alpha = 7.5\%$. In the first case the peak differs from the real situation of about 0.6 MPa and in the second of about 0.2 MPa. Even here, we can notice how rising up the notch values tend to be more suitable, this is due to the fact that the calibration has been done on a specimen with a greater notch than these. In these two cases softening branch does not reflect the shape of the curve obtained from experimental data, having much higher stress values. For the beam with notch $\alpha = 2.5\%$ shown in figure (8.9) ,it is noted that the peak has a good value, close to the reality and even the softening branch began to follow a proper trend. Unfortunately, later on for convergence problems, the program stopped not continuing the simulation.

As might be expected the best case concerns the beam with notch $\alpha = 30\%$. In figure 8.12 it's shown how in this case the results obtained from experimental analysis are in agreement with those obtained from experimental data. The peak is virtually identical and also the performance of the post-peak appears to be very similar to the real one. Regarding this group of beam, the later, with notch $\alpha = 30\%$ appears to be best validation and the only one that can be considered fully acceptable.

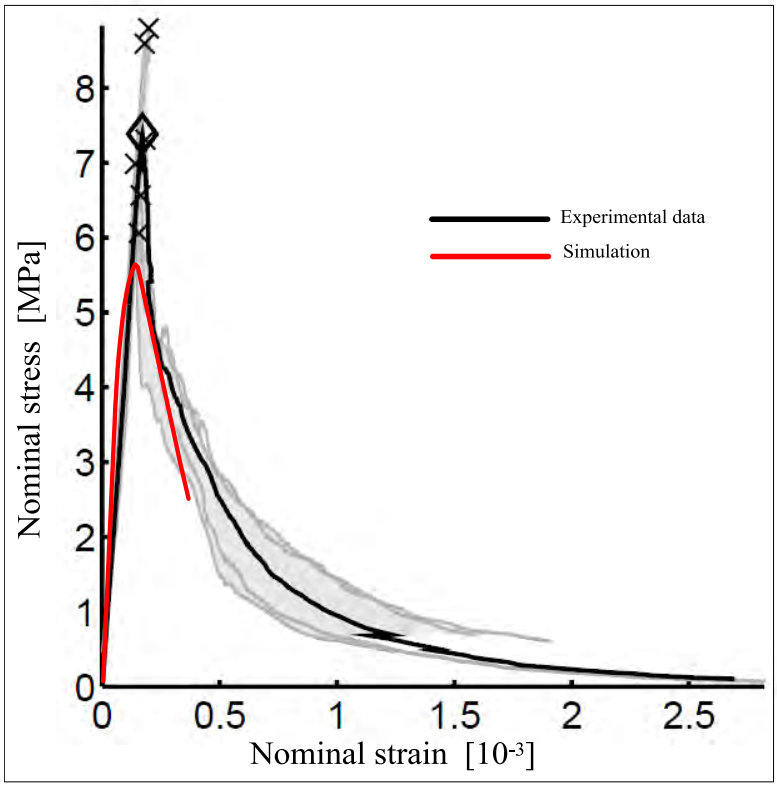


*Figure 8.8: Beam B, without notch, comparison between Simulation-Experimental data*

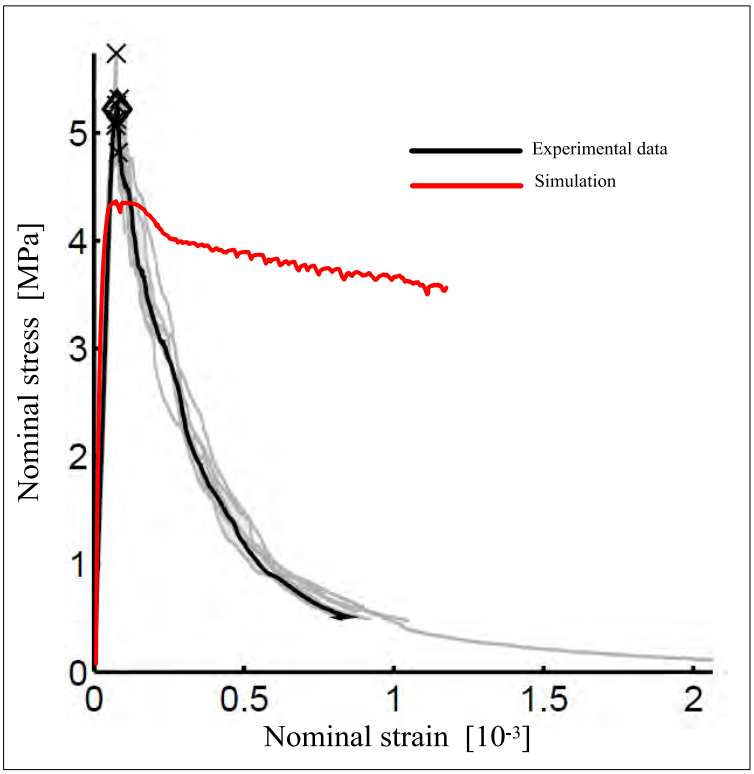


*Figure 8.9: Beam B, notch depth α=2.5%, comparison between Simulation-Experimental data*

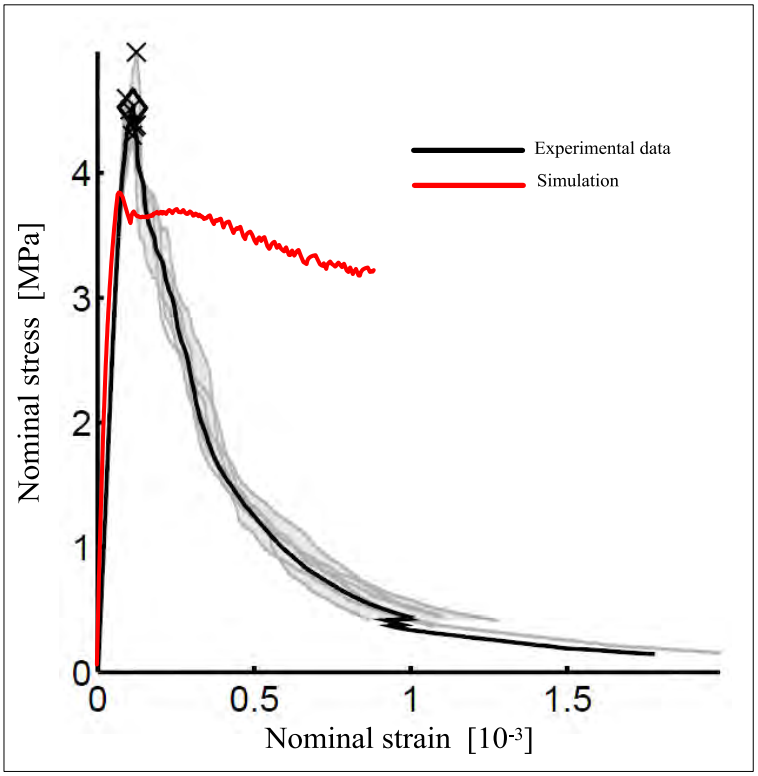


*Figure 8.10: Beam B, notch depth α=7.5%, comparison between Simulation-Experimental data*

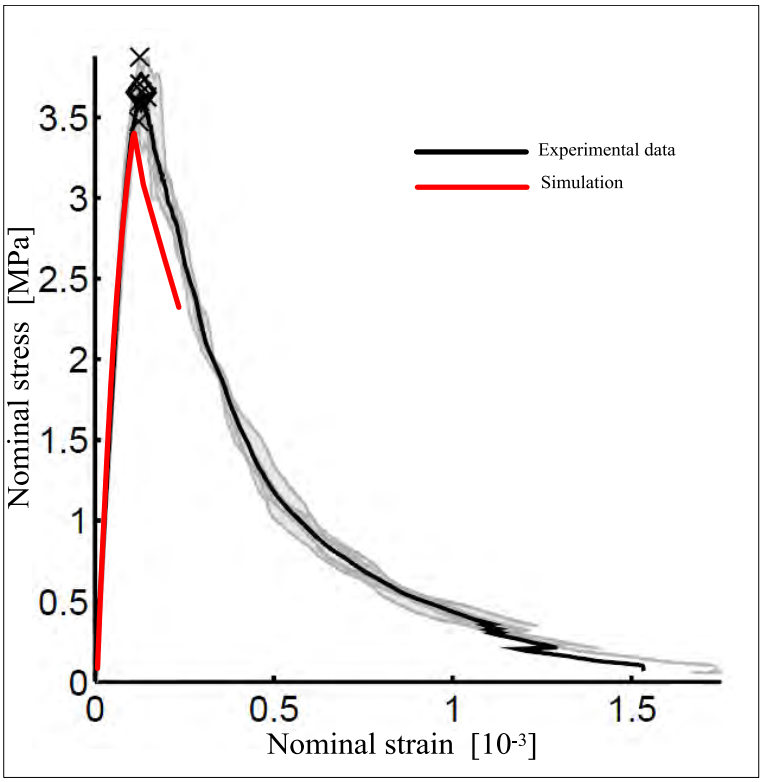


*Figure 8.11: Beam B, notch depth α=15%, comparison between Simulation-Experimental data*

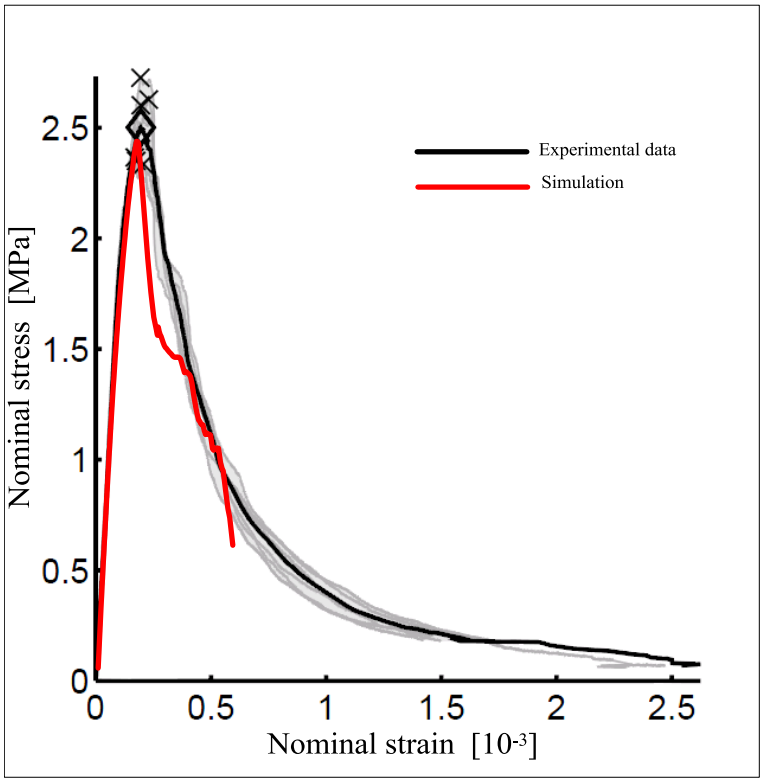


*Figure 8.12: Beam B, notch depth α=30%, comparison between Simulation-Experimental data*

## 8.4 Three-point bending tests of beam A

The last group of beam to be validated is the Beam A. All the limits of the program in this group can be noticed as also the difficulty of analyzing large specimens even after having carried out the calibration on a specimen much smaller. This is also linked to the problem discussed above called "size effect". For all cases except the one with α = 30%, there have been problems in making the nonlinear analysis. Every time Convergence criteria was not satisfied. It has therefore been tried to decrease the prescribe deformation and thus increase the number of steps, reaching in some cases even 500 step but still it has not been able to reach satisfactory solutions. It can be seen in figure (8.13) and (8.14) how the curve obtained by numerical simulation reflects the trends initially but then changes near the peak and

takes on greater strain values than the real ones. In fact, the peak appears even if with almost the right stress values and higher strain values of strain, you can see that the peak obtained is not real but tends to be more rounded instead of having a peak as it should have. The specimen with notch α = 30% is the only one for this group that has led to acceptable results, having a peak a little lower than the real one. The softening branch has not been possible to obtain, not even for this type of notch, even if it can be noticed that the initial post-peak trend is definitely more accurate than the other specimens with notches different to α = 30%.

Concluding, the validation of the beam A has not led to good results because of the too large a size specimen and therefore a high computational load.

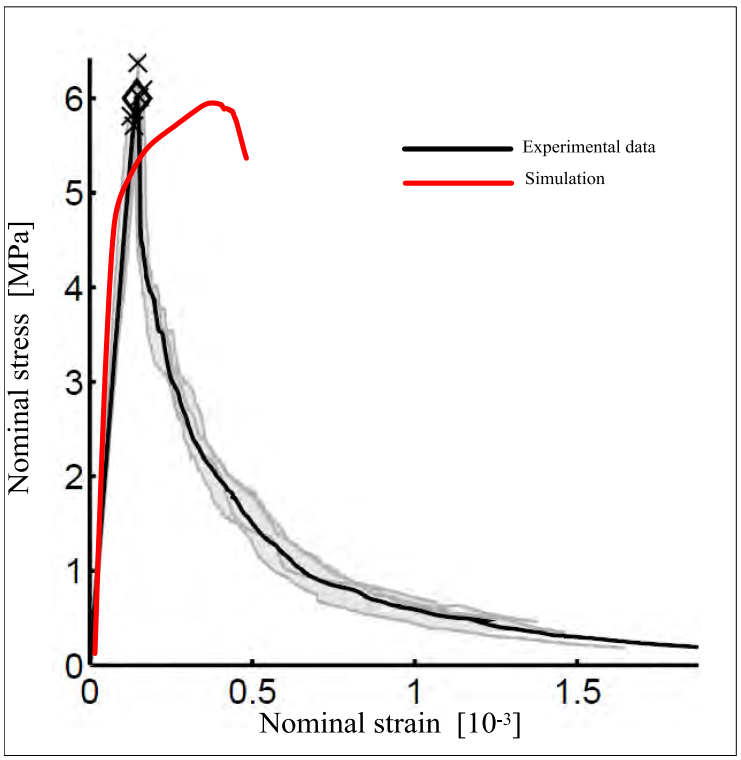


*Figure 8.13: Beam A, without notch, comparison between Simulation-Experimental data*

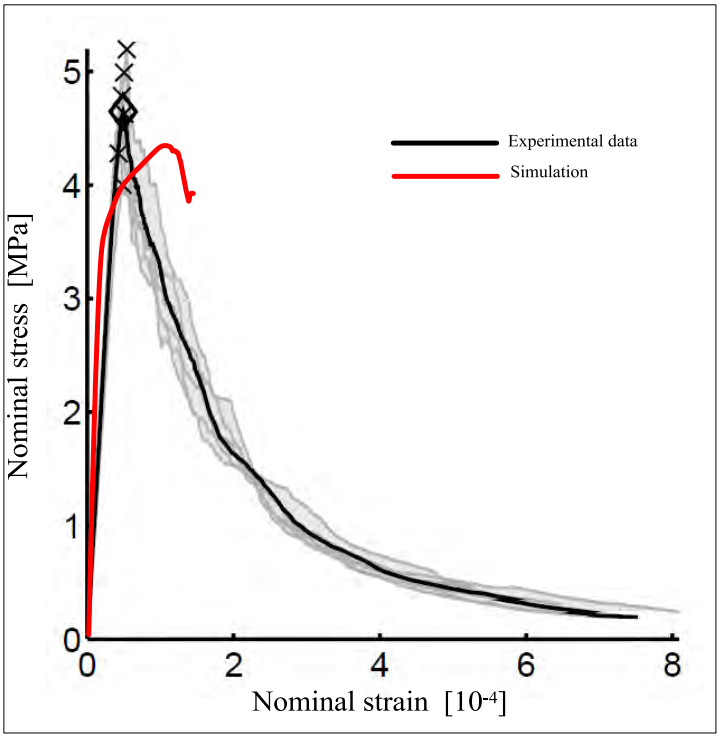


*Figure 8.14: Beam A, notch depth α=2.5%, comparison between Simulation-Experimental data*

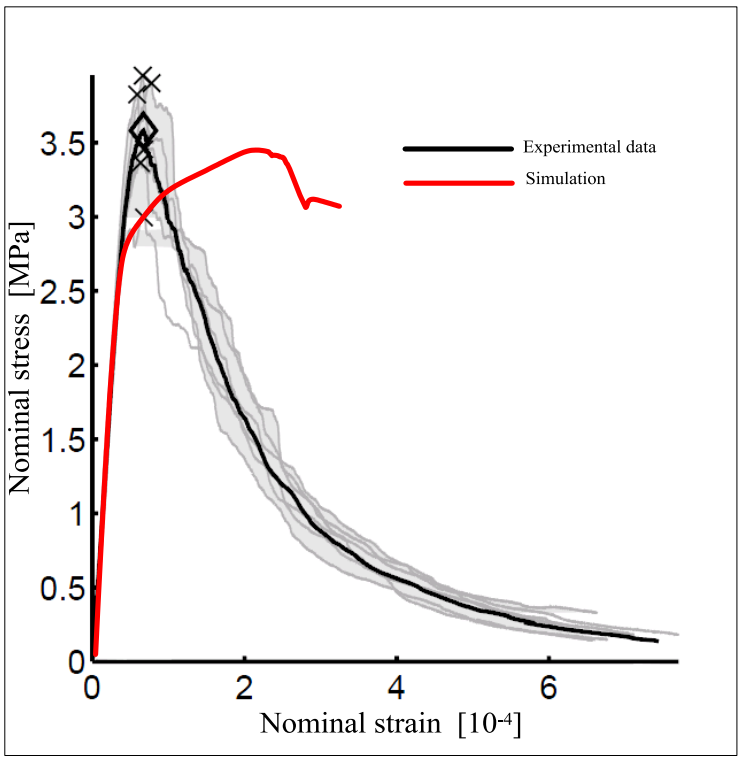


*Figure 8.15: Beam A, notch depth α=7.5%, comparison between Simulation-Experimental data*

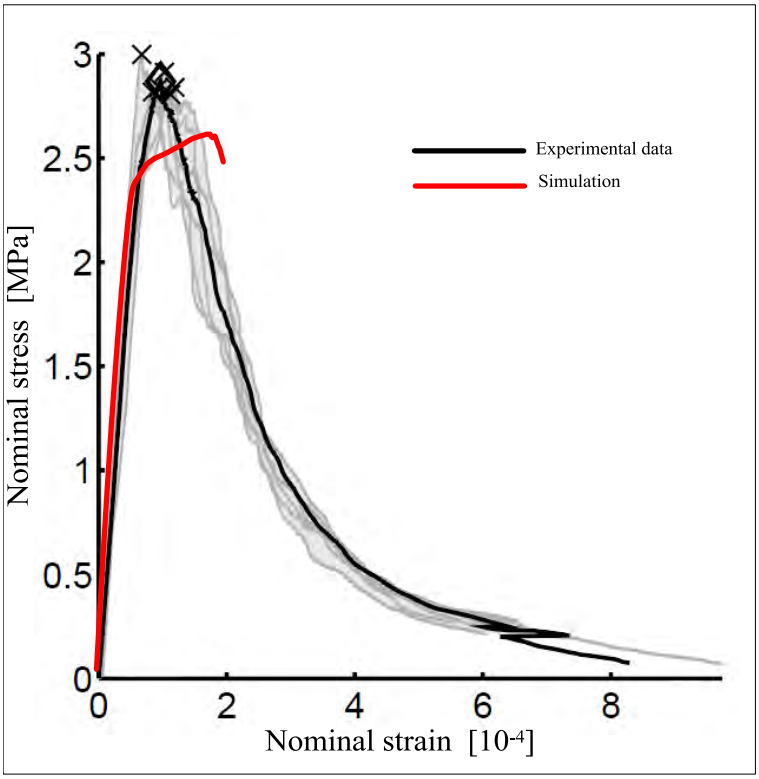


*Figure 8.16: Beam A, notch depth α=15%, comparison between Simulation-Experimental data*

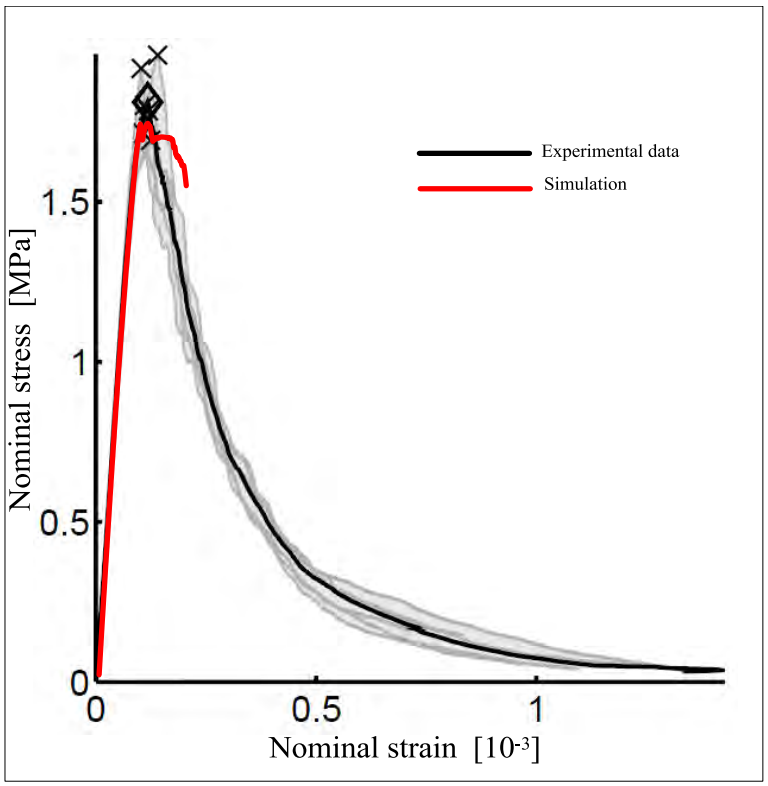


*Figure 8.17: Beam A, notch depth α=30%, comparison between Simulation-Experimental data*

Overall it can be said that the validation of fracture-plastic constitutive model has brought good results for small specimens such as Beam C and beam D but failed to satisfy the requirements for other types of beams. Another important observation is that the validation results tend to be very successful for the specimens with notch $\alpha = 30\%$, that means for the specimens with the same notch used for calibration. Surely if the calibration had been performed on another type of specimen or notch the results of the validation would be different.

# Chapter 9

# CONCLUSION

This research activity has led to a number of important conclusions, showing how the numerical analysis by finite element software has become an essential tool in modern engineering, being able to recreate situations, in the case of laboratory tests treated, increasingly similar to reality.

The importance of the use of laboratory tests made with all specimens from the same batch was very important and essential for a good comparison between the tests, and especially to be able to perform a proper calibration and subsequently a true validation. The set of all the tests performed in the laboratory, which were not all used in this research, may be useful for future research with the aim of improving the development and calibration of the same constitutive model treated in this thesis, or for other constitutive models and other software.

The constitutive model implemented in the program ATENA and used in this research is a three-dimensional model that combines plasticity with fracture. CC3DNonLinCementitious2 is the fracture-plastic model combining constitutive models for the tensile (fracturing) and compressive (plastic) behavior. The fracture model is based on the classical orthotropic smeared crack formulation and crack band model. It employs Rankine failure criteria and exponential softening, and it can be used as a rotated or fixed crack model. The hardening/softening plasticity model is based on the Menétrey- Willam failure surface. The model can be used to simulate concrete cracking, crushing under high confinement, and crack closure due to crushing in other material directions.

Based on the criteria defined in this thesis and the application of the laboratory tests, it is possible to identify the constitutive parameters fracture-plastic model of concrete. The study also serves as a link between the real behavior of concrete and its numerical modelling.

The known material parameters of concrete (compressive strength $f'_c$ and elastic modulus E) are used directly. The other material parameters (tensile strength $f_t$, Poisson's ratio $v$, fracture energy $G_f$, and the end point $W_D$ of the strain-softening curve in compression) of the concrete material model are adjusted to match the measured load-deflection curve and reproduce the observed compression crushing mode of failure.

Thanks to the ATENA program, we managed to recreate the specimen in an identical manner to the real ones, and thanks to the nonlinear analysis implemented in the software, we have been able to reproduce the trend of the tests. The choice of the mesh was important, having used brick elements, it was possible to have a regular mesh, so with less computational load and a more regular solution. Concerning the three-point bending test, for each specimen and for each different notch, the most appropriate mesh has been searched for and this has led to good results. The aim was to thicken the mesh near the notch, this means in the whole central part of the specimen, evaluating from multiple options we managed to find a good solution also useful for the proper performance of the crack.

Through an adequate nonlinear analysis it was possible to recreate the trend of the laboratory tests, and then be able to extrapolate the data necessary to recreate the stress-strain curves to be compared with those obtained from the experimental data. Getting the ultimate load and the trend of the softening branch were two objectives completed. These results were achieved thanks to a step by step analysis where a predetermined deformation has been applied for each of these. The solution method used was the Newton Raphson 's method, which was sufficient for this type of analysis, although for large specimens (*beam A, beam B*) of the three-point bending test, problems like the snap-back have been found .So for future studies, we

recommend the use of solution methods such as arc-length present in the software ATENA. The simulations are found to capture the failure mechanism both qualitatively and quantitatively.

Through certain equations it was possible to recreate the curves from data obtained from linear analysis and make a proper calibration of the model. The next step was to calibrate the constitutive model studying and varying the values of some basic parameters. The calibration was performed in Beam C of the three-point bending and in the 40x40mm cube of the unconfined compression.

The calibration results were suitable. In the search for the most appropriate value for each parameter studied, it was possible to understand the influence of each parameter on the behavior of the material. A better understanding of this was made possible when performing parametric analysis for each parameter. The importance of tensile strength in three-point bending test has been understood through this analysis such as the importance of compressive strength in unconfined compression tests.

Another important aspect that has been considered was the coupling of some parameters, such as the fracture energy $G_f$ and in the $\beta$ parameter. The search for more suitable pairing between these two parameters has led to good results in both the three-point bending tests as in the unconfined compression. The result of the calibration can be considered satisfactory, having found good matches between the values of the parameters used and those obtained from laboratory tests, and noting that the trends of the curves found reflect those obtained with the experimental data. For both tests the peak is virtually identical. In the three-point bending the slope of the softening branch is in agreement with the curve that it is to be compared with, only a lower fracture energy can be noted.

Concluding in the calibration the good agreement between experimental and numerical stress-strain curve can be observed.

Through the use of fracture–plastic constitutive model, after the calibration, the comparisons of the results prove the usefulness of the proposed constitutive model. The other three-point bending notched and unnotched concrete beams and the unconfined compression cube was used to compare the numerical results with the laboratory tests for doing the Validation.

Using fracture–plastic constitutive model enables a proper definition of the failure mechanisms in concrete elements. This constitutive model can be used to model the behavior of concrete and the reinforced concrete structures in advanced states of loadings.

Validation of the constitutive model has provided good results even if some limits have been found. Good results were obtained in the simulations of the beam C and D where the curves obtained are in agreement with the results obtained by experimental data. The size effect is the decisive reason for the use of design criteria based on the fracture mechanism. From the analysis of the three-point bending in 4 different sizes it was found that increasing the dimensions of the specimen, the results deviate more and more from the results obtained by experiment data and it was noticed that for the *beam A* and *beam B* whether the peak or the softening branch are not in complete agreement with the data obtained from the laboratory. A possible solution would be to calibrate the model starting from these specimens, but then the problem will probably reoccur for the simulations of smaller specimens.

The proposed model with the estimated constitutive parameters can successfully serve for analyses of the concrete structures in advanced states of stresses far beyond the limits defined in engineering codes.

To validate the implementation, an experiment from the specific experimental tests used has been analyzed and as a whole the numerical results show good agreement with the experimental data. Results from this research are intended to be used for validation of the numerical model of fatigue material behavior, parameter calibration, further model development and its improvements.

# Reference

Aci: guide for modeling and calculating shrinkage and creep in hardened concrete. Tech. Rep. (2008).

ATENA program documentation, part 1 - Theory, Cervenka consulting, Prague, Czech Republic (2013).

Bazant Z., Cedolin L. Stability of structures. Elastic, inelastic, fracture and damage theories, 2nd edition, Oxford university press, New York (1991).

Bazant z., Oh B. Crack band theory for fracture of concrete. Materials and structures 16, 155-177 (1983).

B.k. Raghu Prasad, Rabindra Kumar Saha1, A.R. Gopalakrishnan. Fracture behavior of plain concrete beams – experimental verification of one parameter model, icces, vol.14, no.3, pp.65-83 (2010).

Carpinteri A, Chiaia B, Ferro G. Multifractal scaling law. An extensive application to nominal strength size effect of concrete structures. Atti del dipartimento di ingegneria strutturale, 2 (50). Italy: politecnico de torino;(1995).

Červenka V. 2002. Computer simulation of failure of concrete structures for practice. Proceedings of the 1st fib congress concrete structures in 21 century, Osaka, Japan. Pp. 289 – 304 (2002).

Christian G. Hoover, Zdene K. P. Bazant, Jan Vorel, Roman Wendne, Mija H. Hubler. Comprehensive concrete fracture tests: description and results, Northwestern university, 2145 Sheridan road, Evanston, Usa, (2013).

Christian G. Hoover, Zdeněk P. Bažant. Cohesive crack, size effect, crack band and work-of-fracture models compared to comprehensive concrete fracture tests international journal of fracture. (2014).

Concrete - part 1: specification, performance, production and conformity (2000).

Eurocode 2: design of concrete structures, part 1-1: general rules and rules for buildings (2004).

Gabet T. and Malecot, Y. Daudeville, L. Triaxial behaviour of concrete under high stresses: inuence of the loading path on compaction and limit states. Cement and concrete research, 403-412 (2008).

Growth in concrete by means of fracture mechanics and finite elements. Cement and concrete research 6, 773-782 (1976).

Han, D.J. Plasticity for structural engineers. J. Ross publishing (2007).

Hillerborg, A. The theoretical basis of a method to determine the fracture energy $G_f$ of concrete. Materials and structures, 291-296 (1985).

Hoover, C.G., Bazant, Z.P. Comprehensive concrete fracture tests: size effects of types 1 & 2, crack length effect and postpeak. Tech. Rep. Cee 12-09/778s, Northwestern university (2012).

Hoover C.G., Bazant Z.P., Vorel J., Wendner R., Hubler M.H. Comprehensive concrete. Fracture tests: description and results. Tech. Rep. Cee 12-09/778d, Northwestern university (2012).

J.C. Matos, J. Batista, P. Cruz & i. Valente. Uncertainty evaluation of reinforced concrete structures behavior, institute for sustainability and innovation in structural engineering, university of Minho, Guimarães, Portugal.

Jiabin Li, Nguyen V. Tue, Ferhun C. Caner. Microplane constitutive model m4l for concrete ii: calibration and validation, institute for structural concrete, Graz university of technology, 8010 Graz, Austria, (2012).

Malvar Jl, Warren Ge. Fracture energy for three-point-bend tests on single-edge-notched beams. 266–72.

Moes N., Dolbow J., Belytschko T. A finite element method for crack growth without Remeshing. International journal for numerical methods in engineering 46(1), 131-150 (1999).

Pryl Dobromil, Cervenka Jan, Pukl Radomir. Material model for finite element modelling of fatigue crack growth in concrete, Cervenka consulting, Na Hrebenkach 44, 150 00 praha 5, Czech Republic, (2010).

R. Raveendra Babu, Gurmail S. Benipal and Arbind K. Singh indian institute of technology, Delhi, indian institute of technology, Guwahati, India, constitutive modelling of concrete: an overview. Asian journal of civil engineering (building and housing) vol. 6, no. 4 (2005), Pages 211-246.

Roman Wendner, Jan Vorel, Zdenek P. Bazant, Gianluca Cusatis, A comprehensive experimental database for the calibration and validation of concrete models, university of natural resources and life sciences Vienna (2013), Austria

S.T. Yang, X.Z. Hu, Z.M. Wu. Influence of local fracture energy distribution on maximum fracture load of three-point-bending notched concrete beams s.t. Department of civil engineering, college of engineering, ocean university of China, Qingdao 266100, China, (2011).

S. Seitl, L. R Outil, J. Klusa K, V. Vesely. The influence of the shape of a saw-cut notch in quasi-brittle 3pb specimens on the critical applied force, ainstitute of physics of materials, academy of sciences of the Czech Republic, 616 62 Brno, Czech Republic, (2008).

Tomasz Jankowiak, Tomasz Odygowski. Identification of parameters of concrete damage plasticity constitutive model, Poznan university of technology, institute of structural engineering (ise) Ul. Piotrowo 5, 60-975 Poznan, Poland, (2005).

Vladimir Cervenka, Jan Cervenka and Radomir Pukl, ATENA.A tool for engineering analysis of fracture in concrete, Sadhana vol. 27, part 4, august 2002, pp. 485–492. India.

# *Ringraziamenti*

I primi ringraziamenti vanno sicuramente ai miei due relatori, il Dott. Ing. Jan Vorel, della Czech Technical University in Prague**,** il quale mi ha aiutato e guidato nello sviluppo di questa tesi, e al Prof. Ing. Carlo Pellegrino, che mi ha seguito fino alla conclusione di questo percorso.

Un sincero ringraziamento va a tutti i miei compagni di studio, diventati veri amici, i quali aiutandomi e supportandomi in tutti questi anni sono stati una fonte preziosa nel conseguimento di questo importante traguardo.

Un particolare grazie va a tutti i miei più cari amici, sempre vicini nei momenti di difficoltà e capaci di farmi svagare e divertire in qualsiasi situazione.

Il ringraziamento più grande va sicuramente alla mia famiglia, a mio padre e a mia madre. Senza di loro non sarei mai riuscito a raggiungere questa impegnativa e fondamentale meta. A loro devo molto, per tutto ciò che mi hanno dato in questi anni.

Un ringraziamento speciale va a tutti gli amici conosciuti durante l'esperienza Erasmus a Praga, dove ho svolto questa tesi, e in maniera particolare voglio ringraziare Marco, con il quale ho stretto una profonda e straordinaria amicizia ed ho condiviso tutto ciò chè si può condividere con un vero amico.